Investigation of phase behaviour of neutral and ionic microgels using scattering, rheology and microscopy techniques

Thesis Submitted to AcSIR for the Award of
the Degree of
DOCTOR OF PHILOSOPHY
In Chemical Sciences

By

KIRAN K. J.
Reg. No. 10CC12A26053

Under the guidance of

Dr. Suresh K. Bhat

CSIR- National Chemical Laboratory
Pune-411008, India

2018

Investigation of phase behaviour of neutral and ionic microgels using scattering, rheology and microscopy techniques

Thesis Submitted to AcSIR for the Award of
the Degree of
DOCTOR OF PHILOSOPHY
In Chemical Sciences

By

KIRAN K. J.
Reg. No. 10CC12A26053

Under the guidance of

Dr. Suresh K. Bhat

CSIR- National Chemical Laboratory
Pune-411008, India

2018

DECLARATION

I hereby declare that the work described in the thesis entitled **"Investigation of phase behaviour of neutral and ionic microgels using scattering, rheology and microscopy techniques"** submitted for the degree of ***Doctor of Philosophy*** in ***Chemical sciences*** to the Academy of Scientific and Innovative Research (AcSIR), New Delhi, has been carried out by me at the Polymer Science and Engineering Division, CSIR-National Chemical Laboratory, Pune-411008, India under the supervision of **Dr. Suresh Bhat**. I further declare that the material obtained from other sources has been duly acknowledged in this thesis. The work is original and has not been submitted in part or fully by me for any other degree or diploma to this or any other university.

Date: 30th January, 2018
CSIR-NCL, Pune

Mr. Kiran K J
(Research Scholar)

राष्ट्रीय रासायनिक प्रयोगशाला
(वैज्ञानिक तथा औद्योगिक अनुसंधान परिषद)
डॉ. होमी भाभा मार्ग पुणे - 411 008. भारत
NATIONAL CHEMICAL LABORATORY
(Council of Scientific & Industrial Research)
Dr. Homi Bhabha Road, Pune - 411 008. India.

CERTIFICATE

This is to certify that the work incorporated in this Ph.D. thesis entitled "**Investigation of phase behaviour of neutral and ionic microgels using scattering, rheology and microscopy techniques**" submitted by Mr. **Kiran K. J.** to Academy of Scientific andInnovative Research (AcSIR) in fulfillment of the requirements for the award of the Degree of**Doctor of Philosophy** in Chemical Sciences, embodies original research work under my supervision/guidance. I further certify that this work has not been submitted to any other University or Institution in part or full for the award of any degree or diploma. Research material obtained from other sources has been duly acknowledged in the thesis. Any text, illustration, table etc., used in the thesis from other sources, have been duly cited and acknowledged.

Kiran K. J.
Reg. No. 10CC12A26053

Dr. Suresh K. Bhat
(Supervisor)

Pune
30.01.2018

Communication Channels
NCL Level DID : 2590
NCL Board No. : +91-20-25902000
EPABX : +91-20-25893300
+91-20-25893400
FAX
Director's Office : +91-20-25893355
COA's Office : +91-20-25893619
COS&P's Office : +91-20-25893008
WEBSITE
www.ncl-india.org

Acknowledgements

I would like to first thank my research advisor, **Dr. Suresh Bhat**, for his motivation, support, and willingness to take me in as his student. His attitude toward research and his availability to his students has provided me with an amazing and supportive environment in the laboratory. I am extremely indebted to **Dr. Priti Mohanty**, my collaborator who was always there when ever I needed him. I owe my gratitude to **Dr. Sharvil Patil**, Assistant Professor, Pune College of Pharmacy, who had been an inspiration for me throughout the work I had done with him. He has been indispensable to my success a field that I knew little about when starting off and in which he is an expert. My special thanks to **Dr. C. Ramesh** who helped me starting my research career in NCL.

My sincere thanks to **Dr. Vyshali S Shinde** and the Doctoral Advisory Committee members **Dr. Amitava Das**, **Dr. Ajith Kumar**, **Dr. Ashootosh Ambade** and **Dr. Manohar Badiger** for evaluating and reviewing my work yearly.

My fellow lab mates, over the years have also provided me with an amazing amount of help. **Dr. Samrudhhi Kamble** and **Dr. Venugopal Edakkal** had the patience and kindness to help me extensively with learning and using the instruments in the lab. It was great fun to work with Fayis, Maya, Anju, and Aswathy on the synthesis and experiments on microgels. A big thanks to Nandhu for helping me drawing the images. I would extend my thanks to my friends in and outside the lab especially Manoj, Mohanraj, Shoy, Leena, Anish, Sunil, Vysakh, Sharath……. They were amazing and reliable. The time spent with them was stress-relieving and really memorable.

I would also extend my gratitude to my parents for supporting my interest in science as far back as I can remember. They have provided me every support both moral and financial to thrive in my whole research career. My warmest thanks are reserved to my wife Sreedevi for everything she has sacrificed for me to make it this far in my career. Thank you for your patience, your compassion, and for your undying love and support. I hope I can provide you with as much as you have given to me. I must be grateful to my brother Arun, from whom I learned many things apart from science and research. I extend my deepest obligation to my cousin Dr. Deepa, who had become Doctor in biological science, and watching her persevere at many times made all the difference in the world to my own levels of motivation.

I acknowledge Council of Scientific and Industrial Research (CSIR) for the research fellowship for my Ph.D. I also extend my thanks to CSIR- National Chemical Laboratory, Pune (CSIR-NCL) for this Ph.D programme and allowing me to avail facilities from this premier research institute in India.

Kiran K. J.

Abstract

The thesis deals with the investigation of structure and dynamics of temperature and pH sensitive microgels of Poly (N-isopropylacrylamide) at very dense concentrations using scattering, rheology and microscopy techniques. The main focus of the work is on understanding how the microgel architecture/structure affects the flow properties as well as in applications. Poly (N-isopropyl acrylamide) microgels were prepared using two different synthesis procedures giving rise to core-shell particles and homogeneous particles respectively. These particles are then used to prepare dense suspensions to study non-linear rheological behaviour in the glassy region. Modern Light scattering techniques, rheology and confocal microscopy are used to investigate the role of microstructure in the flow properties of these dense suspensions. The thesis also deals with electric field induced structure formations in ionic microgels and mixtures. We also look at the effect of microgel particle morphology in a typical application like drug delivery.

Colloids are heterogeneous system where one substance is dispersed as very fine particles in another. The dispersion may be foam, emulsion or sols and are indispensable in or daily life. Study of the processing of all these colloids is important because many of the colloids we use as commercial products in our daily life is subjected to shear when used. They transform from elastic to a plastic state when yielded. The study of yielding in colloids is thus very much important to design the products. In addition to its utility as materials of daily use, colloidal suspensions are extensively used as model systems to study phase behavior of atomic or molecular systems. Phase transitions in colloidal suspensions can be studied in real time using optical techniques and are analogous to phase transitions in liquids. Experiments with colloids are always simpler. The microscopic size scale of colloids allows them to be easily characterized by microscopy and various light scattering techniques. Although lot of work has been done in understanding the yielding mechanism in hard sphere colloids and colloid-polymer mixtures, there is not much progress in understanding the yielding phenomena in soft colloids. **First** chapter sets the motivation and objectives of the study. This chapter also contains a literature survey and introductory remarks on colloids. Hard sphere colloids and soft sphere colloids, their properties, colloidal interactions and phase diagram are described here. A brief history on the investigation of electric field driven assembly of ionic colloids and a background on the drug release studies on model soft microgels are also provided. **Second chapter** provides the details

of the synthesis of homo and copolymer microgels of NIPAm. Some of the preliminary characterizations of microgels using light scattering technique are also provided in this chapter. All the experimental techniques and the methods used in this work to investigate the structure and properties of microgels are explained. The technical part of instruments like 3D- Dynamic Light Scattering, rheology, confocal microscopy, UV-Visible Spectroscopy and Differential Scattering Calorimetry are elaborately discussed in this chapter. Light Scattering techniques are used to find the radius of gyration, hydrodynamic radius, swelling ratio and volume phase transition temperature of PNIPAm microgels. Yielding mechanism in the microgels was elucidated by Large Amplitude Oscillatory Shear experiments in a stress controlled rheometer. Electric field driven assembly of colloids were observed using confocal microscopy. Drug release studies were conducted and percentage release was found by UV-Visible spectroscopy. Subzero temperature DSC was done to analyse the changes thermodynamic property of water associated with the gelling process.

In the **third** chapter, I try to address the yielding mechanism in dense thermosensitive microgels of Poly (N-Isopropylacrylamide) (PNIPAm) in the glassy region as a function of particle morphology and crosslinker content. Electric field driven assembly of negatively charged copolymer microgels of NIPAm and acrylic acid at different concentration regimes are investigated in the **fourth** chapter. The behaviour of a binary mixture of two different sized particles towards applied electric field is also under investigation. The intension of the work is to develop a phase diagram of binary mixture of particles under the electric field with respect to different concentrations and different ratios of particles. **Fifth** chapter covers the study of effect of particle morphology on the drug release from PNIPAm microgel particles. A water-soluble drug and a water insoluble drug were taken for the case study. Percentage drug release was measured using UV-Visible spectroscopy.

The results of the current work are concluded in the **sixth** chapter. Ours is one of the first studies on the understanding of origin of double yielding mechanism in pure PNIPAm microgel system. Although two step yielding has been observed in attraction induced colloidal glasses, we are observing two step yielding in pure PNIPAM microgel glasses, which is otherwise repulsive. Two step yielding disappears with the change in morphology from core-brush type structure to homogeneously crosslinked structure. With increase in crosslinker content, and finally like hard-sphere colloids. Electric field driven assembly can be effectively used to tune the particles

assembly in fluid regime and also at high concentrations. The works may be extended to mixture of oppositely charged particles, active particles and colloids, colloid-metal hybrid particles etc. Drug release ability of microgels can be enhanced by particle morphology changes.

Contents

List of figures

List of tables

CHAPTER 1

INTRODUCTION

1.1. Colloids

Colloid can be called as a dispersion of particles or droplets in a liquid medium where the system is stable against sedimentation or aggregation. The particles or droplets have a size range of 1nm to 1 μm. Many natural materials, from the blood that flows through our body to the milk we drink every day, are colloids. Many of the commercially available products that we use daily like gels, emulsions, foams, paints, pastes, creams etc. contain colloidal suspensions. The extensive work by Sir Albert Einstein on colloids shaped the study of these materials into a different branch named colloid physics. The most important property of colloidal particles is random diffusive motion named Brownian motion.[1] The diffusion coefficient of these moving particles is related to the size of the particles. The bigger the particle, the slower will be the diffusion. Stokes-Einstein- Sutherland equation relates particle diffusion coefficient with the particle radius.[2,3]

$$D = \frac{k_B T}{6\pi\eta r} \qquad 1.1$$

where, r denotes the radius of the diffusing particle and η, the viscosity of the solvent in which the particles are suspended. The numerator k_BT represents the thermal energy of the moving particles where k_B is the Boltzmann constant and T is the temperature which sets the energy scale for all colloidal interactions.

Einstein and Smoluchowski independently found the characteristic time scale of a diffusing particle which later came to be known as Einstein-Smoluchowski relation. This relation is valid only in very dilute solutions, where the particle is considered to be isolated. If the particle can diffuse a distance equal to its radius, the characteristic time scale t is given by the following equation[4]:

$$t = \frac{6\pi\eta r^3}{kBT} \qquad 1.2$$

1.2. Particle interaction and colloidal stability

The diffusion of the colloidal particles in the suspension is greatly dependent on the interaction of the particles. The stability of the particles is also determined by the interaction between particles, which are in turn dependent on interparticle forces. The magnitude and balance between the available attractive and repulsive forces acting on the particle determines the overall stability of the colloidal suspension. DLVO theory developed by Derjaguin and

Landau (1941) and independently by Verwy and Overbeek (1948) quantitatively describe the balance between the most important interactions viz van der Waals attractive interactions and electrostatic repulsion.[5,6] The main attractive forces are Van der Waal's, hydrophobic interaction and depletion attraction. Repulsive interactions include electrostatic and steric repulsion. Classical DLVO theory incorporates only van der Waal's and electrostatic interactions. Total interactive force V_T is a simple addition of van der Waal's and electrostatic interactions. DLVO theory has been modified to incorporate other non-DLVO interactive forces also.[7] The important attractive and repulsive interactions present in a colloidal system are discussed below.[8–11]

1.2.1. Van der Waal's attraction

These are short range interaction with a range of several hundreds of A°. These forces emerge due to the dipole-dipole interaction and induced dipole interactions between colloidal particles. Van der Waals interactions are weak in very dilute solutions since the particles are far enough to feel the attraction. But as the concentration increases, the van der Waal's attractive potential causes the colloidal particles to attract, stick and aggregate. So, it is important to stabilize the colloidal particles by repulsive forces. Electrostatic repulsion occurring due to columbic effects, steric stabilization and entropic effects are frequently used for stabilizing the colloidal particles. Van der Waal's force between two spherical particles in a medium is given by the expression:

$$F\,(D) = \frac{-A}{6D^2}\left[\frac{R_1 R_2}{R_1 + R_2}\right] \qquad 1.3$$

where A is called Hamaker constant, A= $\pi^2 C \rho_1 \rho_2$, D is the centre to centre distance between two particles and R_1 and R_2 are radii of particles.

1.2.2. Hydrophobic interactions

Presence of hydrophobes or nonpolar molecules in the aqueous system may cause disruption of hydrogen bonds between the water molecules and hydrophilic groups. This disruption causes phase separation of the particles and the water molecules. This type of interaction is very much important in the case of thermoresponsive hydrogels (in our case PNIPAm and its ionic counterparts) since hydrophobic interaction boosts phase transition in this system. Hydrophobic interactions are relatively stronger than van der Waal's interactions and may be effective upto several tens of nanometers depending on the solvent. It is expressed as:

$$F(D) = \frac{-2\gamma_i}{\lambda_0} e^{-D/\lambda_0} \quad 1.4$$

where D is the centre to centre distance between two particles, λ_i is the interfacial energy and λ_0 is the characteristic exponential decay length.

1.2.3. Depletion interactions

In a colloidal suspension of two different sized particles, the presence of the smaller particles produces an attractive force between the larger ones. This is called the depletion force. Depletion force range is determined by the size difference between the particles.

$$F(D) = 2\pi R R_g \rho k_B T \quad 1.5$$

where R is the particle radius, R_g is the radius of gyration of non-adsorbing polymer, ρ is the number density, k_B is Boltzmann constant and T temperature in K.

This interaction causes the larger particle to come together and aggregate. Addition of sufficient concentration of non-adsorbing polymers to a colloidal suspension causes the colloidal particles to deplete or exclude the non-adsorbing polymers from the overlap region between the particles. This creates an osmotic pressure imbalance between the overlap region and the bulk solvent. This pressure around the colloidal particles drives them towards each other (Figure 1.1).

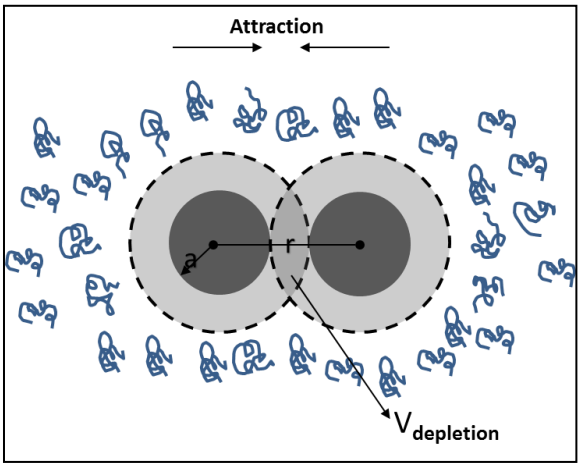

Figure 1.1: Depletion interaction between two hard spheres caused by the addition of small polymer fragments.

1.2.4. Electrostatic repulsion

The electrostatic forces arise due to the charges on the surface of colloidal particles dispersed in a solvent. Surface charge is formed due to the dissociation of ionisable functional

groups, adsorbed free ions or surfactants. The dissociated counter ions will form an oppositely charged layer over the charged group leading to the formation of a double layer. The particles are excluded from each other and kept away from aggregation due to the repulsion of this double layer. The potential at the hypothetical boundary of the diffusive layer is called the zeta potential. The magnitude of the zeta potential gives an indication of the potential stability of the colloidal system. Dispersion of particles with zeta potential more positive than 30mV or more negative than -30mV are normally considered to be stable. Debye length (κ) characterizes the interaction range. Typical values for the Debye length ranges from 0.3- 300 nm. The extend of these types of forces ranges up to hundreds of nanometers depending on surface charge density, particle size and solvent ion concentrations. Consider the centre to centre distance between two particles be D, then the repulsive force acting between them is given by:

$$F(D) = 2\pi \mathrm{R}\varepsilon\varepsilon_0\kappa\psi_0 e^{-\kappa D} \qquad 1.6$$

where R is the particle radius, ε is the dielectric constant of the medium, ε_0 the permittivity of the suspending medium and ψ is the surface charge potential.

1.2.5. Steric repulsion

This occurs due to the presence of bulky side groups or can be induced by grafting a short polymer chain (~50nm length) or surfactant molecules on to the surface of the particles. This is another way of stabilizing the colloid. Usually these interactions are very short and extend upto only 1- 2 nm, in the case of grafted polymer chains, these can extend to 10 times the radius of gyration of the coil. The grafting density and length of the side chain determines the magnitude and range of the repulsion. In order to prevent particles from coagulation, the above parameters are chosen in a way that the range of the steric interaction is larger than the range of the Van der Waals attraction between the colloids. The steric repulsion can be expressed as:

$$F\,(D) = f_0 e^{-D/\lambda_0} \qquad 1.7$$

where f_0 is force at D=0, D is the centre to centre distance between the particles and λ_0 is the exponential decay length.

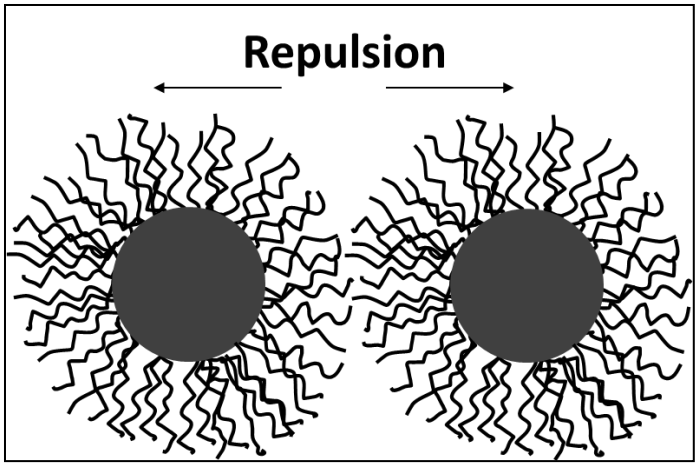

Figure 1.2: Steric repulsion provided by linear chains of polymer on the surface of particles.

Colloidal suspensions exhibit different structural ordering namely, fluid, crystal and even glass with necessary conditions, a property similar to that of atomic systems.[12,13] Moreover, larger interparticle length scales (in μm range) and slower dynamics (10^{-6} sec -10^{3} sec) give the colloids an easy experimental access compared to atomic level studies. Hence colloidal suspensions serve as model system to investigate atomic or molecular systems to understand crystal nucleation and structural phase transitions.[14–19] Experiments with colloids are far simpler compared to atomic or molecular level studies. The microscopic size scale of colloids allows them to be easily characterized by microscopy and various light scattering techniques.[20–24] Moreover, the synthesis of monodisperse colloidal particles which is essential for a system to behave as a model system becomes much easier with the advent of appropriate synthetic routes.[25–28] Many of the industrial processes and applications involve shearing of the colloidal suspensions where they undergo deformation. At very low concentrations, the suspension flows like a Newtonian fluid where the viscosity of the suspension is independent of the applied stress.[29] But dense suspension of colloids show shear thickening or thinning property depending upon the sample. As the name indicates, viscosity increases with stress in shear thickening while viscosity decreases with increasing stress in shear thinning fluids. The non-linear mechanical response of many materials when subjected to large deformation or stress, changes from being predominantly elastic to predominantly plastic. It is called yielding.[30] One of the experimental techniques to investigate the non-linear response of soft materials involves subjecting them to oscillatory shear flow in which the shear strain is varied by ramping its amplitude at a constant frequency. Investigation of yielding of colloids by rheology is of significant value for appropriate

formulation of many industrial products containing colloids such as medicines, food items, paints, cosmetics etc. and thereby increasing shelf life and application.

1.3. Hard sphere colloids

Hard sphere colloids like silica, poly(methyl methacrylate), poly(styrene) etc. are the simplest examples of colloidal systems. Conventional hard sphere colloids have a fixed size and cannot be compressed above some extent. Particles in hard sphere system do not interact directly with each other. Hard sphere colloids interact exclusively through excluded volume interaction. The only control parameter to vary phase behavior of hard sphere colloidal suspensions is the volume fraction φ. Temperature-induced size change cannot be used as an experimental parameter in their case. While hard sphere particles has a fixed size and can be altered only by changing the synthesis parameters, the size of soft sphere colloids like microgels can be adjusted by adjusting external parameters like temperature and pH. Soft spheres unlike hard spheres can be compressed to a volume fraction much higher than 1. Star polymers, microgels, surfactants etc. come under the category of soft colloids. Temperature can be used as a controllable parameter to study the phase behaviour of microgels. Temperature acts as a parameter to adjust the concentration without addition of particles to the system. Moreover, adjusting temperature is far more accurate than varying volume fraction. Recently there has been considerable interest in studying the phase behaviour of soft colloids owing to their wide applications in industry and daily life. Two important model soft colloids viz star polymers and microgels are briefly discussed here.

1.4. Multi-arm star polymers

Multi-arm star polymers are very good examples of soft colloidal particles. Because of the presence of arms at the surface, they show polymer/colloid duality. This duality property greatly depends on the length and number of arms of the star. If the functionality (f) of the arms and the length of the arms are sufficiently large, the star polymers have a dense core-brush like morphology. This allows them to behave like colloids with a soft interaction potential. When the functionality is sufficiently small (~1-4), then the polymeric property dominate, whereas at very large or infinite functionality, the behaviour is colloidal in nature. Unlike hard spheres, the brushlike surface of star colloids can interpenetrate, thereby making it possible to attain effective volume fractions very much larger than 1.[31] The interpenetration of the brushes results in

complex dynamics in dense suspension of stars.[32] But since the synthesis of these multi arm star polymers are difficult, microgel dominate the field of model system for soft colloid glasses.[33]

1.5. Microgels as model colloids

A gel, by IUPAC definition, is a non-fluid colloidal network or polymer network that is expanded throughout its whole volume by a fluid.[34] Microgels are soft colloidal particles with crosslinked network of polymer chains. This intramolecular link distinguishes these systems from other polymer systems and offer many striking properties. They exhibit both liquid and solid-like behaviour owing to the crosslinks present among the polymer chains extending throughout the systems and diluted by a specific solvent. The crosslink networks present helps the gel to attain a particular structure. Gels exhibits both fluidity and elasticity and so can be called viscoelastic.[35] With sizes ranging from nanometers to micrometers and with greatly tunable properties, microgels can mimic many biological components and can act as model colloids.[36,37] These model colloids can be used to study phase behavior of atomic or molecular systems. Phase transitions in colloidal suspensions can be studied in real time using optical techniques like light scattering and confocal microscopy and are analogous to phase transitions in liquids.[38–41]

1.5.1. Polymeric microgels

Sub-micron sized hydrogel particles are called microgels, the word being first used in 1949 by W.O. Baker to represent his styrene butadiene.[42] As stated earlier, microgels are soft colloidal particles with crosslinked network of polymer chains. Owing to their many possible applications in templated synthesis of nanoparticles and hybrid microgels,[43–48] water filtration and purification,[49] enhanced oil recovery,[50–52] targeted drug delivery,[53–58] photonic crystal fabrication[59–62] and sensors,[63–66] polymeric microgels have achieved extreme importance in materials science and medical field. All the important applications of microgels make use of the specific property known as stimuli-responsiveness. Polymeric microgels respond to several external stimuli like temperature,[67–70] pH,[71–74] ionic strength,[75,76] some chemicals,[77] solvent quality,[78] electric and magnetic fields,[79–81] light[82] etc. enabling them applicable in medical field and for sensor applications. The stimuli responsive property is the result of the balance between the intramolecular hydrophobic repulsive interactions and hydrophilic attractive forces. The most important of all these stimuli responses is the thermal stimulus. This imparts a property called

lower critical solution temperature (LCST) in the case of a linear polymer and volume phase transition temperature (VPTT) in the case of polymer microgel. The property and mechanism of VPTT is explained in subsequent chapter.

1.5.1.1. Neutral microgels

The microgels can be of neutral or charged depending on the availability of functional groups on the microgel structure. Poly(N-isopropyl acrylamide) simply called PNIPAm, a polymer of N-isopropyl acrylamide is a well-known neutral microgel, which has gained enormous attention since the advent of well-defined and easy synthetic process by Pelton and Chibante in 1986.[26] In general, acrylamides and Poly (vinyl caprolactam) are neural microgels, while there are anionic (Poly(acrylic acid)) and cationic microgels (Poly(dimethyl amino ethyl methacrylate)).

1.5.1.2. Ionic microgels

Incorporation of ionic comonomers like methacrylic acid, acrylic acid, DMAEMA, vinyl pyridine etc. to NIPAm introduces additional stimuli responses like pH and ionic strength. This addition also helps to shift the volume phase transition temperature (VPTT) of the polymer microgel to desired range. We obtain another parameter to play with and adjust to get desired properties. Moreover, electric and magnetic field driven assembly of microgel suspensions are achieved with the addition of ionic comonomers to the otherwise neutral NIPAm.

1.6. Phase behaviour of hard colloids

Hard sphere suspension shows different phase behaviour depending on concentration of particles. As stated earlier, volume fraction is a more decent parameter representing concentration of particles. As concentration is varied hard sphere shows different phases as shown in figure 1.3.

The phase behavior for hard sphere colloids was first observed by Pusey and van Megen[83] and has been confirmed by various experimental and theoretical investigations. At volume fractions less than 0.49, hard sphere suspension flows like an ergodic fluid where the particles can freely diffuse around in the system. At volume fractions between 0.49 and 0.54, the system has a coexistence phase of liquid and crystal. As the number density is increased from 0.54, crystalline phases start forming; mainly FCC or HCP.

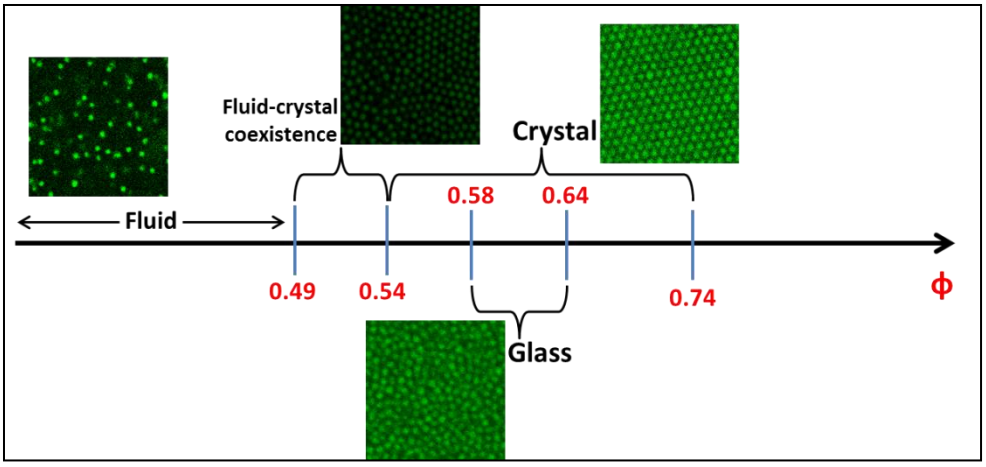

Figure 1.3: Phase diagram for hard-sphere suspension.

Hard sphere colloids attain hexagonal close packing at the maximum volume fraction they can be packed i.e. φ_{hcp}= 0.74. Colloidal glasses can be formed when the suspension with sufficiently high volume fraction (φ>0.58) is quenched. When the system is quenched, suspension stops flow due to sudden increase in viscosity.[84] The microstructure in this case is similar to that of a fluid. The critical volume fraction at which this abrupt change from predominantly fluid to disordered solid occurs is called glass transition volume fraction (φ_g). Glassy state is observed in hard sphere colloids with volume fraction above that of random close packing (φ_{rcp} ~0.64). Above glass transition, suspension becomes viscoelastic with predominantly elastic property.

Crystal formation on annealing occurs in particles with high monodispersity. For the glass transition to occur there must be some amount of polydispersity in the system. Size polydispersity of around 0.8% is required to develop glass transition.[85,86] For highly charged hard sphere colloids the phase boundaries shift to lower values,[87] while the boundaries of the phase diagram shift to higher values for a slightly polydisperse system.[88] The particle diffusive motion is hindered by nearby particles as the concentration increases, eventually a kinetic arrest reaches. That is what is happening during glass transition. Due to the crowding of particles, individual particles are considered to be trapped inside a cage formed by the neighbouring particles. This effect, called the "cage effect" is well explained by Pusey and van Megen in 1986.[83]

The cage effect is shown in figure 1.4. The cage effect was first proposed in 1986 and was extensively used to study dynamics of colloidal systems in last 2 decades.[89–93] At higher packing, due to the topological constraints on a particle by its nearest neighbours, particles

cannot diffuse over longer distances.[94] However, these particles can move within the cages. Two types of relaxation of the particles can occur in cage model viz α-relaxation and β-relaxation. The β-relaxation, where a single particle under consideration moves inside the constraints made by the neighbours, is a faster mode of relaxation and occurs at a characteristic frequency of the system called β-relaxation frequency (ω_β). The α-relaxation, also called the structural relaxation is slower when compared to the β-relaxation. In this case the particle eventually escapes out of the cage by a co-operative motion of the surrounding particles. This occurs at α -relaxation frequency (ω_α). If we take the inverse of the characteristic frequencies, we get the corresponding relaxation times ($t_\alpha=1/\omega_\alpha$& $t_\beta=1/\omega_\beta$).

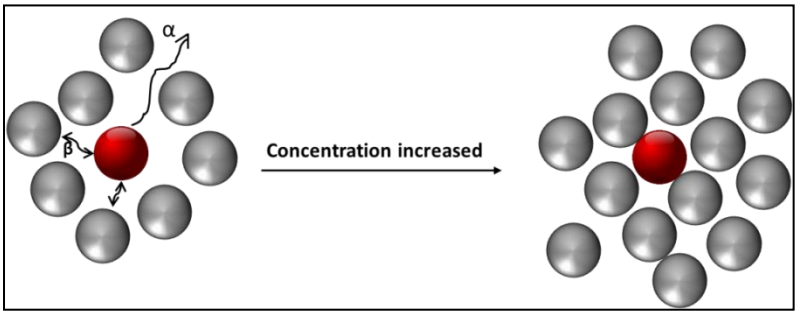

Figure 1.4: Cage effect due to topological constraints on a particle by nearest neighbours.

Short range attractions can be induced on otherwise repulsive hard spheres by adding softness to the system. Short range attractions are induced by depletion interaction. Depletion is achieved by adding nonadsorbing linear polymer fragments to the hard sphere systems, which eventually leads to attraction and aggregation of the hard spheres.[95,96] Recently soft microgels were also used to induce attraction in hard sphere colloids.[97] Recent reviews also show importance of application of induced attractive interaction.[98] The incorporation of attraction drastically changes the phase behaviour of the colloids. The strength of the interaction depends strongly upon the size and amount of polymer fragments added to the system. For hard spheres at high concentration near glass, induced depletion interaction causes another glass transition through a fluid phase. At very short range attraction, glass melts and forms a fluid-crystal coexistence phase. On increasing the attraction further, the system reenters into another glass phase. Thus a glass-to-glass transition through a short-term fluid phase occurs at higher attractive strength. These two non-ergodic phases are called repulsive glass and attractive glass based on the strength of interparticle attractive force.[99]

1.7. Colloidal glasses and gels

As discussed in the previous section, hard sphere forms types of glasses depending upon the strength of the interparticle attraction induced in the system. Based on the findings by Poon et al in 2002, Sciortino et al in 2003 found a phase diagram for hard spheres where hard spheres have repulsive glass and attractive glass phases.[100] Later Zaccarelli and Poon modified the phase diagram by renaming repulsive glass as non-bonded repulsive glass and attractive glass as bonded repulsive glass.[93] In the case of soft spheres, where weak attraction occurs between particles, the phase behaviour is different.

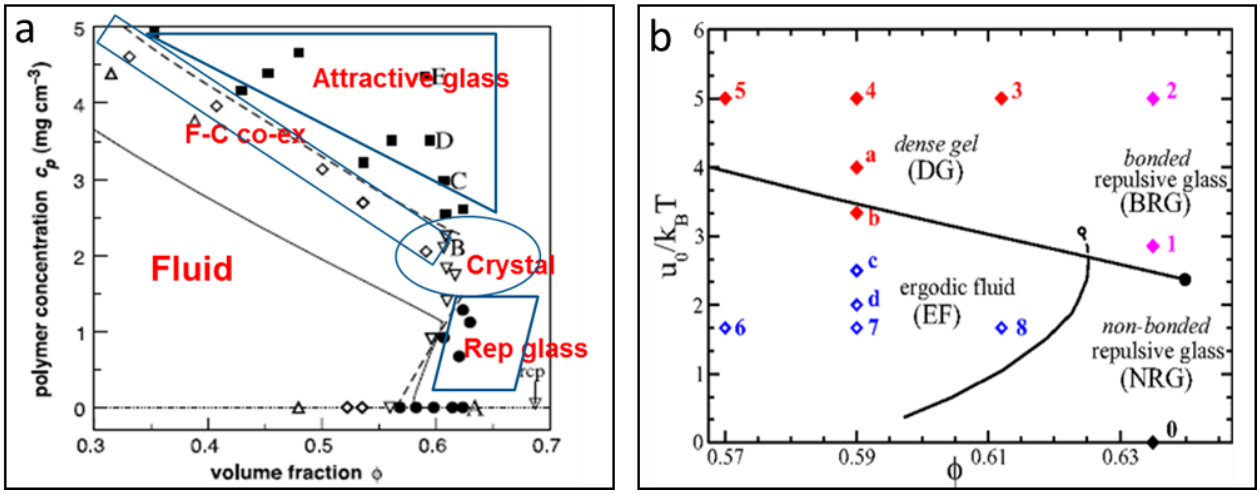

Figure 1.5: (a) Phase diagram of hard spheres with induced short range attraction showing re-entrant glass transition. [Pham *et al*. (2002) (Reprinted with permission-from AAAS©).] (b) Revisited phase diagram of colloidal-polymer mixture (Zaccarelli and Poon, 2009) [Reprinted with permission from Proceedings of National Academy of Sciences©].

Gelation of colloids takes place when the particle concentration is very low but at higher interparticle attractions with short range. This causes the particles to aggregate and form clusters which will percolate through and get kinetically arrested. When compared to colloidal glasses, gels have more open structure. Zacarelli and Poon, in their modified phase diagram, stated the gels formed by very high attractions from the ergodic fluid as “dense gels”. So unlike the old phase diagram by Sciortino et al, the new phase diagram has shown a glass-gel transition also along with a glass-glass transition by the interplay between concentration and interparticle potential.

Kinetic arrest in the colloidal suspensions can be determined by light scattering techniques, microscopy and simulations etc. Visually, a non-flowing colloidal suspension in an inverted tube is a clear indication of kinetic arrest. Autocorrelation function $g_2(\tau)$ obtained from the dynamic light scattering will give us the idea on dynamic arrest. A colloidal suspension at low concentrations with diffusing particles will have a decaying autocorrelation function. As the particle concentration is increased, the diffusion slows down and the decay gets delayed. So the decay curve slowly gets flattened. As the concentration nears glass transition, $g_2(\tau)$ reaches an intermediate plateau before decaying to zero. This plateau shows the double relaxation of microgels in glassy state. Microgels at glass transition have two types of relaxation called α-relaxation and β-relaxation. The intermediate plateau formed shows the onset of β-relaxation of particle from the cage. The long decay to zero after the plateau is the α-relaxation where particles escape from the cage formed by other particles around. If we further increase the concentration of the particles the long time decay will be further delayed that it cannot be observed within experimental timescale. In this case the system will be completely arrested since the decay is not reaching to zero.[101]

The dynamics at glassy state is also observed mechanically by rheological measurements. The storage and loss modulus curves in a range of frequencies at strains in linear regime provide information about the relaxation and arrested states. In the frequency sweep curve, the shallow minimum of the G" curve indicates the β-relaxation frequency (ω_β), characteristic to the system. The α-relaxation is typically out of the range of frequencies accessible experimentally at which the sample "age". Ageing is the phenomenon of decaying of properties of a colloidal glass with time. It is important to study the ageing of material since it is not desirable for a material to age during experiment. Ageing studies are carried out in colloidal materials by flowing the material at very high shear rates well above its yield stress and wait for the material to age until its material property attains a quasi-plateau value.[102] Ageing time can also found by observing temporal mean square displacement (MSD) as a function of waiting time.[103]

1.8. Yielding in dense colloidal suspensions

The deformation and flow study of colloids is a rich area of different aspects since they are viscoelastic in nature. The mechanical properties of these complex fluids lie between that of pure solids and pure liquid. They possess both the properties of solids and liquids. The mechanical properties of many important commercial products which composed of dense

colloidal suspensions are affected by the shear due to induced flow in the microstructure while processing. So it is important to study the structure-property relations in these complex fluids over a range of length and time scales, both under dormant conditions, and under shear. Enormous number of literatures on the rheology of soft and hard sphere glasses reported worldwide shows the relevance of the study.[83,104–109] Dynamic oscillatory shear measurements of complex fluids provide viscoelastic properties of the fluid. Small amplitude oscillatory shear experiments are being conducted to study the linear viscoelastic properties in the dormant conditions while large amplitude oscillatory shear (LAOS) tests provide insights into the microstructural changes in the colloids at very high strains.[110] The rheological properties of hard spheres vary much with that of soft spheres like microgels and star polymers. Soft colloids display much richer rheological properties than hard spheres.

Soft colloids at very low concentrations behave like liquids, where particles are in constant Brownian motion. But at high concentrations, colloids behave like crystals or glasses (colloidal crystals or colloidal glasses). At this high concentration, when they are subjected to shear strain, their response will be elastic at low strains and viscous at higher strains.[111] In colloidal suspensions at high concentration, the motion of particles is restricted by neighbouring particles where local cages are formed. When strain is applied, particles escape out of the system by two relaxations, β-relaxation, representing the fast localized motion of particles inside the cage and α-relaxation, which is slower than the β-relaxation, representing a collective diffusion of particles out of the cage (cage break). When the particle concentration is increased further, the structural relaxation time increases. This relaxation time exceeds the measurable range of time at some stage, where the system is said to be nonergodic.[23] Colloids when subject to strong shear will transform from elastic to plastic. This transformation is called yielding.[30] A colloidal glass yields by a shear induced cage breaking process. Yielding occurs by the cage breaking process on application of oscillatory strains at a constant frequency. In a typical strain sweep experiment, the soft colloids yield at a particular strain value indicated by a crossover of G' and G". It is called critical strain. G' is the in-phase component called "storage" modulus and G″ is the out-of phase component known as the "loss" modulus. If $G' > G''$ then the fluid is predominantly elastic, and if the $G' < G''$ then the response is predominantly viscous. Corresponding stress is called yield stress.

After the critical strain, there will be a monotonic decrease in storage modulus with increasing strain, while loss modulus shows a non-monotonic dependence, with a peak at the crossover of G' and G", marking the yield point. Hard spheres having repulsive interaction show yielding with a single peak in G". But in suspensions with weak attractions, a double yielding phenomenon is observed (i.e. double peak in G"). These weak physical attractions in the system are termed as bonds and are not covalent bonds. The increasing deformation first breaks the bonds that results in the first peak in G" followed by the cage breaking peak at higher strains. Anisotropic particles have also shown a double yielding behavior where attraction is induced by the anisotropy in the surface charge distribution. However, a strongly repulsive or a strongly attractive colloidal system does not show a double yielding.[112] Star polymers, having long hair-like star arms, at high concentrations also show a double peak in G" due to the disentanglement of the interpenetrated star arms, followed by the cage breaking process. In case of star polymers, second peak in loss modulus is observable at higher frequency also.[113] Recently, it was found that the double yielding mechanism was shown by surfactant pastes containing abrasive particles.[114] There is a recent work by Joshi and Tata which investigates the double yielding mechanism in pure PNIPAM microgel system.[115]

1.9. Electric field driven assembly of colloids

Microgels behave similar to atoms and molecules and they can be observed in real space. Manipulating their phase behaviour by external means opens up wide scope for variety of applications. The second part of my thesis consists of the electric field driven assembly of colloidal particles. The structure and interaction between the particles in the presence of an external electric field was investigated in terms of particle concentration. All our electric field studies use micrometer-sized poly(NIPAM-AAc) spherical soft colloids, labeled with a fluorescent dye for confocal microscopy, and suspended in water. The details of the samples and synthesis methods followed can be found in section 2.6 of chapter 2.

The investigation of effect of electromagnetic field on colloidal suspension dates back to early 1940s by W M Winslow and he published his findings in 1949.[116] Applying external electric and magnetic fields on colloids induce some structural changes to the macroscopic properties by directed assembly of the colloidal particles.[16,117,118] This occurs due to the difference in dielectric constant of the particles from that of the solvent, they will acquire an induced dipole moment. Within fraction of seconds, increase in viscosity of the suspension is

observed. This property is said to be fully reversible, as the electric field is switched off. This behaviour is known as the 'electro-rheological effect'.[119,120] The brisk switching from one state to another has given rise to variety of applications in hydraulic valves, clutches,[120] in advanced materials like photonic crystals for displays.[121] There had been many reviews on electrorheological fluids since 1990.[122–125] This field-induced phase behavior in colloids is controlled by interplay between hard-sphere repulsions and dipole–dipole interaction, which in turn can be tuned by the electric field strength.[80] Crystal to crystal transitions and complex phases are possible by the inclusion of forces like electrostatic repulsion supplementary to hard-sphere potential and dipolar interaction.

Hard spheres were the subject of electric field-driven assembly. Many works have been published on the field-driven assembly of hard spheres like silica gel, PMMA etc.[126–128] Only recently, soft spheres were introduced in to this field of research. As stated earlier, cross-linked microgels of poly(N-isopropylacrylamide) have been used as excellent model systems for soft colloids. They can be packed into high volume fractions well above 1 and hence they exhibit different phase behaviour to hard spheres.

Ionic microgels having a very soft repulsive interaction would be a good candidate for electric field self-assembly studies. Their interaction potential ranges from Yukawa type interaction to very soft-repulsive ones when the interparticle distance decreases. Because of the soft potential, these microgels can be packed to very high effective volume fractions.[79] Introducing charge on PNIPAm allows one to play with external stimuli like pH, ionic strength, electric and magnetic field etc. Moreover, ionic charge in the system makes the soft colloid softer, enriching the phase behaviour with many crystalline states.[13,129] Phase behaviour of ionic microgels can be tuned by use of external electric field. External electric fields are straightforward, efficient and powerful way to maneuver and assemble colloidal particles. Many reports have come where people use AC electric field to assemble highly monodisperse particles into well-defined arrays which can be tuned by the field strength and position.[79,130–132] The electric field studies on charged colloids are fairly a new idea which gained attention recently. Some recent works on single type of particles system proved the existence of different structures influenced by the field.[80] Field studies on binary mixture of colloidal particles of different sizes, different structures or opposite charges also provide insights into the microstructural property changes of the systems with external effects. The interpretations from the field effect studies on

the binary systems may be helpful in designing and producing multifunctional materials, where one can make use of the directional assembly properties of the particles. Some recent works on binary colloidal mixtures provide different perspectives like formation of strings of binary particles,[133] self-healing colloidal crystal formation,[134] core-shell formation with oppositely charged microgels,[135] heteroaggregation of particles[136] etc. Theoretical studies have also been carried out and come up with exciting results making use of Monte Carlo simulations.[137–140]

1.10. Application of soft colloids in targeted drug delivery

1.10.1. Drug delivery

Drug delivery is the process of introduction of drug or a pharmaceutical compound in to the body of a patient for the treatment of a disease. There are different routes to introduce drug into the body viz oral, transdermal, parenteral, inhalation etc. Oral drug delivery is the oldest route of conventional drug delivery. Because of the ease of administration and comfort, this is highly preferred one. Transdermal drug delivery is done through body surfaces like skin. This type of delivery is fast because the drug is transferred directly to the blood stream rather than gastrointestinal metabolism. Parenteral route of drug delivery is another means of introducing drug to the body through routes like intra-arterial, intramuscular, intravenous and subcutaneous route rather than oral. When the drug is introduced by inhalation route, it will directly reach the lungs. This will avoid systemic effect i.e., increase the bioavailability of the drug in the system and is preferred one for treating respiratory diseases.

1.10.2. Targeted drug delivery

Conventional delivery systems have the limitations as high dose in one go, delivery in unwanted areas of the body etc. Intelligent targeted drug delivery systems and controlled release using smart microgel particles eliminates these limitations to some extent. Many advantages of microgels like size tunability (from nanometers to microns), easy incorporation of drugs inside, swelling and deswelling in response to several stimuli etc. made them attractive drug delivery carriers.[141]

1.10.3. Microgels in drug delivery

The quality of life of patients depends greatly on the amount and efficiency of drug administered by reducing the frequency of administration and increasing the efficiency of the drug. The drug delivery technology has emerged a lot with the advent of new biomaterials. Smart

polymeric materials offer extreme possibilities to control the delivery and dosage of drugs to particular area of the body. Smart materials are materials that respond to external stimuli like temperature, pH, ionic strength, electric and magnetic fields, and metabolites like glucose. Swelling controlled release systems like polymeric microgels come under these "smart" materials whose structure can be tuned to respond to some environmental conditions, such as temperature, pH or ionic strength.[142–144] There are potential limitations to this application such as accumulation in the body, problem with prolongation of delivery etc. Still, as a proof-of-concept, many researchers are using polymeric microgels of N-Isopropyl acrylamide as a drug delivery vehicle.[56,145–148] The ability to absorb water and to swell multifold allow PNIPAm microgels to absorb and store small molecules and ions with water. This property along with their nanometer size range makes these microgels ideal for drug delivery applications. Absorbed water molecules along with the other molecules will be released at a particular temperature (~32°C) which is called volume phase transition temperature (VPTT) and subsequent shrinkage of microgel particle occurs. Since the VPTT can be tuned to human physiological temperature, PNIPAm microgel can conveniently be used as drug delivery vehicle. VPTT can be tuned by addition of comonomers to the system which is explained in section 2.5.2 of chapter 2. Addition of carboxylic acid comonomers provides additional stimuli responses to pH, ionic strength etc. Interaction between the microgel particles and the drug molecules can also be tuned by appropriate selection of monomers. Since 90% of the microgel is water, it produces very low inflammatory response when used in human body. The hydrophilic nature of the microgel can pose some problems in delivering hydrophobic drugs in to the system. So PNIPAm microgels can be used to deliver hydrophilic drugs allowing free release of drugs along with the release of water at VPTT. Due to the heterogeneous morphology of PNIPAm with a highly crosslinked core and loosely bound brush-like surface, there are limitations for the drugs to get loaded into the particle. With a homogeneously crosslinked structure, more drugs can be incorporated into the microgel and subsequently more drugs will be delivered to the target. A comparison of drug release from two different types of microgel morphologies i.e. core-brush type made by conventional synthesis method and homogeneous type made by two-step synthesis method.

1.11. Objectives of the work

- **Synthesis of microgels:** Synthesizing monodisperse microgel particles of N-Isopropylacrylamide (NIPAm) and copolymer microgels of NIPAm and acrylic acid (AAc) of different required sizes for the experimental studies. Particles with different sizes ranging from 150 nm to 1.3 μm are synthesized by employing changes in amount of reactants and reaction conditions to achieve different sizes and morphologies.
- **Basic characterizations:** Determination particle size by light scattering. Conducting static light scattering (SLS) on dilute samples to find radius of gyration and dynamic light scattering (DLS) to fine hydrodynamic radius, volume phase transition temperature (VPTT) and swelling ratio. Effective volume fraction of particles is found by using capillary viscometry.
- **Structure and dynamics of microgels with crosslinking density effects:** Influence of particle morphology and crosslinking density on the yielding dynamics of the microgels by large amplitude oscillatory shear (LAOS) rheology. Small amplitude oscillatory shear characterizations are intended.
- **Electric field driven assembly of binary colloidal mixture:** Confocal microscopy is used to investigate the dynamics of fluorescently labelled ionic microgels of NIPAm and AAc. Experiments are designed in such a way to conduct at low concentrations and at high concentrations when particles interact. Mixture of two distinct sized PNIPAm-AAc particles in different ratios is being investigated. The microgels were distinguished by using different fluorescent dyes for different samples.
- **Application of PNIPAm microgels in targeted drug delivery:** A comparison of drug release ability of PNIPAm microgels with two different morphologies viz core-shell and homogeneous. A hydrophilic and a hydrophobic drug were selected for the study.

1.12. Organisation of thesis chapters

My thesis is divided into 6 chapters

1. **First** chapter sets the motivation and objectives of the study. This chapter also contains a literature survey and introductory remarks on colloids, colloidal interactions, glass transition, model for colloidal glasses, yielding in colloidal glasses, electric field driven assembly of colloids, drug release studies on model soft microgels etc.
2. **Second** chapter provides the details of the synthesis of homo and copolymer microgels of NIPAm. Some of the preliminary characterizations of microgels using light scattering technique are also provided in this chapter. All the experimental techniques and the methods used in this work to investigate the structure and properties of microgels are explained in this chapter.
3. **Third** chapter includes the rheological characterization of the microgels. The property changes with morphology are thoroughly studied here. Large amplitude oscillatory shear experiments were conducted on the samples to elucidate the microstructural changes in the microgel. This chapter also investigates the effect of crosslinker content on the dynamic properties of the microgels.
4. Electric field driven assembly of negatively charged copolymer microgels of NIPAm and acrylic acid at different concentration regimes were investigated in the **fourth** chapter. The behaviour of a binary mixture of two different sized particles towards applied electric field is also under investigation.
5. **Fifth** chapter deals with the comparison of drug release from PNIPAm microgels of two different particle morphologies.
6. Conclusion and future perspective: In the **sixth** chapter, a summary of the important conclusive points from each chapter is given. The chapter ends with some recommendations for future investigations in the field of study.

1.13. References

1 R. Brown, *Ray Soc. by R. Hardwicke, London*, 1985, **1**, 358–371.

2 A. Einstein, *Ann. Phys.*, 1905, **322**, 549–560.

3 W. Sutherland, *Philos. Mag. Ser. 6*, 1905, **9**, 781–785.

4 M. von Smoluchowski, *Ann. Phys.*, 1906, **326**, 756–780.

5 B. Derjaguin and L. Landau, *Acta Physicochim. URSS*, 1941, **14**, 633–662.

6 E. J. W. Verwey and Overbeek, *J. Phys. Chem.*, 1946, **1**, 631–636.

7 D. Grasso, K. Subramaniam, M. Butkus, K. Strevett and J. Bergendahl, *Rev. Environ. Sci. Biotechnol.*, 2002, **1**, 17–38.

8 P. C. Hiemenz and R. Rajagopalan, *Principles of Colloid and Surface Chemistry*, Marcel Dekker Inc.,New York, 1997.

9 R. A. L. Jones, *Soft Condensed Matter*, Oxford University Press, 2003.

10 D. F. Evans and H. Wennerström, *The colloidal domain: Where physics, chemistry, biology, and technology meet*, Wiley-VCH, 1999, vol. 1.

11 J. N. Israelachvili, *Intermolecular and Surface Forces: Intermolecular and Surface Forces*, Academic Press, 2011.

12 B. V. R. Tata and S. S. Jena, *Solid State Commun.*, 2006, **139**, 562–580.

13 P. S. Mohanty and W. Richtering, *J. Phys. Chem. B*, 2008, **112**, 14692–14697.

14 K.-Q. Zhang and X. Y. Liu, *Nature*, 2004, **429**, 739–743.

15 U. Gasser, E. R. Weeks, A. Schofield, P. N. Pusey and D. A. Weitz, *Science (80-.).*, 2001, **292**, 258–262.

16 A. Yethiraj and A. Van Blaaderen, *Nature*, 2003, **421**, 513–517.

17 T. Palberg, *J. Phys. Condens. Matter*, 1999, 11, R323–R360.

18 P. Schall, I. Cohen, D. A. Weitz and F. Spaepen, *Nature*, 2006, **440**, 319–323.

19 P. Schall, D. A. Weitz and F. Spaepen, *Science (80-.).*, 2007, **318**, 1895–1899.

20 M. H. Chestnut, *Curr. Opin. Colloid Interface Sci.*, 1997, **2**, 158–161.

21 V. Prasad, D. Semwogerere and E. R. Weeks, *J. Phys. Condens. Matter*, 2007, **19**, 1–25.

22 A. D. Dinsmore, E. R. Weeks, V. Prasad, A. C. Levitt and D. A. Weitz, *Appl. Opt.*, 2001, **40**, 4152.

23 W. Van Megen and P. N. Pusey, *Phys. Rev. A*, 1991, **43**, 5429–5441.

24 W. Van Megen and S. M. Underwood, *Phys. Rev. E*, 1994, **49**, 4206–4220.

25 A. van Blaaderen and A. Vrij, *Langmuir*, 1992, **8**, 2921–2931.
26 R. H. Pelton and P. Chibante, *Colloids and Surfaces*, 1986, **20**, 247–256.
27 G. Bosma, C. Pathmamanoharan, E. H. A. De Hoog, W. K. Kegel, A. Van Blaaderen and H. N. W. Lekkerkerker, *J. Colloid Interface Sci.*, 2002, **245**, 292–300.
28 A. I. Campbell and P. Bartlett, *J. Colloid Interface Sci.*, 2002, **256**, 325–330.
29 N. J. Wagner and J. F. Brady, *Phys. Today*, 2009, **62**, 27–32.
30 F. Chambon, Z. S. Petrovic, W. J. MacKnight and H. H. Winter, *Macromolecules*, 1986, **19**, 2146–2149.
31 D. Vlassopoulos, *J. Polym. Sci. Part B Polym. Phys.*, 2004, 42, 2931–2941.
32 M. Kapnistos, A. N. Semenov, D. Vlassopoulos and J. Roovers, *J. Chem. Phys.*, 1999, **111**, 1753–1759.
33 J. Roovers, L. L. Zhou, P. M. Toporowski, M. van der Zwan, H. Iatrou and N. Hadjichristidis, *Macromolecules*, 1993, **26**, 4324–4331.
34 R. G. Jones, J. Kahovec, R. Stepto, E. S. Wilks, M. Hess, T. Kitayama and W. V. Metanomski, in *Compendium of Polymer Terminology and Nomenclature*, eds. R. G. Jones, J. Kahovec, R. Stepto, E. S. Wilks, M. Hess, T. Kitayama and W. V. Metanomski, Royal Society of Chemistry, Cambridge, 2009, pp. 211–236.
35 H. B. Bohidar, *Curr. Sci.*, 2001, **80**, 1008–1017.
36 B. Saunders, *Adv. Colloid Interface Sci.*, 1999, **80**, 1–25.
37 L. A. Lyon and A. Fernandez-Nieves, *Annu. Rev. Phys. Chem.*, 2012, **63**, 25–43.
38 P. A. Hiltner and I. M. Krieger, *J. Phys. Chem.*, 1969, **73**, 2386–2389.
39 P. A. Hiltner, Y. S. Papir and I. M. Krieger, *J. Phys. Chem.*, 1971, **75**, 1881–1886.
40 D. J. W. Aastuen, N. A. Clark, L. K. Cotter and B. J. Ackerson, *Phys. Rev. Lett.*, 1986, **57**, 1733–1736.
41 E. B. Sirota, H. D. Ou-Yang, S. K. Sinha, P. M. Chaikin, J. D. Axe and Y. Fujii, *Phys. Rev. Lett.*, 1989, **62**, 1524–1527.
42 W. O. Baker, *Rubber Chem. Technol.*, 1949, **22**, 935–955.
43 J. Zhang, S. Xu and E. Kumacheva, *J. Am. Chem. Soc.*, 2004, **126**, 7908–7914.
44 D. Suzuki and H. Kawaguchi, *Langmuir*, 2005, **21**, 8175–8179.
45 Y. Lu, Y. Mei, M. Drechsler and M. Ballauff, *Angew. Chemie - Int. Ed.*, 2006, **45**, 813–816.

46 N. Singh and L. A. Lyon, *Chem. Mater.*, 2007, **19**, 719–726.

47 R. Contreras-Cáceres, A. Sánchez-Iglesias, M. Karg, I. Pastoriza-Santos, J. Pérez-Juste, J. Pacifico, T. Hellweg, A. Fernández-Barbero and L. M. Liz-Marzán, *Adv. Mater.*, 2008, **20**, 1666–1670.

48 M. Karg and T. Hellweg, *Curr. Opin. Colloid Interface Sci.*, 2009, **14**, 438–450.

49 P. Nilsson and P. Hansson, *J. Phys. Chem. B*, 2005, **109**, 23843–23856.

50 H. Yu, Y. Wang, W. Ji, J. Zhang, P. Zhang, K. Li and S. Wang, *Pet. Sci. Technol.*, 2011, **29**, 715–727.

51 R. K. Prudhomme, J. T. Uhl, J. P. Poinsatte and F. Halverson, *Soc. Pet. Eng. J.*, 1983, **23**, 804–808.

52 S. M. Vargas-Vasquez and L. B. Romero-Zerón, *Pet. Sci. Technol.*, 2008, 26, 481–498.

53 A. S. Hoffman, *J. Control. Release*, 1987, **6**, 297–305.

54 L. E. Bromberg and E. S. Ron, *Adv. Drug Deliv. Rev.*, 1998, **31**, 197–221.

55 J. Gu, F. Xia, Y. Wu, X. Qu, Z. Yang and L. Jiang, *J. Control. Release*, 2007, **117**, 396–402.

56 T. R. Hoare and D. S. Kohane, *Polymer (Guildf).*, 2008, 49, 1993–2007.

57 S. Vinogradov, *Curr. Pharm. Des.*, 2006, **12**, 4703–4712.

58 S. Nayak, H. Lee, J. Chmielewski and L. A. Lyon, *J. Am. Chem. Soc.*, 2004, **126**, 10258–10259.

59 M. Zhou, F. Xing, M. Ren, Y. Feng, Y. Zhao, H. Qiu, X. Wang, C. Gao, F. Sun, Y. He, Z. Ma, P. Wen and J. Gao, *ChemPhysChem*, 2009, **10**, 523–526.

60 S. Xu, J. Zhang, C. Paquet, Y. Lin and E. Kumacheva, *Adv. Funct. Mater.*, 2003, **13**, 468–472.

61 L. A. Lyon, J. D. Debord, S. B. Debord, C. D. Jones, J. G. McGrath and M. J. Serpe, *J. Phys. Chem. B*, 2004, **108**, 19099–19108.

62 X. Li, J. Weng, Y. Guan and Y. Zhang, *Langmuir*, 2016, **32**, 3977–3982.

63 T. Hoare and R. Pelton, *Macromolecules*, 2007, **40**, 670–678.

64 V. Lapeyre, I. Gosse, S. Chevreux and V. Ravaine, *Biomacromolecules*, 2006, **7**, 3356–3363.

65 G. E. Morris, B. Vincent and M. J. Snowden, *Prog. Colloid Polym. Sci.*, 1997, **105**, 16–22.

66 G. Bazin and X. X. Zhu, *Prog. Polym. Sci.*, 2013, 38, 406–419.

67 Y. Hirokawa and T. Tanaka, *J. Chem. Phys.*, 1984, **81**, 6379–6380.

68 R. H. Peltor, H. M. Pelton, A. Morphesis and R. L. Rowell, *Langmuir*, 1989, **5**, 816–818.

69 Y. H. Bae, T. Okano and S. W. Kim, *J. Polym. Sci. Part B Polym. Phys.*, 1990, **28**, 923–936.

70 T. Hoare and R. Pelton, *Macromolecules*, 2004, **37**, 2544–2550.

71 M. J. Snowden, B. Z. Chowdhry, B. Vincent and G. E. Morris, *J. Chem. Soc. - Faraday Trans.*, 1996, **92**, 5013–5016.

72 L. Brannon-Peppas and N. A. Peppas, *Chem. Eng. Sci.*, 1991, **46**, 715–722.

73 G. Chen and A. S. Hoffman, *Nature*, 1995, **373**, 49–52.

74 Y. L. Guan, L. Shao, J. Liu and K. D. Yao, *J. Appl. Polym. Sci.*, 1996, **62**, 1253–1258.

75 S. Neyret and B. Vincent, *Polymer (Guildf).*, 1997, **38**, 6129–6134.

76 M. Shibayama, F. Ikkai, S. Inamoto, S. Nomura and C. C. Han, *J. Chem. Phys.*, 1996, **105**, 4358–4366.

77 J. H. Holtz and S. A. Asher, *Nature*, 1997, **389**, 829–832.

78 C. Shi, X. Chen, L. Chen, M. Chen and R. Jiang, *J. Appl. Polym. Sci.*, 2013, **128**, 3034–3042.

79 P. S. Mohanty, A. Yethiraj and P. Schurtenberger, *Soft Matter*, 2012, **8**, 10819.

80 S. Nöjd, P. S. Mohanty, P. Bagheri, A. Yethiraj and P. Schurtenberger, *Soft Matter*, 2013, **9**, 9199.

81 P. S. Mohanty, D. Paloli, J. J. Crassous, E. Zaccarelli and P. Schurtenberger, *J. Chem. Phys.*, 2014, **140**, 094901.

82 K. Fan, M. Bradley and B. Vincent, *J. Colloid Interface Sci.*, 2012, **368**, 287–291.

83 P. N. Pusey and W. Van Megen, *Nature*, 1986, **320**, 340–342.

84 S. P. Meeker, W. C. K. Poon and P. N. Pusey, *Phys. Rev. E - Stat. Physics, Plasmas, Fluids, Relat. Interdiscip. Top.*, 1997, **55**, 5718–5722.

85 S. Auer and D. Frenkel, *Nature*, 2001, **413**, 711–713.

86 E. Zaccarelli, C. Valeriani, E. Sanz, W. C. K. Poon, M. E. Cates and P. N. Pusey, *Phys. Rev. Lett.*, 2009, **103**, 135704.

87 A. P. Hynninen and M. Dijkstra, *Phys. Rev. E - Stat. Physics, Plasmas, Fluids, Relat. Interdiscip. Top.*, 2003, **68**, 8.

88 M. Fasolo and P. Sollich, *Phys. Rev. Lett.*, 2003, **91**, 068301.

89 Y. M. Joshi, *J. Chem. Phys.*, 2007, **127**, 081102.

90 E. Di Cola, A. Moussad, M. Sztucki, T. Narayanan and E. Zaccarelli, *J. Chem. Phys.*, 2009, **131**, 144903.

91 J. M. Brader, M. Siebenbürger, M. Ballauff, K. Reinheimer, M. Wilhelm, S. J. Frey, F. Weysser and M. Fuchs, *Phys. Rev. E - Stat. Nonlinear, Soft Matter Phys.*, 2010, **82**, 1–20.

92 E. R. Weeks and D. A. Weitz, *Phys. Rev. Lett.*, 2002, **89**, 095704.

93 E. Zaccarelli and W. C. K. Poon, *Proc. Natl. Acad. Sci.*, 2009, **106**, 15203–15208.

94 J. C. Conrad, P. P. Dhillon, E. R. Weeks, D. R. Reichman and D. A. Weitz, *Phys. Rev. Lett.*, 2006, **97**, 265701.

95 T. Eckert and E. Bartsch, *Phys. Rev. Lett.*, 2002, **89**, 125701.

96 S. Yang, D. Yan, H. Tan and A. C. Shi, *Phys. Rev. E - Stat. Nonlinear, Soft Matter Phys.*, 2006, **74**, 041808.

97 J. Luo, G. Yuan, C. Zhao, C. C. Han, J. Chen and Y. Liu, *Soft Matter*, 2015, **11**, 2494–2503.

98 R. Tuinier, T. H. Fan and T. Taniguchi, *Curr. Opin. Colloid Interface Sci.*, 2015, **20**, 66–70.

99 K. N. Pham, A. M. Puertas, J. Bergenholtz, S. U. Egelhaaf, A. Moussaid, P. N. Pusey, A. B. Schofield, M. E. Cates, M. Fuchs and W. C. K. Poon, *Science (80-.).*, 2002, **296**, 104–106.

100 F. Sciortino, P. Tartaglia and E. Zaccarelli, *Phys. Rev. Lett.*, 2003, **91**, 268301.

101 W. Hartl, *Curr. Opin. Colloid Interface Sci.*, 2001, **6**, 479–483.

102 B. M. Erwin, D. Vlassopoulos and M. Cloitre, *J. Rheol. (N. Y. N. Y).*, 2010, **54**, 915–939.

103 R. E. Courtland and E. R. Weeks, *J. Phys. Condens. Matter*, 2003, **15**, S359–S365.

104 H. Senff and W. Richtering, *J. Chem. Phys.*, 1999, **111**, 1705–1711.

105 G. Petekidis, D. Vlassopoulos and P. N. Pusey, *J. Phys. Condens. Matter*, 2004, **16**, 287–302.

106 K. N. Pham, G. Petekidis, D. Vlassopoulos, S. U. Egelhaaf, P. N. Pusey and W. C. K. Poon, *Europhys. Lett.*, 2006, **75**, 624–630.

107 K. N. Pham, G. Petekidis, D. Vlassopoulos, S. U. Egelhaaf, W. C. K. Poon and P. N. Pusey, *J. Rheol. (N. Y. N. Y).*, 2008, **52**, 649–676.

108 G. Petekidis, D. Vlassopoulos and P. N. Pusey, *Faraday Discuss.*, 2003, **123**, 287–302.

109 P. N. Pusey and W. Van Megen, *Phys. Rev. Lett.*, 1987, **59**, 2083–2086.

110 J. Mewis and N. J. Wagner, *Colloidal suspension rheology*, Cambridge University Press, Cambridge, 2011, vol. 9780521515.

111 W. B. Russel, D. A. Saville and W. R. Schowalter, *Colloidal dispersions*, Cambridge University Press, Cambridge, UK, 1989, vol. 1.

112 R. C. Kramb and C. F. Zukoski, *J. Phys. Condens. Matter*, , DOI:10.1088/0953-8984/23/3/035102.

113 M. E. Helgeson, N. J. Wagner and D. Vlassopoulos, *J. Rheol. (N. Y. N. Y).*, 2007, **51**, 297–316.

114 A. Shukla, S. Arnipally, M. Dagaonkar and Y. M. Joshi, *Rheol. Acta*, 2015, **54**, 353–364.

115 R. G. Joshi and B. V. R. Tata, *Colloid Polym. Sci.*, 2017, **295**, 1671–1683.

116 W. M. Winslow, *J. Appl. Phys.*, 1949, **20**, 1137–1140.

117 T. C. Halsey and W. Toor, *Phys. Rev. Lett.*, 1990, **65**, 2820–2823.

118 M. E. Leunissen, H. R. Vutukuri and A. Van Blaaderen, *Adv. Mater.*, 2009, **21**, 3116–3120.

119 A. P. Gast and C. F. Zukoski, *Adv. Colloid Interface Sci.*, 1989, 30, 153–202.

120 M. Parthasarathy and D. J. Klingenberg, *Mater. Sci. Eng. R Reports*, 1996, 17, 57–103.

121 W. Wen, C. Weisbuch, D. M. Phuong, G. Lu, W. Ge, C. T. Chan and P. Sheng, *Nanotechnology*, 2005, **16**, 598–601.

122 T. C. Halsey, *Science (80-.).*, 1992, **258**, 761–766.

123 C. F. Zukoski, *Annu. Rev. Mater. Sci.*, 1993, **23**, 45–78.

124 W. Wen, X. Huang and P. Sheng, *Soft Matter*, 2008, **4**, 200.

125 P. Sheng and W. Wen, *Annu. Rev. Fluid Mech.*, 2012, **44**, 143–174.

126 A. Van Blaaderen, *MRS Bull.*, 2004, **29**, 85–90.

127 M. E. Leunissen, C. G. Christova, A.-P. Hynninen, C. P. Royall, A. I. Campbell, A. Imhof, M. Dijkstra, R. van Roij and A. van Blaaderen, *Nature*, 2005, **437**, 235–240.

128 A. van Blaaderen, M. Dijkstra, R. van Roij, A. Imhof, M. Kamp, B. W. Kwaadgras, T. Vissers and B. Liu, *Eur. Phys. J. Spec. Top.*, 2013, **222**, 2895–2909.

129 D. Gottwald, C. N. Likos, G. Kahl and H. Löwen, *J. Chem. Phys.*, 2005, **122**, 1–11.

130 J. Dobnikar, A. Snezhko and A. Yethiraj, *Soft Matter*, 2013, **9**, 3693.

131 H. Löwen, *Eur. Phys. J. Spec. Top.*, 2013, **222**, 2727–2737.

132 D. Gottwald, C. N. Likos, G. Kahl and H. Löwen, *Phys. Rev. Lett.*, 2004, **92**, 068301.

133 D. R. E. Snoswell, T. J. Rogers, A. M. Howe and B. Vincent, *Langmuir*, 2005, **21**, 11439–11445.

134 A. S. J. Iyer and L. A. Lyon, *Angew. Chemie - Int. Ed.*, 2009, **48**, 4562–4566.

135 Y. Hou, J. Ye, X. Wei and G. Zhang, *J. Phys. Chem. B*, 2009, **113**, 7457–7461.

136 R. J. Hall, V. T. Pinkrah, B. Z. Chowdhry and M. J. Snowden, *Colloids Surfaces A Physicochem. Eng. Asp.*, 2004, **233**, 25–38.

137 F. Smallenburg, H. R. Vutukuri, A. Imhof, A. Van Blaaderen and M. Dijkstra, *J. Phys. Condens. Matter*, 2012, **24**, 464113.

138 B. Bharti and O. D. Velev, *Zeitschrift für Phys. Chemie*, 2015, **229**, 1075–1088.

139 B. Bharti, F. Kogler, C. K. Hall, S. H. L. Klapp and O. D. Velev, *Soft Matter*, 2016, **12**, 7747–7758.

140 J. Zhou and F. Schmid, *Eur. Phys. J. Spec. Top.*, 2013, **222**, 2911–2922.

141 C. Ramkissoon-Ganorkar, F. Liu, M. Baudyš and S. W. Kim, *J. Control. Release*, 1999, **59**, 287–298.

142 D. Chakraborty, *Front. Biosci.*, 2013, **18**, 1030.

143 K. S. Soppimath, A. R. Kulkarni and T. M. Aminabhavi, *J. Control. Release*, 2001, **75**, 331–45.

144 D. J. Bharali, S. K. Sahoo, S. Mozumdar and A. Maitra, *J. Colloid Interface Sci.*, 2003, **258**, 415–423.

145 N. Murthy, M. Xu, S. Schuck, J. Kunisawa, N. Shastri and J. M. J. Fréchet, *Proc. Natl. Acad. Sci. U. S. A.*, 2003, **100**, 4995–5000.

146 V. C. Lopez, J. Hadgraft and M. J. Snowden, *Int. J. Pharm.*, 2005, **292**, 137–147.

147 W. Xiong, W. Wang, Y. Wang, Y. Zhao, H. Chen, H. Xu and X. Yang, *Colloids Surfaces B Biointerfaces*, 2011, **84**, 447–453.

148 K. Madhusudana Rao, B. Mallikarjuna, K. S. V Krishna Rao, S. Siraj, K. Chowdoji Rao and M. C. S. Subha, *Colloids Surf. B. Biointerfaces*, 2013, **102**, 891–7.

CHAPTER 2

MATERIAL SYNTHESIS AND CHARACTERIZATION TOOLS

A detailed synthesis procedure of PNIPAm microgels used for all the experiments in my work is provided in this chapter. This also gives background information on the all the experimental procedures and methods that are relevant to the results presented in the following chapters. This chapter begins with a brief background on the structure and phase transition property of PNIPAm microgels and continues with the synthesis procedure of all microgels used for the studies in this thesis. The last part of the chapter describes various characterisation techniques such as Static Light Scattering (SLS), Dynamics light scattering (DLS), Confocal Laser Scanning Microscopy (CLSM), Linear and Non-Linear Rheology and other important techniques.

2.1. Introduction

Synthesis of PNIPAm microgels can be done by free radical polymerization mechanism and emulsion polymerization technique which gives gels of different desired sizes. The synthesis procedure was well-structured by Robert Pelton and his student Chibante in 1986.[1] The synthesis procedure for small particles typically less than 500 nm size involves the presence of an initiator, a crosslinker and a surfactant. The procedure is often referred to as precipitation polymerization because the reaction is performed above the volume phase transition temperature (VPTT) of the microgel. In our work, we also use surfactant-free emulsion polymerization (SFRP) for synthesizing bigger particles of micron (μm) sizes which is done without the presence of a surfactant. Different properties of the microgels like size, softness, swelling property, morphology and optical properties can be tuned by the adjusting synthesis conditions and the composition of the reactants.

The amount of surfactant decides the size of the microgel. Surfactant stabilises the precursor particle during the synthesis and lowers the diameter of the primary particles leading to an increase in the number of particles. In some previous work,[2] it was shown that for surfactant sodium dodecyl sulfate (SDS) concentration in the range of 0.2 to 4 mM, the relation between the hydrodynamic diameter of microgel and the SDS molarity is given by a relation:

$$\boldsymbol{D \propto [SDS]^{-0.71}} \qquad 2.1$$

Suspensions of microgels containing smaller particles of size below 200 nm would be transparent while large sized particles of around 1 μm appear to be turbid. Thus the optical density depends much upon the size of the particles in the system and also the refractive index

difference between the particles and the solvent. Crosslinker also plays a pivotal role in deciding the optical property. Compared to a lower cross-linked microgel, a highly cross-linked microgel will have greater refractive index contrast with the solvent. It was found that the crosslinker N,N'-Methylene bis acrylamide (BIS) used in the synthesis reacts faster than the monomer NIPAm leading to the formation of spherical particles of hard core having more BIS content and brush-like surface of long PNIPAm chains.[2] The amount of crosslinker, its density and distribution over the particle radius have a profound effect on the properties of microgels, such as swelling, optical properties, and their interaction with functional molecules like DNA, enzymes etc. and in the morphology of the microgel and interparticle pair potential at high concentrations.[3] Recently, Roberta Acciaro et al found out a new synthetic strategy through which it can form particles with the cross-linking density homogenous over the particle radius. They could prove that even the larger sized microgel suspension with homogeneous crosslink density would appear transparent.[4] The crosslinker content determines the softness and swelling capability also.[5] Amount of initiator also decides the size and swelling behaviour of particles formed in the system.[6] Thus the control over the reaction temperature and reactants can provide desired size and morphology of the microgel. Controlling the microstructure of the microgel was important in this work since it plays a pivotal role in the dynamics of dense suspensions. This was mainly achieved by changing the amount of crosslinker, surfactant and temperature of the reaction.

In this work, different characterization techniques were used for deducing different properties of the microgels. The size of the microgel was characterized by Static Light Scattering (SLS) and Dynamic Light Scattering (DLS). The dynamic properties and yielding behaviour of dense microgel suspension with respect to different crosslinker ratio was studied by rheology. UV- Visible spectroscopy was used to determine the absorption of drug loaded microgels. This chapter gives the properties of poly (N-isopropyl acrylamide) microgel and a detailed description of the synthesis of all microgels used in the work. Subsequent sections in this chapter describe all the characterization techniques and the testing protocols on the samples.

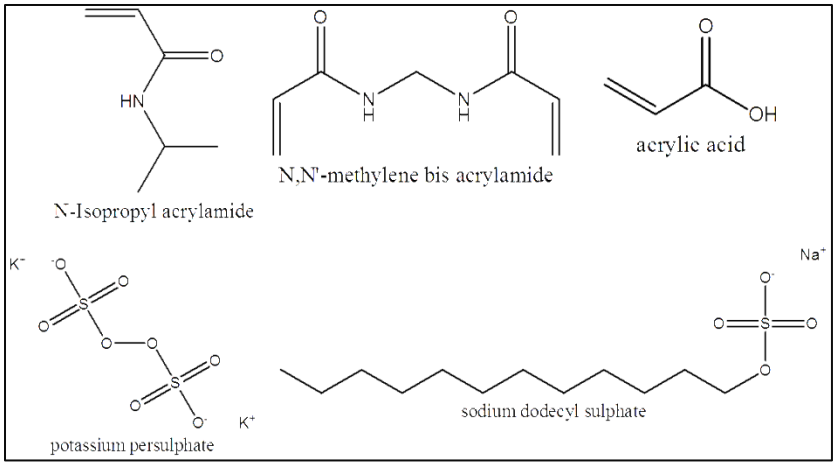

Figure 2.1: Structure of NIPAm (monomer), acrylic acid (comonomer), BIS (crosslinker), KPS (free radical initiator) and SDS (surfactant) used for the synthesis of microgel.

2.2. Poly(N-Isopropyl acrylamide) microgels

As stated earlier, polymer microgel is a network of a high molecular weight polymer crosslinked by a suitable crosslinker. Hydrophilic microgels swell to multifold size in water due to presence of polar groups on their polymeric backbone. Due to the non-covalent interaction between the polar group and water molecule, reversible swelling and deswelling of microgels is possible with the adjustment of the interaction. This can be accomplished through external stimuli such as temperature,[7] pH, ionic strength[8,9] and electric and magnetic fields,[10,11] making the microgels responsive "smart materials". Temperature and pH stimuli were widely investigated stimuli because of the convenience to handle experimentally. Temperature is the most widely used stimulus in smart polymer systems as it does not require the need for other solvents, co-polymerization agents, or any externally applied trigger.[12] Thermoresponsiveness becomes a favourite property when applied in targeted drug delivery.

Poly(N-Isopropyl acrylamide) or simply PNIPAm is a widely studied thermoresponsive polymer due to its desirable properties and potential applications in many fields especially biomedical and in nanotechnology.[13,14] The most important property of PNIPAm which made it favourite candidate in most applications is its lower critical solution temperature. Linear PNIPAm is water-soluble and it undergoes a hydrophilic to hydrophobic transition, referred as "coil-to-globule transition", at a particular temperature called lower critical solution temperature (LCST). The property is retained even when the polymer is made in to a microgel by covalent crosslinking. In the case of crosslinked PNIPAm microgels, the particular temperature at which

the hydrophilic property changes to hydrophobic is called Volume phase transition temperature (VPTT). Both the LCST of the linear polymer and the VPTT of the crosslinked microgel is at around 32°C. Since VPTT is near human physiological temperature, this exclusive behavior makes PNIPAm microgels engaging in biomedical applications especially targeted drug delivery. The crosslinking of microgel is achieved by the addition of a difunctional comonomers, namely N, N'-methylene-bis-acrylamide (BIS), as crosslinker agent. Diacrylates are other class of crosslinkers used. As said earlier, the synthesis parameters and reactants play a major role in deciding the size and properties of PNIPAm microgels. PNIPAm crosslinked microgels are highly monodisperse and are resistant to aggregation due to the surface charges formed from the initiator and surfactant molecules. High monodispersity of these microgels allow one to use it as model system to study colloidal dispersion and colloidal crystal.

2.3. Ionic microgels of NIPAm with acrylic acid: Effect of temperature, pH and ionic strength

Pure PNIPAm microgels exhibit thermoresponsive property only. The addition of ionic comonomers to the system opens up possibility for extra stimuli responses like pH, ionic strength, electric field and the like. In our study, we used acrylic acid as a comonomer in order to explore the effect of electric field on the assembly of the microgel. The synthesis procedure followed is same as that for the pure PNIPAm, the amount of acrylic acid taken is 10% of total monomer content unless otherwise stated. The effect of temperature, pH and ionic strength were studied on the p(NIPAm-AAc) system. Presence of acrylic acid moiety in the structure enhances the VPTT of the microgels. It was proved that the hydrodynamic diameter of PNIPAm-AAc copolymer microgel particles increase as a function of pH at a constant temperature and ionic strength, while with increasing ionic strength, the hydrodynamic diameter tends to decrease to a minimum at a pH above the pK_a value of acrylic acid i.e. 4.25 at 25 °C.[8]

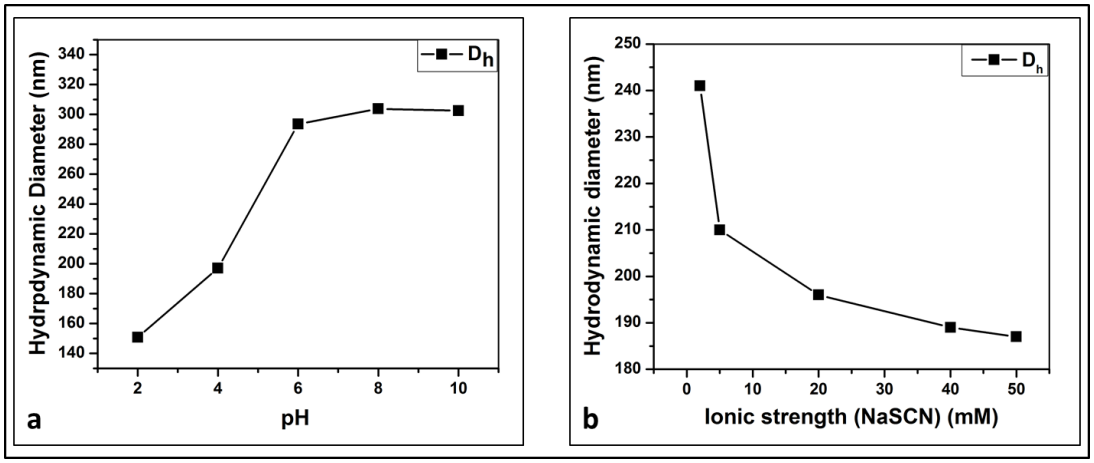

Figure 2.2: The hydrodynamic diameter of P(NIPAm-AAc) microgel particles (5% AAc) as a function of (a) pH at 23°C and (b) as a function of ionic strength of NaSCN at 23°C at a pH of ~6.

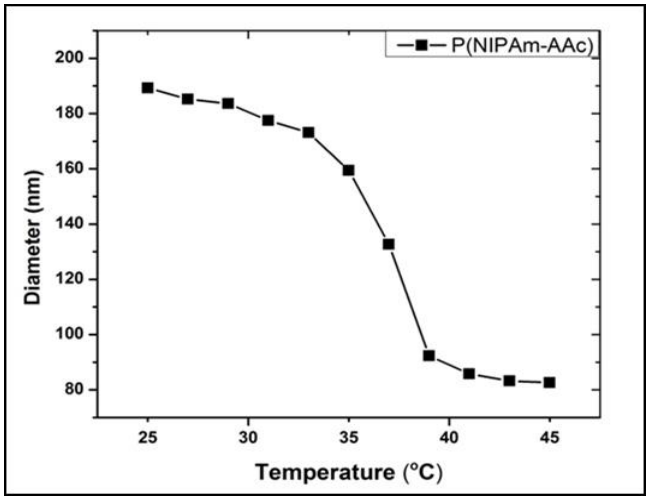

Figure 2.3: The hydrodynamic diameter of P(NIPAm-AAc) microgel particles (10% AAc) as a function of temperature. A shift in the VPTT (37°C) from that of PNIPAm (~32°C) is observed.

2.4. Structure of the microgels: Effect off crosslinker

Structure of PNIPAm microgels is different from that of hard spheres. In contrast to hard sphere colloids, PNIPAm exhibits core-brush morphology very similar to that of a hyper branched star polymer. The analogy in particle morphology along with the luxury of monodispersity and ease of preparation provide microgels an edge over the star colloids to be used as model systems for soft colloidal glasses. The amount of crosslinker greatly affects the physical properties of the microgels. Several literatures prove the effect of crosslinker on the

properties like size, internal structure, swelling behaviour, temperature sensitivity, mechanical properties etc.[3,15–17] Owing to the difference in the reaction rates of the monomer and the cross-linker, the microgel obtains its core-brush morphology. The cross-linker BIS reacts at a faster rate compared to the monomer NIPAm, and gets consumed faster than the monomer during synthesis.[2] Hence the crosslinking density at the center of the microgel is higher than that at the surface. This result in a gradient in the radial density profile in the form of a densely cross-linked core and a loosely cross-linked brush-like surface, see figure 2.4. The loosely cross-linked brush at the particle surface provides steric stabilization and weakens the van der Waals attraction.

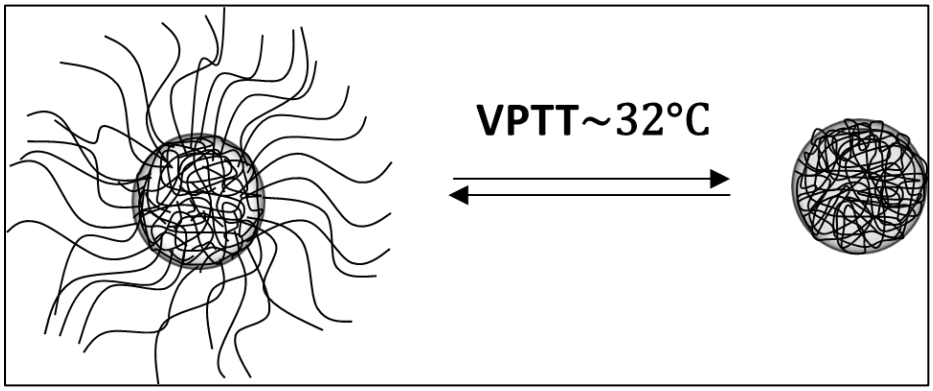

Figure 2.4: Schematic of a PNIPAm microgel showing a radial density profile and also the volume change in response to change in temperature.

Many theoretical predictions gave insights to the core-shell structure of PNIPAm microgels which were backed by experimental studies using light and neutron scattering.[18–20] At higher temperature, the long brushes on the surface of the colloid collapse to the shell essentially behaving like a hard sphere colloid thereafter. Very small sized particles having hydrodynamic diameter typically less than 100 nm with a homogeneous crosslinked structure could be made by conducting polymerisation with high amount of surfactant.[21] There were attempts to make homogeneously crosslinked PNIPAm by many researchers in the recent past. It was shown by Roberta Acciaro's group that a two-step synthesis strategy involving a continuous feed of appropriate amount of monomer and cross-linker with a syringe pump during the course of reaction could earn microgels with a homogenous distribution of the cross-linking density.[4] By constantly checking the kinetics of the cross-linker incorporation into the reaction mixture and there by controlling the monomer to crosslinker ratio in the system, they could achieve homogenously cross-linked PNIPAm particles. They could prove that even the larger sized

microgel suspension with homogeneous crosslink density would appear transparent. The experimental protocol followed in this thesis for the preparation of homogeneously crosslinked microgel was based on this paper. The preparation procedure is explained in section 2.6.3 of this chapter. Although the paper explains only the synthesis of pure PNIPAm, we use the same protocol for ionic counterparts of NIPAm also. We did not find any difference in the basic morphology by the alteration of monomer ratio. Tim Still et al also tried a similar strategy, a semi-batch synthesis method they call, to produce particles with uniform crosslinker density and with precise adjustment of particle diameter.[22] Very recently, To Ngai group has come up with a controlled synthesis method to prepare micrometer-sized, multiresponsive copolymer of NIPAm with Methacrylic acid (P(NIPAm-MAA)).[23]

2.5. Volume phase transition in PNIPAm

2.5.1. Volume phase transition temperature (VPTT)

The presence of both hydrophilic and hydrophobic group on the same monomer (NIPAm) helps in achieving the special property of volume phase transition. NIPAm contains a hydrophilic amide group and an isopropyl hydrophobic group as shown in Figure 2.5. The amide group on each repeating unit of the polymer forms hydrogen bonds with water molecules involving protic hydrogen (R'– NH….OH_2) and carbonyl oxygen (R–C=O….H–O–H). Isopropyl group at the side chain end will remain repelled at lower temperature. On increasing the temperature, when the thermal energy necessary to break the hydrogen bond reaches, the hydrogen bonds between acrylamide and water molecule breaks down. These water molecules surrounding the side group will be expelled out of the polymer molecule at higher temperature. This causes a hydrophobic interaction between isopropyl groups of opposite chains resulting in a collapse of the chains. At volume phase transition temperature, the hydrophobic interaction dominates leading to a coil-to-globule conversion.

The entropy of the hydrophobic interaction overcomes the enthalpy of H- bonding leads to the release of water molecules and subsequent shrinkage of the particle. This temperature at which phase transition occurs is called volume phase transition temperature (VPTT). The VPTT largely depends on the hydrogen-bonding abilities of the constituent monomer units. Many other factors also affect the phase transition, which is discussed in the subsequent section.

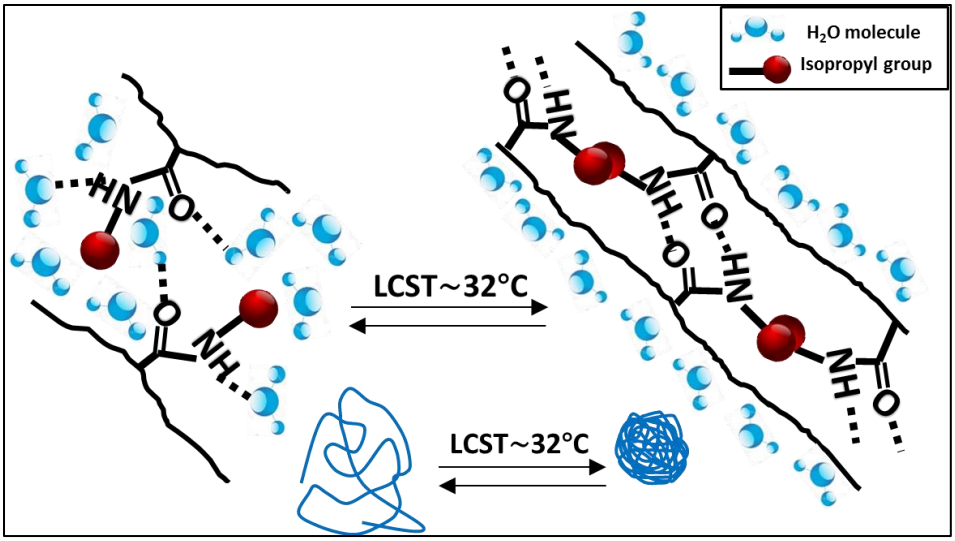

Figure 2.5: Schematic representation of the mechanism of coil-globule transition in PNIPAm aqueous suspension.

2.5.2. Factors affecting the volume phase transition

The hydrophilic- hydrophobic balance in the system decides the collapse during phase transition. Thus VPTT can be tuned to some extent by changing the factors which influence the hydrophilicity of the system. Additions of different comonomers to the NIPAm system, changing the solvent properties etc. are some methods to tune the VPTT. Hydrophilic comonomers like acrylic acid, methacrylic acid and vinyl acetic acid would shift the VPTT to higher values, while addition of comonomers like t-butyl acrylate, vinyl pyridines etc. will shift the VPTT to lower values.[5,24] Many other factors like ionic concentration, added surfactants etc. also affect the VPTT of PNIPAm.[8,25]

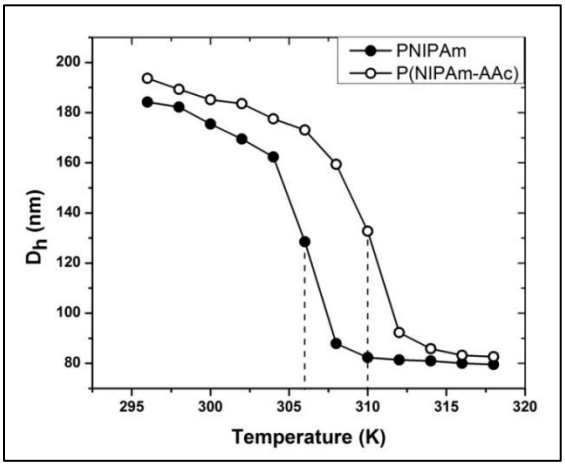

Figure 2.6: Comparison of VPTT of neutral and ionic microgels of NIPAm.

Figure 2.6 shows the phase transition for PNIPAm and PNIPAm-co-acrylic acid made with same cross-linker density (~5% by weight of monomer); however the size of the copolymer is slightly larger than the homo-polymer. The VPTT also changes from 306K to 310K. More number of hydrophilic groups (-COOH) from acrylic acid counterpart are present in the copolymer and all are involved in hydrogen bonding. So higher energy is required to break the extra number and much stronger hydrogen bonds between water and the acidic groups leading to higher temperature for phase transition. The swelling ability of the microgel also gets affected by comonomers.[24] The higher the amount of comonomer, the broader the VPTT will be.

2.5.3. Effect of solvent on volume phase transition

Water and some organic solvents like methanol, ethanol etc. are pure solvents for PNIPAm. But a mixture of water and methanol/ethanol will be a non-solvent for PNIPAm depending on the ratio of water and alcohol. This effect is called co-nonsolvency.[26] The ratio of water to alcohol decides the sample dissolution. The volume phase transition occurs below the transition temperature usually observed in pure water.

2.6. Synthesis of PNIPAm microgels

2.6.1. Materials

The monomer N-isopropylacrylamide (NIPAm) procured from Acros Organics, USA was recrystallized at room temperature after dissolving in a 3:1 mixture of toluene and hexane at 40°C. Comonomer acrylic acid (AAc) (Merck, Germany) was used as received. Crosslinker N, N'-methylene-bisacrylamide (BIS) bought from Merck, Germany was recrystallized from HPLC grade methanol. Initiator used was ammonium persulfate (APS) bought from Merck Germany, was recrystallized from deionised water. Surfactant used for small particles was sodium dodecyl sulphate (SDS) and was used as received. All the reactants after purification were stored in refrigerator.

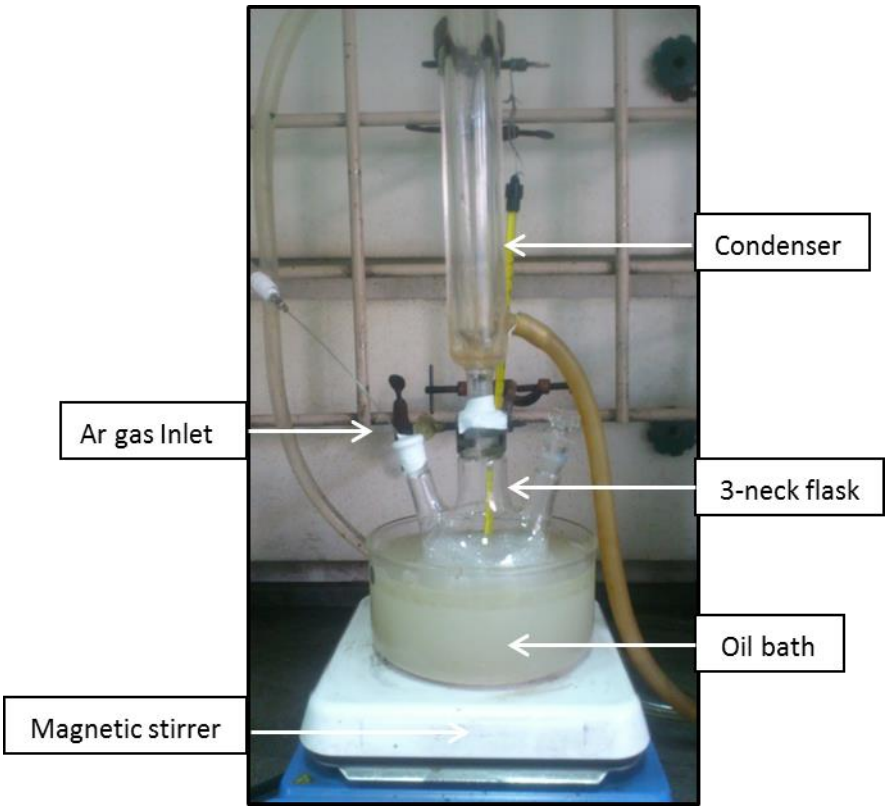

Figure 2.7: Microgel synthesis setup.

2.6.2. Synthesis of small PNIPAm microgels

PNIPAm microgel of small sized particles (less than 500 nm) was synthesized by emulsion polymerization technique via radical polymerization using a free radical initiator. The reaction was carried out in a 3-neck glass reactor fitted with a condenser, an inlet for Argon gas and inlet for monomer feed. The reaction mixture was stirred using a magnetic stirrer (IKA Instruments) at 200 rpm. The temperature of the reaction was maintained by keeping the 3- neck flask in an oil bath.

Necessary amount of distilled, deionised water (Milli-Q Gradient A10, Millipore) was purged with Argon gas for 1 hour prior to the reaction and was used for preparing the solutions. The purified reactants, monomer NIPAm, cross linker BIS and stabilizer SDS were dissolved in Argon-purged DI water and stirred in the flask at room temperature for 1 hour under a continuous slow purging of Argon. The temperature was then increased to 80 °C. After complete mixing of these reactants and the sufficient temperature is reached, the initiator APS dissolved in Argon-purged DI water was added to the reaction mixture. The reaction mixture colour change from transparent to turbid in 5-10 minutes after addition of the initiator indicates the

polymerisation initiation. Although the polymerisation completes within first half an hour, the reaction was allowed to proceed for 3 more hours with continuous stirring at 80°C to ensure complete conversion of monomers. After that, the temperature was then reduced to room temperature and the dispersion formed was stirred overnight at 100 rpm. This procedure gave microgels of hydrodynamic size well below 500 nm in diameter at 23°C.

2.6.3. Synthesis of small PNIPAm microgels with homogeneous crosslink density

This synthesis procedure is adopted from the paper by Roberta Acciaro.[4] This synthesis is a two-step strategy: reactor and feed. The preparation of reactants for the first step was done similarly to the batch synthesis: i.e. calculated amount of deionised water (Milli Q water) was degassed with Argon gas for 1 hour before the reaction to remove oxygen. Then it was transferred to the reaction vessel. Reaction vessel is a 3-neck flask fitted with a condenser, an inlet for Argon gas and inlet for monomer feed. The temperature of the reactor was set to 80°C, and the water was stirred (~300 rpm). Calculated amounts of NIPAm monomer and BIS cross-linker were dissolved in 18 mL of Milli-Q water prepurged with Argon gas and fed to the reactor. After the injection of the monomers, 1 mL of SDS solution was also injected into the reactor and then the reaction was initiated by the addition of 1 mL of APS solution after 1 minute. The amount of NIPAm and BIS in the feed in the second step is different to that of batch synthesis. To prepare microgel particles with a homogeneous cross-link density, the ratio of the NIPAm and BIS was set to 50 in the reactor. One minute after the initiation of the polymerization the feeding of NIPAm and BIS monomers to the reaction mixture was turned on. To make monomer feeding possible, the monomers were dissolved in water. The ratio of the NIPAm and BIS was 20 in the feeding solution. The solution was degassed, filled into a 60 ml syringe, and a total volume of 28.6 ml was fed into the reaction mixture with a feeding rate of 200 µl/min by means of a syringe pump (Harvard Apparatus PHD2000). After 143 min the feeding was stopped and the reaction was quenched by plunging the reactor in ice to decrease the temperature from 80 to 15°C.

2.6.4. Synthesis of large P(NIPAm-AAc) copolymer microgels

The synthesis of large sized copolymer microgels of NIPAm with acrylic acid was done for the electric field study under a confocal microscope. The synthesis protocol was similar to that mentioned in the previous section except that here the polymerisation was conducted in the

absence of the surfactant. The initiator used here was potassium persulphate (KPS). Consequently the purification of the microgels was easier. This procedure gave large size microgels above 500 nm in diameter at 23°C.

Calculated amount of distilled, deionised water (Milli-Q Gradient A10, Millipore) was purged with inert gas (Ar) for 1 hour before the reaction and was used for preparing the solutions. The purified reactants, monomers NIPAm, acrylic acid and cross linker BIS were dissolved in Argon-purged DI water and stirred in the flask at room temperature for 1 hour under a continuous slow purging of Argon. The dyes used to tag the microgels were methacryloxyethyl thiocarbamoyl rhodamine B (MRB) for 670 nm particles and Fluorescein isothiocyanate (FITC) for 1300 nm particles. The MRB dye (4mg/ml) was dissolved in DMSO and FITC (4mg/ml) was dissolved in ethanol. The temperature was then increased to 60 °C. For larger particles, the temperature was set first at 40 °C and then slowly increased to 60 °C in 1 hour. A very small amount of SDS was used while synthesizing smaller particles to control the size. After complete mixing of the reactants and the sufficient temperature is reached, the initiator KPS dissolved in Argon-purged DI water was added to the reaction mixture. The reaction mixture colour change from transparent to turbid in 5-10 minutes after addition of the initiator indicates the polymerisation initiation. Although the polymerisation completes within first half an hour, the reaction was allowed to proceed for 3 hours with continuous stirring at 60°C to ensure complete conversion of monomers. The temperature was then reduced to room temperature and the dispersion formed was stirred overnight at 100 rpm. Size of the microgel particles were controlled by controlling the amount of initiator and time and temperature of reaction.

2.7. Purification and storage of synthesized microgels

All microgel dispersions made by above given procedures were purified by dialysis against deionised water for about two weeks with changing water every 8 hours and keeping the medium stirring at 200 rpm for whole time at room temperature. This removes unreacted reactants and especially the surfactant from the polymer. Dialysis bags (Sigma Aldrich, USA) having a molecular weight cut-off of 14,000 was used. Dialysis of microgels made without using surfactant was done for 1 week. After dialysis, the samples were frozen in liquid nitrogen, and then freeze dried in freeze dryer (ScanVac CoolSafe, Denmark). The freeze dried microgel powder was stored in desiccator under vacuum. Freeze drying the microgels done to avoid bacterial and fungal growth which occurs in aqueous suspensions. This method is sufficient in

case the microgels are to be stored for a longer time. For preparing specific concentration of samples, freeze dried powder was redispersed in filtered DI water. Ion-exchange resins were added to further deionize the water. Complete list of reactants and synthesis parameters for each of microgel is given in the following tables (2.1- 2.3).

Sample	NIPAm (g)	BIS (g)	APS (g)	SDS (g)
CS1	3.378	0.023	0.108	0.051
CS2	4.3	0.11716	0.08214	0.08
CS3	4.3	0.2343	0.08214	0.08
CS4	4.3	0.4686	0.08214	0.08
CS5	4.3	0.9373	0.08214	0.08

Table 2.1: Material details for the synthesis of core-shell (CS) microgel particles using the conventional synthesis method.

Sample	NIPAm (g)		BIS (g)		SDS (g)		APS (g)	
	Reactor	Feed	Reactor	Feed	Reactor	Feed	Reactor	Feed
HM1	0.43	4.4099	0.011	0.0221	0.08	--	0.044	--
HM2	0.43	4.4099	0.011	0.11	0.08	--	0.044	--
HM3	0.43	4.4099	0.011	0.2205	0.08	--	0.044	--
HM4	0.43	4.4099	0.011	0.441	0.08	--	0.044	--
HM5	0.43	4.4099	0.011	0.882	0.08	--	0.044	--

Table 2.2: Material details for the synthesis of homogeneous (HM) microgel particles using the continuous feed method.

Sample notation	NIPAm (g)	AAc (g)	BIS (g)	KPS (g)	SDS (g)	Dye (ml)	DI H_2O (ml)	Reaction Temperature (°C)	Time (hrs)
RNA670	1.935	0.215	0.117	0.03	0.008	1.25	150	60	3
FNA1300	1.935	0.215	0.117	0.05	--	1.25	150	40 (1 hr), 60 (2 hrs)	3

Table 2.3: Parameters for synthesis of microgel particles for electric field studies.

Sample	BIS content (% of monomer)	Diameter at 23°C (nm)	Diameter at 43°C (nm)	VPTT (°C)	Swelling Ratio ($R_{h(43)}/R_{h(23)}$)
CS1	0.5	284	97.1	33	0.342
CS2	2.5	198.7	83.78	33	0.422
CS3	5	180.6	84.6	34	0.468
CS4	10	165	95.6	35	0.581
CS5	20	166	113	35	0.679
HM1	0.5	212.96	82	32	0.385
HM2	2.5	232.96	103.2	34	0.443
HM3	5	245	105	34	0.429
HM4	10	268	150	36	0.52
HM5	20	220	140	36	0.63

Table 2.4: Size and swelling ratio of microgel particles.

2.8. Experimental methods

2.8.1. Capillary Viscometry: Determination of effective volume fraction (φ_{eff})

Viscometry, a branch of rheology, deals with the determination of viscosity of fluids. In a capillary viscometer, the velocity gradient needed to measure the viscosity is formed by the laminar flow within a capillary tube. Technically, the time required for a given volume of fluid to flow through a defined length of capillary under its own hydrostatic head is measured. The flow time is directly related to the viscosity.

The microgel suspension behaves like a soft solid only when $\varphi_{eff} > \varphi_g$, where φ_g is the volume fraction at which glass transition occurs. Thus it is important to determine the effective volume fraction of the PNIPAm microgel suspension. We followed the method described by Senff and Richtering.[27] A series of dilute aqueous solutions of PNIPAm microgels of different known concentrations were prepared and their relative viscosities were measured using a viscometer (SCHOTT GERATE CT 1650 Viscometer, Germany) at 23°C. Effective volume fraction (φ_{eff}) can be determined from the relative viscosity, η_{rel}, by an expression named Batchelor equation (equation 2.2):

$$\boldsymbol{\eta_{rel} = \left[\frac{\eta_0}{\eta_s}\right] = 1 + 2.5\kappa c + 5.9(\kappa c)^2} \qquad 2.2$$

Here, η_0 and η_s are the viscosities of the sample and the solvent (water) respectively; c represents the sample concentration (in weight %) and κ is a shift factor for converting the weight fraction to effective volume fraction. Since all the concentrations selected were in the fluid regime itself, the second order is neglected from the equation and fitted with a linear fit keeping the intercept 1. The relative viscosity of dilute suspensions was measured as a function of particle concentration. The obtained viscosity was plotted against corresponding concentration and then the data obtained were fitted with the Batchelor relation to determine the volume fraction.

2.8.2. Light Scattering

Light scattering is a non-invasive technique for measuring the size and related properties of polymers and other molecules especially in the sub-micron region dispersed in a solvent. Light scattering covers a broad range of macromolecules and emulsions including nanoparticles. Most importantly, light scattering permits measurement of the solution properties of the molecules and can be conducted with in short duration of time. With this comparatively short experimental time along with the absolute determination of molecular weight, particle size, and second virial coefficient make light scattering the preferable technique for accurate and fast macromolecular characterization. To dichotomize, light scattering can be of Static Light Scattering (SLS) and Dynamic Light Scattering (DLS). Both techniques are used in colloidal characterization, and have a range of applications. The theory and application of SLS and DLS are discussed in the subsequent sections.

2.8.2.1. Static Light Scattering

A light beam when hits a particle in its path will be scattered by the particle in different directions. In a light scattering instrument, a detector catches this scattered light and measures the scattering intensity as a function of the scattering angle θ. In static light scattering, the mean scattered intensity is measured as a function of the scattering vector q which is a measure of the scattering angle. The scattering vector is defined as the difference between incident beam vector and the scattered beam vector, and depends on the refractive index of the sample (n), the angle between incident and scattered light (θ) and the wavelength of light (λ) (equation 2.3).

$$\boldsymbol{q = \frac{4\pi n}{\lambda} \sin(\theta/2)} \qquad 2.3$$

The scattering vector is inversely proportional to the wavelength, thus smaller the wavelength of the incident radiation, larger the structures that can be investigated with a scattering experiment.[28] The scattered intensity I_q is proportional to the scattering cross section which is a product of the particle form factor P_q and the static structure factor S_q (equation 2.4). Form factor gives an idea about the size and shape of the particle while structure factor gives information about the interaction between the particles.

$$\boldsymbol{I_q \propto P_q * S_q} \quad 2.4$$

$$\boldsymbol{I_q = N a^6 * P_q * S_q} \quad 2.5$$

where, N= the number of the particles and a= diameter of the particle.

The total scattering cross section σ(q) or its differential $\frac{d\sigma(q)}{d\Omega}$ is an important parameter, where Ω is the solid angle formed by the scattered intensity I_s to the incident intensity I_o. This determines the dependence of the scattered intensity on the scattering vector q. The scattered intensity and differential scattering cross section are proportional to the wavelength (λ) and polarizability (α) of the light used (equation 2.6).

$$\boldsymbol{\frac{d\sigma(q)}{d\Omega} = \frac{I_q R^2}{I_0} = \frac{16\pi^2\alpha^2}{\lambda^4}} \quad 2.6$$

where, R is the distance of the detector from the source of light.

Many important properties of polymers like weight average molecular weight (M_w), radius of gyration (R_g), second virial coefficient (A_2) etc. can be determined from the scattered intensity by conducting static light scattering experiment. Bruno Zimm determined the molecular weight of polystyrene particles using static light scattering experiments and set a well-defined method for determining molecular weight (M_w) and Second virial coefficient (A_2).[29] The following equation (2.7) is used to determine these parameters of colloidal dispersion and/or polymer solutions (Zimm equation).

$$\boldsymbol{\frac{Kc}{\mathcal{R}_{ex}} = \frac{1}{M_w P_q} + 2A_2 c = \frac{1}{M_w}\left(1 + \frac{q^2 {R_g}^2}{3}\right) + 2A_2 c} \quad 2.7$$

where M_w= weight average molecular weight of the particle, $\mathcal{R}_{ex}$ the excess Rayleigh ratio, K is the scattering wave vector and P(q) is the particle form factor which is described in the next section. Excess Rayleigh ratio, the scattering wave vector and particle form factor are given by the following expressions:

$$\boldsymbol{\mathcal{R}_{ex} = \frac{I_{soln} - I_{solv}}{I_{std}} * \frac{n_0^2}{n_T^2} * R_T} \quad 2.8$$

$$\boldsymbol{K = \frac{4\pi^2 n^2 \left(dn/dc\right)^2}{N_A \lambda^4}} \quad 2.9$$

where, n = refractive index of the solvent, c = particle concentration (mass/volume), dn/dc= refractive index increment, N_A= Avogadro's number and λ= wavelength of the incident light.

2.8.2.1.1. Form factor

The scattered intensity from the particle I_q is the superposition of the light scattered from all volume elements within a particle. Here interference effects due to the different optical path lengths from the volume elements to the detector results in the particle form factor P_q which is given by the scattering intensity I_q divided by the scattering intensity without interference effects in forward direction $I_{q=0}$. $P_q = I_q / I_{q=0}$. Form factor decreases from unity at q=0 and shows an angular dependence, which is characteristic of the size and form of the particle.

Rayleigh scattering occurs when the particles are small compared to the wavelength of the light and if there is only a small contrast between the particles and the solvent. The form factor can be calculated using the Rayleigh-Gans-Debye (RGD) approximation the basic ideas of which including derivations from integration were formulated by Rayleigh in 1881[30] and later derived and applied independently by Debye in 1915.[31] The first assumption in the theory is that each of the small volume elements sees the same incident light wave.

$$\boldsymbol{P_q = \left[1/V \int e^{iqR} dv\right]^2} \quad 2.10$$

Evaluation of the integral after conversion to spherical co-ordinates gives:

$$\boldsymbol{P_q = \left[\frac{3}{(qR)^3}(sin(qR) - qR\, cos(qR))\right]^2} \quad 2.11$$

Expanding the above expression (equation 2.11) in powers of q and using $R_{g,\,sphere} = \sqrt{3/5}\,R$ we get

$$P_q = e^{\left[\frac{q^2 R_g{}^2}{3}\right]} \qquad 2.12$$

This expression named as the Guinier approximation is used to determine the radius of gyration R_g which is a well-defined measure of size of any object as obtained from small q-scattering (i.e., $qR_g<1$). Hence the plot of the corrected intensity or the excess Rayleigh ratio R_{ex} versus q^2 will give a slope $R_g{}^2/3$. Thus by using the Guinier approximation, radius of gyration can be determined by a single concentration, rather than using equation which requires atleast three concentrations.

Soft particles like microgels, unlike hard particles, have a radial density gradient with a highly cross-linked core and a loose brush-like surface require a modified form of RGD.[32] The following expression (equation 2.13) is the modified form of RGD equation which gives the form factor.

$$P_q = \left[I_q\right]^2 = \left[\frac{\left(3e^{\left((-\sigma q)^2\right)/2}\right)(\sin qR - qR\cos qR)}{(qR)^3}\right]^2 \qquad 2.13$$

Figure 2.8 shows the form factor for PNIPAm microgel suspensions at 20°C.

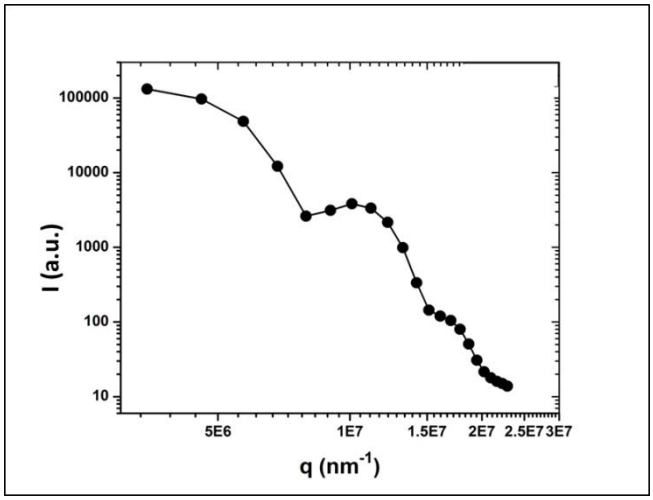

Figure 2.8: Particle form factor P_q as a function of scattering vector q for PNIPAm particle of size ~1μm.

2.8.2.1.2. Structure factor

While the form factor provides information on the size and shape of the particle, the static structure factor S_q describes the local structures taking into account the inter-particle interference. Thus static structure factor is a measure of order in the system. For very small particle concentrations, where particle interactions are negligible, structure factor value is equal to 1, whereas at higher concentrations, particles interact each other, and a destructive interference effect appears at small scattering vectors.

2.8.2.2. Dynamic light scattering

Dynamic light scattering is also called photon correlation spectroscopy or quasi elastic light scattering (QELS). As the name indicates DLS measures the dynamics of particles in the system. The particles in a colloidal suspension always exhibit Brownian motion due to the thermal motion of solvent particles causing fluctuations in the intensity of scattered light with time.[33] These intensity fluctuations gives information about the time scale of the movement of the Brownian particles, or more physically, their diffusion process in terms of a time correlation function and hence can be used to obtain the information about the dynamics of colloidal particles. DLS technique basically works on the principle of diffusion. The instrument measures the diffusion of particles in the suspension. Diffusion largely depends on size of the particles i.e. the smaller particles diffuse very fast while large particles diffuse slowly.

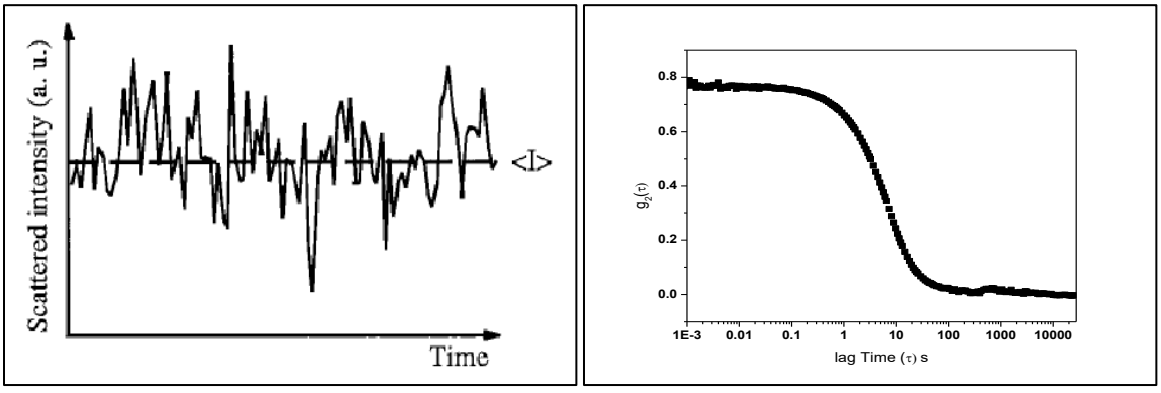

Figure 2.9: (a) Scattering intensity vs time in a DLS experiment and (b) Auto Correlation function g_2 (τ), of a PNIPAm microgel suspension.

The scattered intensity is fed to a correlator through an avalanche photo diode (APD). A correlator is a signal comparer where it compares the intensity at a given time and a short time after (t and t+τ). If the time gap is short, the intensity will have a strong correlation. As time

goes, the correlation decays. So eventually we get a decay curve, the shape of which gives idea about the particle size. Because smaller particles decay faster while larger particles decay slowly. Essentially what we get from the instrument is the autocorrelation function g_2 (τ). The scattering intensity autocorrelation function g_2 (τ) and the electric field autocorrelation function g_1 (τ) are related to each other by Siegert relation (equation 2.16).

$$\boldsymbol{g_2}\,(\boldsymbol{\tau}) = \frac{<\boldsymbol{I_t}.\boldsymbol{I_{t+\tau}}>}{<\boldsymbol{I_t}>^2} \qquad 2.14$$

$$\boldsymbol{g_1}(\boldsymbol{\tau}) =< \boldsymbol{E}(\boldsymbol{t}).\boldsymbol{E}(\boldsymbol{t}+\boldsymbol{\tau}) > \qquad 2.15$$

$$\boldsymbol{g_2}\,(\boldsymbol{\tau}) =< \boldsymbol{I} >^2 + |\boldsymbol{g_1}(\boldsymbol{\tau})|^2 \qquad 2.16$$

The electric field autocorrelation function g_1 (τ) is related to the relaxation time Γ by the equation 2.17. The relaxation time in turn is a measure of diffusion coefficient D (equation 2.18). q is the scattering vector which is a measurement of angle. Diffusion coefficient obtained from equation 2.18 is substituted in Stoke-Einstein equation (equation 2.19) to find the hydrodynamic radius (R_h).

$$\boldsymbol{g_1}(\boldsymbol{\tau}) = \boldsymbol{e}^{-\boldsymbol{\Gamma\tau}} \qquad 2.17$$

$$\boldsymbol{\Gamma} = \boldsymbol{Dq^2} \qquad 2.18$$

$$\boldsymbol{R_h} = \frac{\boldsymbol{k_B T}}{\boldsymbol{6\pi\eta D}} \qquad 2.19$$

where, R_h is hydrodynamic radius, D is diffusion coefficient, k_B is Boltzmann's constant, T absolute temperature and η the solvent viscosity.

Both SLS and DLS techniques are valid on one assumption that the light is scattered by a single scattering event or negligibly small multiple scattering. However, in real situations this assumption is valid only if the sample is very dilute. But in real life, concentrated or turbid samples also have to be investigated from an industrial as well as research point of view. Additional averaging due to multiple scattering occurs both in static as well as in dynamic light scattering. The static experiment shows a shift of scattered intensity towards larger scattering angles. The dynamic experiment shows additional spectral components at higher frequencies. Both experiments show a decreased resolution.[34] Thus, investigation or characterization of turbid systems cannot be achieved by conventional static or dynamic light scattering methods.

Many researchers have come up with new techniques and methods to reduce the problem of multiple scattering like the three dimensional dynamic light scattering (3DDLS),[35,36] cross-correlation scheme,[37] the diffusing wave spectroscopy (DWS),[38] use of thin flat cells[39] etc. We use a special instrument in which we can use turbid samples for characterization. The problem of multiple scattering is avoided here by the combination of cross-correlation technique and 3D-DLS where two light scattering measurements were performed simultaneously at the same scattering vector on the same sample volume. Thus the contribution from single scattering volume will be identical in both experiments, while multiple scattering contributions will not. The correlation of both experiments with each other results in a cross-correlation function, which contains only the single scattering contribution.

Coming to the components of the 3D-DLS instrument (figure 2.10) with cross-correlation technique, it has a source of light, basically a LASER. A single beam of He-Ne laser (632.8 nm) is usually used because it is easy to use, long life and comparatively cheap. A beam splitter divides the single beam into three equal beams; two of which are used for the experiment and the central one is used for alignment of the whole system. A plano-convex lens converges the two beams and focuses to the sample chamber. The same plano-convex lens system is there on the detector end also which captures the scattered light and fed into the detector. At the detector end, two single mode fibres which collect the scattered intensity and fed into a highly sensitive avalanche photodiode (APD) which can detect even feeble intensity light. The sample is kept in a toluene bath because toluene has the least scattering and we can control the temperature of the sample externally using a chiller. Both the sample chamber and the detector can move around. The detector goniometer move around from 5° to 150° angles. The scattering level of the particles differs with angles. Lower angles will show particles which are bigger in size (forward scattering). So for a binary mixture of particles of two sizes, in order to get the complete information on both sizes, we use a multi-angle measurement. Similarly, if we have a sample in which particles aggregate with time, we have to run the experiment at different angles. Finally the intensity is fed into a cross-correlator through the APD where it is processed and shown in the monitor.

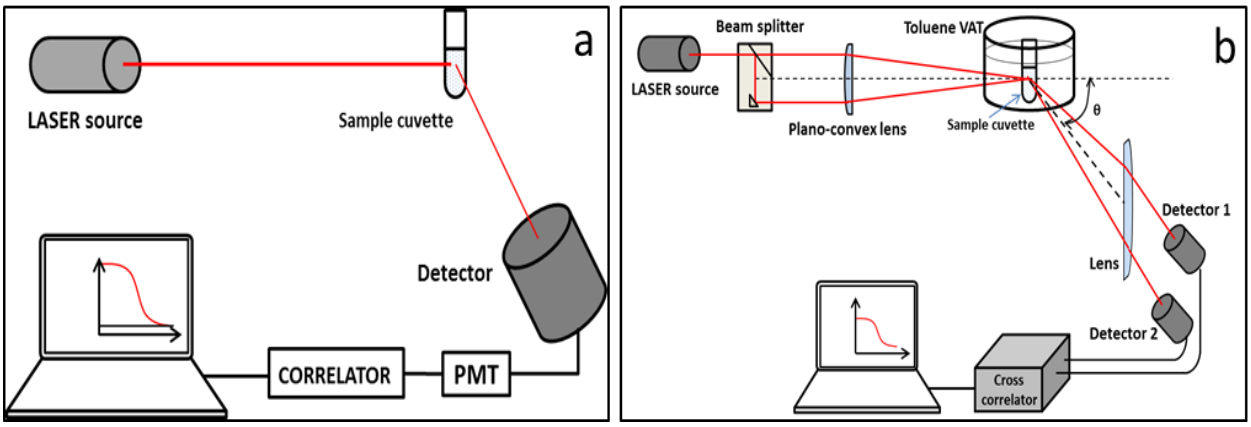

Figure 2.10: Schematic diagram of (a) a simple light scattering set up and (b) 3D- DLS light scattering set up with cross correlation technique showing the components.

2.8.3. Rheology

Rheology is the study of deformation and flow of materials by applying external shear. The external flow could be a steady shear flow or a dynamic oscillatory flow. The structure-property relationship study of viscoelastic materials uses rheology as an important tool. Rheology is applied to such materials having a complex structure like suspensions, pastes, polymers etc. The instrument used to conduct rheological experiments in a laboratory scale is called a rheometer. Deformations like shear, extension are applied on the system and the resulting response of the material is measured using the rheometer. There are strain-controlled rheometers which measure the torque or stress on a material with applied strain. Alternatively, if a stress is imposed on the material and the corresponding strain response is measured, it is called a stress-controlled rheometer. All rheological experiments conducted in this work are dynamic oscillatory strain measurements. The most important properties obtained from the oscillatory rheology are the storage (elastic) modulus G' and the loss (viscous) modulus G". Since viscoelastic fluids exhibit both these properties, the rheological measurements of these fluids are very relevant. Dynamic oscillatory shear tests are of two: Small Amplitude Oscillatory Shear (SAOS) which probes the linear viscoelastic properties of the material and Large Amplitude Oscillatory Shear (LAOS) which investigates the non-linear properties. All rheology measurements in my work were conducted on Anton Paar Physica MCR301 strain-controlled rheometer with a cone and plate geometry having a cone radius 25 mm.

2.8.3.1. Small Amplitude Oscillatory Shear (SAOS)

The stress response of a viscoelastic material on application of a sinusoidal strain can be divided into two components: the in-phase and out-of-phase components. The in-phase component represents the elastic property of the material while the out-of-phase component is its viscous property. When a sinusoidal shear strain of the form $\gamma(t) = \gamma_0 \sin(\omega t)$ of small amplitude γ_0 and frequency ω is imposed on a viscoelastic fluid, the stress response is given by:

$$\boldsymbol{\sigma(t,\omega) = \gamma_0[G'(\omega)\sin(\omega t) + G''(\omega)\cos(\omega t)]} \qquad 2.20$$

where, G′ is the in-phase component called as storage modulus and G″ is the out-of phase component known as the loss modulus and are functions of the angular frequency (ω).[40] Storage modulus is the stored component of the energy of the material while loss modulus is the dissipated energy. Two routine experiments conducted on viscoelastic materials in linear regime are strain sweep experiment and frequency sweep experiment. In strain sweep (amplitude sweep) experiment, the amplitude of the sinusoidal strain is increased and the resulting response in terms of G' and G" is measured while the frequency is kept constant. The material is predominantly elastic if G'> G" and the material is predominantly viscous if G"> G'. Property change from elastic to viscous while undergoing deformation is said to be the onset of gelation or structural arrest due to topological constraints in high concentrated suspensions of colloids. In frequency sweep experiment, the frequency of the oscillation is increased while the stress in kept constant. Frequency sweep experiments are conducted to ascertain the relaxation times of the material under dormant conditions.

2.8.3.2. Large Amplitude Oscillatory Shear (LAOS)

The sample characterization is complete with both the linear and nonlinear test methods because during most of the processing or application of the soft matter, the deformations occurring in the material will be rapid and large and at that point the nonlinear properties control the response of the system. Large Amplitude Oscillatory Shear (LAOS) tests are used to investigate and quantify the nonlinear viscoelastic behavior of complex fluids.[41] While SAOS contribute to the linear viscoelastic properties of the material, LAOS is conferred with non-linear behaviour also.[42] Strain amplitude and frequency of relevant range should be selected for LAOS and SAOS as experimental inputs; but the material response varies for both. At large strain amplitude, response will be nonlinear in LAOS and at that point SAOS tests become irrelevant.

Since the nonlinear stress response becomes non-sinusoidal, linear viscoelastic moduli (storage and loss) cannot be used to quantify nonlinear response under LAOS conditions. The stress generated in the material is related to the applied strain in a non-linear fashion at sufficiently large strains. Consequently, for each oscillatory strain amplitude, the full wave form of the stress response is resolved by large-amplitude oscillatory shear (LAOS) and it will thus contain higher harmonics which are interpreted in terms of harmonic moduli G'_n and G''_n (subscript n refers to the n^{th} harmonic). These are functions of both the strain amplitude and the angular frequency.

$$\boldsymbol{\sigma(t,\omega,\gamma_0) = \gamma_0 \sum_{n=1,3,5\ldots} [G'_n(\omega,\gamma_0)\sin(n\omega t) + G''_n(\omega,\gamma_0)\cos n\omega t]} \qquad 2.21$$

Non-linear response of viscoelastic materials shows a peak in G" which is called yielding of material. G' peak start to droop from the linear region (Figure 2.11).

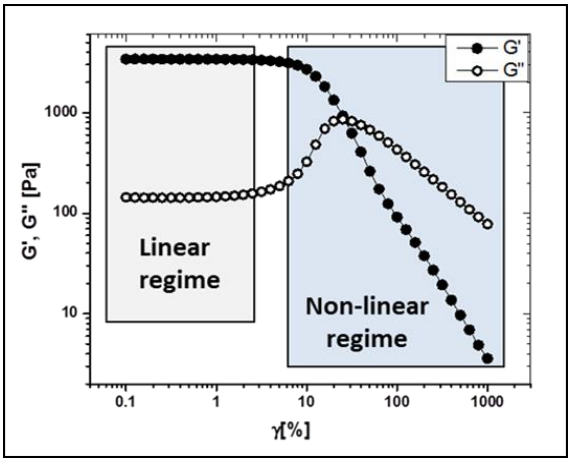

Figure 2.11: Strain sweep curves for microgel suspension showing the linear and non-linear regimes.

Strain sweep and frequency sweep experiments and large amplitude Oscillatory shear experiments on PNIPAm microgel particles and its response with respect to particle morphology and crosslinking density are detailed in chapter 3.

2.8.4. Confocal Microscopy

Marvin Minsky invented confocal microscopy in 1955[43] and is now one of the recently evolved microscopy techniques providing quality images and many more. It provides information at single particle level with precise qualitative analysis. More complex systems like colloidal glasses and gels can be easily analyzed using confocal microscopy.[44–46] Although this

technique is preferred for biological specimen, it has been now widely used to investigate the colloidal systems also. Recent developments in confocal microscopy have made enormous impact on research in colloidal science especially microrheology and particle tracking.[47,48]

If a molecule is shined with light, it will emit different coloured light. This is called fluorescence. Principally, the molecule will absorb high energy radiation and emit photon with less energy. The colour of light excited and emitted depends on the material.

A dichroic mirror is an important part of a microscope, which reflects light shorter than a particular wavelength while pass light longer than that. This uses the objective to illuminate the sample from above. This fluorescence is called epifluorescence. The most important part of a confocal microscope is the pinhole. Rays of different wavelengths are emitted from different parts of the sample resulting in a blurred image. We get a clear image only if the light rays with wavelength originating from the focal point of the lens system. The idea of blocking all the out-of-focus rays by placing a screen with a pinhole is the core of confocal microscopy. The pinhole is positioned in such a way that the focal point of the objective lens forms the image at the pinhole. This means the pinhole is **con**jugate to the **focal** point of the objective, and thus the name confocal. The practical importance of this pinhole comes when an image from a very thin sliced sample is taken.

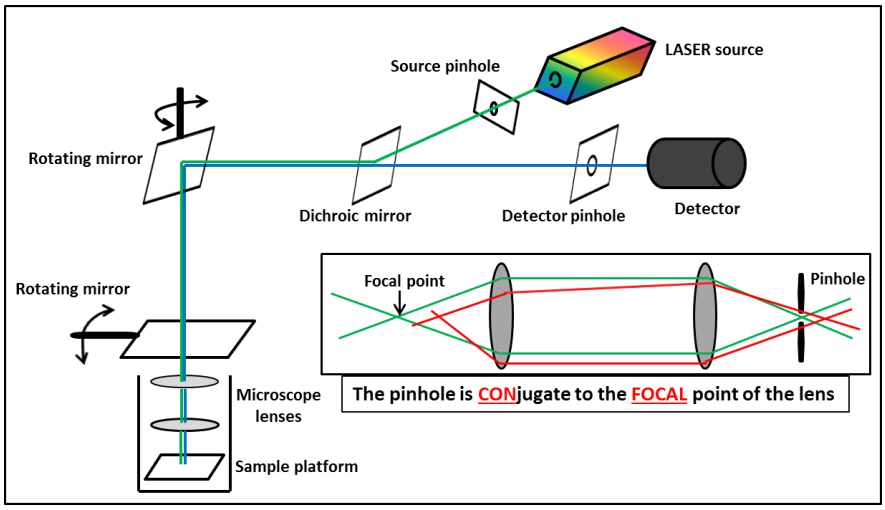

Figure 2.12: Pictorial representation of a typical confocal microscopy setup. Inset shows how the pinhole is cutting out-of-focus rays.

2.8.5. UV-Visible spectroscopy

When light of wavelength in the ultraviolet region (190-380 nm) is absorbed by a molecule, the electrons get excited from the ground state to higher energy states. The spectrum

formed by the absorption is UV spectrum. If the absorption range covers lights of higher wavelengths from 380 nm to 750 nm (visible region), it is called UV-Visible spectroscopy. Beer Lambert's law forms the basis of UV-Visible spectroscopy.

Beer Lambert's law provides a direct correlation between the absorbance and concentration of the absorbing molecule.[49] According to Beer-Lambert law, the absorbance A, of a solution is directly proportional to the concentration of the absorbing species in the solution and the path length of L. The greater the number of molecules capable of absorbing light of a given wavelength, the greater the extent of absorption. This can be expressed as:

$$A = \log (I_0/I) = \epsilon cL \qquad 2.22$$

A = absorbance

I_0 = intensity incident light

I = intensity of transmitted light

c = Concentration of absorbing species

L = path length through the sample

ϵ = molar absorptivity

2.8.6. Differential Scanning Calorimetry (DSC)

Differential Scanning Calorimetry (DSC) is the most often used calorimetric method because it is rapid, easy to operate and readily available. DSC is a technique in which a controlled temperature programme is given to the system with the substance and a reference material is kept in the controlled environment and the difference of heat flow into a substance and reference material is measured as a function of temperature.[50] The substance under testing or the specimen of small mass contained in an appropriate holder (pan) and an empty reference holder of the same material and size are placed in the DSC cell in the sample and reference positions. Aluminium pans are usually used for both reference and sample. Reference pan will be kept empty. These are then put through a temperature profile, by applying power to heaters in the system be it a heating and/or cooling or isothermal treatment and the equipment measures the difference in heat flow between the sample and reference. The temperature of the sample will lag behind that of the empty pan according to the capacity of material to take up heat. The temperature difference between the two is small, and the heat flowing into the sample is measured.

2.9. References

1 R. H. Pelton and P. Chibante, *Colloids and Surfaces*, 1986, **20**, 247–256.

2 X. Wu, R. H. Pelton, a E. Hamielec, D. R. Woods and W. McPhee, *Colloid Polym. Sci.*, 1994, **272**, 467–477.

3 I. Varga, T. Gilányi, R. Mészáros, G. Filipcsei and M. Zrínyi, *J. Phys. Chem. B*, 2001, **105**, 9071–9076.

4 R. Acciaro, T. Gilányi and I. Varga, *Langmuir*, 2011, **27**, 7917–7925.

5 Q. S. Zhang, L. S. Zha, J. H. Ma and B. R. Liang, *J. Appl. Polym. Sci.*, 2007, **103**, 2962–2967.

6 X. C. Xiao, *Express Polym. Lett.*, 2007, **1**, 232–235.

7 R. H. Peltor, H. M. Pelton, A. Morphesis and R. L. Rowell, *Langmuir*, 1989, **5**, 816–818.

8 M. J. Snowden, B. Z. Chowdhry, B. Vincent and G. E. Morris, *J. Chem. Soc. - Faraday Trans.*, 1996, **92**, 5013–5016.

9 M. Shibayama, F. Ikkai, S. Inamoto, S. Nomura and C. C. Han, *J. Chem. Phys.*, 1996, **105**, 4358–4366.

10 T. C. Halsey and W. Toor, *Phys. Rev. Lett.*, 1990, **65**, 2820–2823.

11 J. Martin, J. Odinek, T. Halsey and R. Kamien, *Phys. Rev. E*, 1998, **57**, 756–775.

12 E. Ruel-Gariépy and J. C. Leroux, *Eur. J. Pharm. Biopharm.*, 2004, 58, 409–426.

13 B. R. Saunders, N. Laajam, E. Daly, S. Teow, X. Hu and R. Stepto, *Adv. Colloid Interface Sci.*, 2009, **147**–**148**, 251–262.

14 S. Nayak and L. Andrew Lyon, *Angew. Chemie - Int. Ed.*, 2005, **44**, 7686–7708.

15 C. Obeso-Vera, J. M. Cornejo-Bravo, A. Serrano-Medina and A. Licea-Claverie, *Polym. Bull.*, 2013, **70**, 653–664.

16 A. Burmistrova, M. Richter, C. Uzum and R. V. Klitzing, *Colloid Polym. Sci.*, 2011, **289**, 613–624.

17 M. Wiemann, N. Willenbacher and E. Bartsch, *Colloids Surfaces A Physicochem. Eng. Asp.*, 2012, **413**, 78–83.

18 B. R. Saunders, *Langmuir*, 2004, **20**, 3925–3932.

19 M. Stieger, J. S. Pedersen, P. Lindner and W. Richtering, *Langmuir*, 2004, **20**, 7283–7292.

20 F. Scheffold, P. Díaz-Leyva, M. Reufer, N. Ben Braham, I. Lynch and J. L. Harden, *Phys. Rev. Lett.*, 2010, **104**, 1–4.

21 L. Arleth, X. Xia, R. P. Hjelm, J. Wu and H. U. Zhibinc, *J. Polym. Sci. Part B Polym. Phys.*, 2005, **43**, 849–860.

22 T. Still, K. Chen, A. M. Alsayed, K. B. Aptowicz and A. G. Yodh, *J. Colloid Interface Sci.*, 2013, **405**, 96–102.

23 M. H. Kwok, Z. Li and T. Ngai, *Langmuir*, 2013, **29**, 9581–9591.

24 S. Zhou and B. Chu, *J. Phys. Chem. B*, 1998, **102**, 1364–1371.

25 M. Andersson and S. L. Maunu, *J. Polym. Sci. Part B Polym. Phys.*, 2006, **44**, 3305–3314.

26 F. M. Winnik, H. Ringsdorf and J. Venzmer, *Macromolecules*, 1990, **23**, 2415–2416.

27 H. Senff and W. Richtering, *J. Chem. Phys.*, 1999, **111**, 1705–1711.

28 R. Pecora, Ed., *Dynamic Light Scattering*, Springer US, Boston, MA, 1985.

29 B. H. Zimm, *J. Chem. Phys.*, 1948, **16**, 1099–1116.

30 Lord Rayleigh, *Philos. Mag. Ser. 5*, 1881, **12**, 81–101.

31 P. Debye, *Ann. Phys.*, 1915, **351**, 809–823.

32 M. Reufer, P. Díaz-Leyva, I. Lynch and F. Scheffold, *Eur. Phys. J. E*, 2009, **28**, 165–171.

33 B. J. Berne and R. Pecora, *Dyn. Light Scatt. With Appl. to Chem. Biol. physics., by Berne, B. J.; Pecora, R.. New York, NY Wiley-Interscience, 8 + 376 p.*

34 K. Schatzel, M. Drewel and J. Ahrens, *J. Phys. Condens. Matter*, 1990, **2**, SA393-SA398.

35 C. Urban and P. Schurtenberger, *J. Colloid Interface Sci.*, 1998, **207**, 150–158.

36 C. Urban, S. Romer, F. Scheffold and P. Schurtenberger, *Macromol. Symp.*, 2000, **162**, 235–247.

37 K. Schätzel, *J. Mod. Opt.*, 1991, **38**, 1849–1865.

38 D. J. Pine, D. A. Weitz, P. M. Chaikin and E. Herbolzheimer, *Phys. Rev. Lett.*, 1988, **60**, 1134–1137.

39 M. Medebach, C. Moitzi, N. Freiberger and O. Glatter, *J. Colloid Interface Sci.*, 2007, **305**, 88–93.

40 J. D. Ferry, *Viscoelastic Properties of Polymers*, Wiley, 1980.

41 J. Mewis and N. J. Wagner, *Colloidal suspension rheology*, Cambridge University Press, Cambridge, 2011, vol. 9780521515.

42 R. H. Ewoldt, G. H. McKinley and A. E. Hosoi, *J. Rheol. (N. Y. N. Y).*, 2007, **52**, 1427–1458.

43 M. Minsky, *Scanning*, 1988, **10**, 128–138.

44 M. H. Chestnut, *Curr. Opin. Colloid Interface Sci.*, 1997, **2**, 158–161.

45 V. Prasad, D. Semwogerere and E. R. Weeks, *J. Phys. Condens. Matter*, 2007, **19**, 1–25.

46 M. C. Jenkins and S. U. Egelhaaf, *Adv. Colloid Interface Sci.*, 2008, **136**, 65–92.

47 T. Moschakis, B. S. Murray and E. Dickinson, *Langmuir*, 2006, **22**, 4710–4719.

48 C. P. Royall, A. A. Louis and H. Tanaka, *J. Chem. Phys.*, 2007, **127**, 044507.

49 D. F. Swinehart, *J. Chem. Educ.*, 1962, **39**, 333.

50 M. E. Brown, *Introduction to thermal analysis: techniques and applications*, 1988.

CHAPTER 3

DYNAMICS OF PNIPAM COLLOIDAL MICROGELS: ROLE OF PARTICLE MORPHOLOGY

In this chapter, the dynamics of PNIPAm glasses were investigated under large amplitude oscillatory shear (LAOS). Here the effect of the particle morphology on the nonlinear rheological behaviour of the microgel is investigated. Particles with different radial density profile were used for the study. The effect of the amount of crosslinker on the nonlinear rheological behaviour of the microgel is also studied in the second part of this chapter. Particles with five different crosslink densities were synthesized for this study. Large amplitude oscillatory shear provides the information about non-linear behaviours like shear thinning, shear thickening etc. All the samples were highly dense with a range of volume fractions from $\phi = 1$ to $\phi = 2$.

3.1. Introduction

The mechanical properties of many important commercial products which are composed of dense colloidal suspensions are affected by the shear due to induced flow in the microstructure while processing. An understanding on how microstructure affects the rheology of these materials will help to tailor the processability conditions to make useful products from these materials. So it is important to study the structure-property relations in these complex fluids over a range of length and time scales, both under dormant conditions, and under shear. These materials, usually viscoelastic in nature, also possess yield stress, a minimum stress required to induce flow in these materials. A prominent method for understanding the yielding in materials is to use oscillatory rheology technique in which an oscillatory flow field with increasing stress (strain) is applied to a yield stress material. For small stress or strain, the elastic moduli (G') as well as viscous moduli (G") remain constant with G'>G". With increase in strain, the viscous modulus increases from its linear value and reaches a maximum value (peak) before decreasing, while G' decreases monotonically with strain and crosses below G" at the yield point. This behaviour at higher strains were reported for soft colloidal glasses,[1] emulsions[2,3] and gels.[4]

Linear stress strain experiments give lot of information on the linear response of viscoelastic fluids. Colloidal glasses under quiescent conditions show predominantly elastic response in a small amplitude oscillatory shear (SAOS) tests. SAOS can provide linear viscoelastic properties of complex fluids in dormant conditions. Easily executable test protocols and strong theoretical background strengthens the use of SAOS for probing linear viscoelastic properties of complex fluids.[5,6] The sample characterization is complete with both the linear and nonlinear test methods because during most of the processing or application of the soft matter, the deformations occurring in the material will be brisk and large and at that point the nonlinear

properties control the response of the system. Large amplitude oscillatory shear (LAOS) tests are used to investigate and quantify the nonlinear viscoelastic behavior of complex fluids.[7] LAOS is a tool of paramount importance for a rheologist for analyzing deep into the non-linear behaviour of colloids and other complex materials. While SAOS contribute to the linear viscoelastic properties of the material, LAOS is conferred with non-linear behaviour also.[8] Strain amplitude and frequency of relevant range should be selected for LAOS and SAOS as experimental inputs; but the material response varies for both. At large strain amplitude, response will be nonlinear in LAOS and at that point SAOS tests become irrelevant. Since the nonlinear stress response becomes non sinusoidal, linear viscoelastic moduli (storage and loss) cannot be used to quantify nonlinear response under LAOS conditions. Consequently, for each oscillatory strain amplitude, the full wave form of the stress response is documented and resolved by large-amplitude oscillatory shear (LAOS) and it will thus contain higher harmonics which are interpreted in terms of harmonic moduli G'_n and G''_n (subscript n refers to the n^{th} harmonic). These are functions of both the strain amplitude and the angular frequency. Reviews have been published depicting the use and sensitiveness of SAOS and LAOS of complex fluids and showed that LAOS behaviour was very much sensitive to shear-induced microstructure formation.[6]

Highly monodisperse dense suspensions of PNIPAm microgels at volume fractions above 1 are investigated in this chapter. At high volume fractions, the loose brushes on the surface of the particles are expected to interpenetrate and interact.[9] The interparticle potential of PNIPAm microgels measured in dilute suspensions, changes from soft repulsive to attractive, below and above the volume phase transition temperature, respectively.[10–12] This potential change occurring due to the interpenetration of chains may vary with the morphology. The complex yielding behavior of PNIPAm microgel suspensions with two different particle morphologies are investigated in detail in this chapter. A phenomenon of double peak in G" was observed when the strain amplitude sweeps were performed at higher strains. Double yielding phenomenon was observed earlier in star polymers where the second peak is attributed to the relaxation of long star arms[13,14] and also in attraction induced particles,[15] where the two peaks were attributed to cage breaking and bond breaking. Present study on PNIPAM microgel suspension investigates deep into the mechanism of double yielding.

The second part of this chapter provides an insight into the effect of amount of crosslinker added to the reaction medium in the morphology and yielding behaviour of the

microgel. PNIPAm microgels with 5 different crosslinker contents were prepared for the study. Both core-shell type and homogeneous type morphologies were investigated.

3.2 Synthesis of microgels

The synthesis was done by free radical precipitation polymerization with sodium dodecyl sulphate (SDS) as the surfactant to achieve smaller particle size. The detailed synthesis procedure is explained in the section 2.6 of chapter 2. The batch synthesis of PNIPAM microgels was based on a conventional method developed by R. Pelton and P. Chibante[16] while the synthesis procedure for particles with homogeneous crosslink density is based on a paper by Roberta Acciaro.[17] Core-shell samples with 5 different crosslinker contents viz 0.5%, 2.5%, 5%, 10% and 20% were synthesized and labelled as CS1, CS2, CS3, CS4 and CS5 respectively. Similarly, 5 homogeneous microgel particles were also made with 5 different crosslinker content. They were labelled as HM1, HM2, HM3, HM4 and HM5 with 0.5%, 2.5%, 5%, 10% and 20% BIS content respectively. Amount of crosslinker is represented in % per % of monomer content.

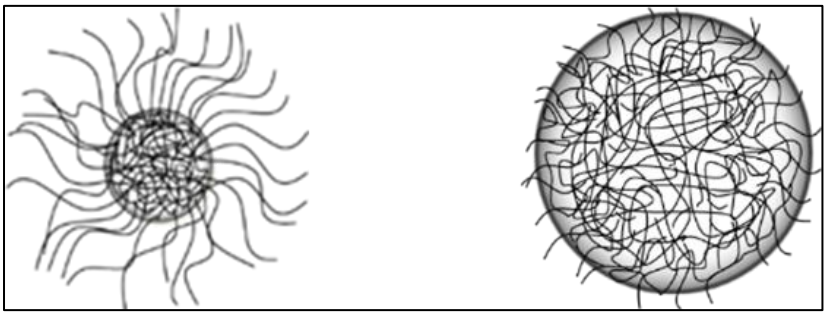

Figure 3.1: PNIPAm particles of two different morphologies achieved by different synthesis strategy.

Required concentration for characterizations were made by redispersing calculated amount of freeze dried samples in DI water after determining the volume fraction.

3.3. Determination of effective volume fraction

Effective volume fractions of all samples were determined by viscometry. We followed the method described by Senff and Richtering. The procedure is detailed in experimental methods section (section 2.8.1) of second chapter. The volume fraction`ϕ'of all our samples investigated in this work is much above 1 and hence are in a dense glassy state. Table 3.1 summarizes the volume fraction details of the samples used in our study.

Sample	Slope	Shift factor (κ)	Volume fraction @C= 1 wt%
CS1	1.08	0.4326	0.4326
CS2	0.5735	0.2294	0.2294
CS3	0.4762	0.1905	0.1905
CS4	0.3041	0.1216	0.1216
CS5	0.165	0.066	0.066
HM1	1.13	0.452	0.452
HM2	0.7594	0.3038	0.3038
HM3	0.6784	0.271	0.271
HM4	0.7097	0.2839	0.2839
HM5	0.2438	0.0975	0.0975

Table 3.1: Volume fraction of samples CS and HM determined by capillary viscometry.

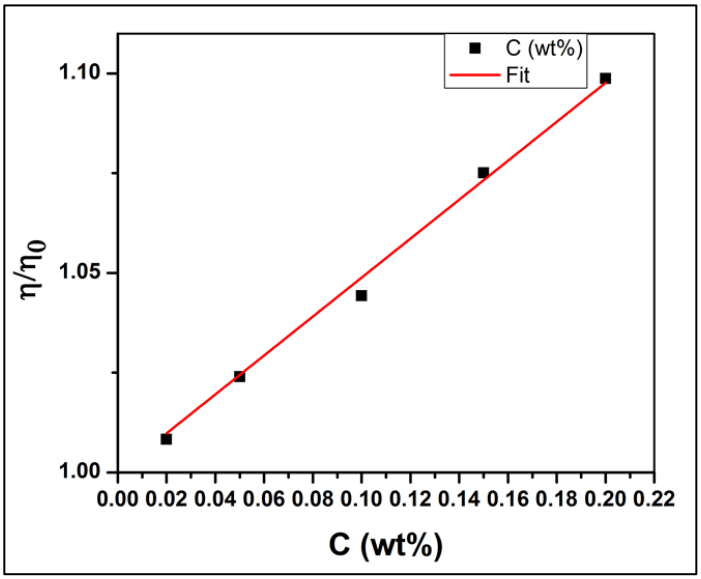

Figure 3.2: Relative viscosity as a function of concentration for PNIPAm microgel suspension.

3.4 Characterization

3.4.1. Static & Dynamic light scattering

The hydrodynamic particle size (R_h) was measured as a function of temperature using 3D- dynamic light scattering (LS Instruments AG, Switzerland) with a laser wavelength of 632.8 nm. The 3D-DLS technique is used to get the structure and dynamics of highly turbid suspensions.[18] It uses a special beam splitter to generate two identical parallel laser beams from

the H-Ne laser and uses cross-correlation geometry to eliminate the contributions from multiple scattering. The temperature of the sample was maintained using a refrigerated bath circulator with water circulating channels around a toluene bath where the sample is kept. The particle size was measured at an angle of $\theta = 90^{o}$, which corresponds to a scattering vector $q = 1.868 \times 10^{7}\ m^{-1}$. The scattering vector is defined as

$$q = \left(\frac{4\pi n}{\lambda}\right) sin\left(\frac{\theta}{2}\right) \quad 3.1$$

where, 'n' is the refractive index of the solvent in which the particles are dispersed, 'λ' is the wavelength of the laser and 'θ' is the scattering angle. Swelling ratios of the particles $R_h(43)/R_h(23)$ were found for each sample. Here, $R_h(43)$ is the hydrodynamic radius of the microgel particle at 43°C and $R_h(23)$ is the hydrodynamic radius at 23°C. Table 3.2 provides the hydrodynamic diameter D_h, the volume phase transition temperature (VPTT) and swelling ratio of all the samples. Static light scattering measurements were also done using the same experimental setup to find the radius of gyration (R_g) and shape factor R_g/R_h for all the samples. Table 3.3 provides the hydrodynamic radius R_h, the radius of gyration (R_g) and the shape factor R_g/R_h obtained from static and dynamic light scattering experiments for the samples.

3.4.2. Rheology

All rheology experiments were done on a stress controlled rheometer (Physica MCR301, Anton Paar). The geometry used was a cone and plate (cone angle 1°, diameter 25mm). To minimize water evaporation, a solvent trap was placed around the sample during the rheological experiments. To exclude the thermal and deformation history of the sample, fresh sample was loaded for each measurement and the temperature of loading (T_{load}= 28°C) was kept at a higher temperature than the measurement temperature (T_{exp}= 20°C). After loading the sample, it was incubated for 10 minutes before starting the experiment. Loading the sample at a higher temperature than experimental temperature allows the sample to swell a little bit and gives it a controlled history. It was made sure that the loading and the experiment was done well below the VPTT of the sample to avoid aggregation of the particles.

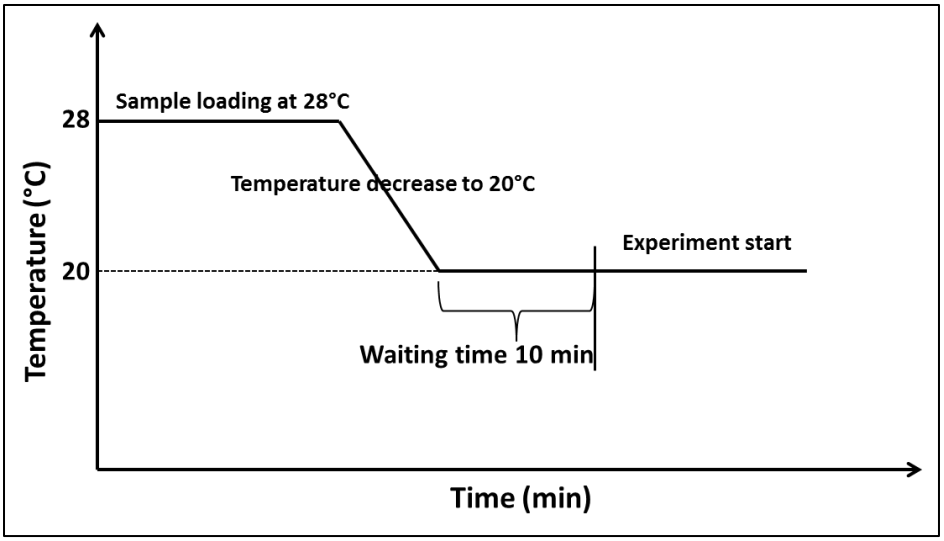

Figure 3.3: Experiment protocol scheme showing loading temperature, experiment temperature and waiting time before rheological measurements.

3.5. Results and discussion

The PNIPAM microgel particles are temperature sensitive. The size and the apparent volume fraction (ϕ_{eff}) of the microgel particles changes with temperature. The apparent volume fraction (ϕ_{eff}) can be tuned without changing the number density of particles. Moreover, the interaction potential between the microgel particles changes from repulsive to attractive above the volume phase transition temperature (VPTT).[19,20] However, in all our experiments, the investigation is carried out at temperatures well below the VPTT. The volume fractions of all our samples are above 1 and hence they are in a dense glassy state. In this chapter, the results of investigation on the origin of double yielding in soft colloidal glasses and the effect of particle morphology are provided. We use non-linear rheology to investigate the yielding behavior of the microgel suspensions.

3.5.1. Static & Dynamic Light Scattering

The particle size of the synthesized microgels was measured using 3D-dynamic light scattering technique. The particle size as a function of temperature for both the core-shell (CS3) particles as well as homogeneous particles (HM3) is plotted in figure 3.4 and the details are summarized in table 3.2.

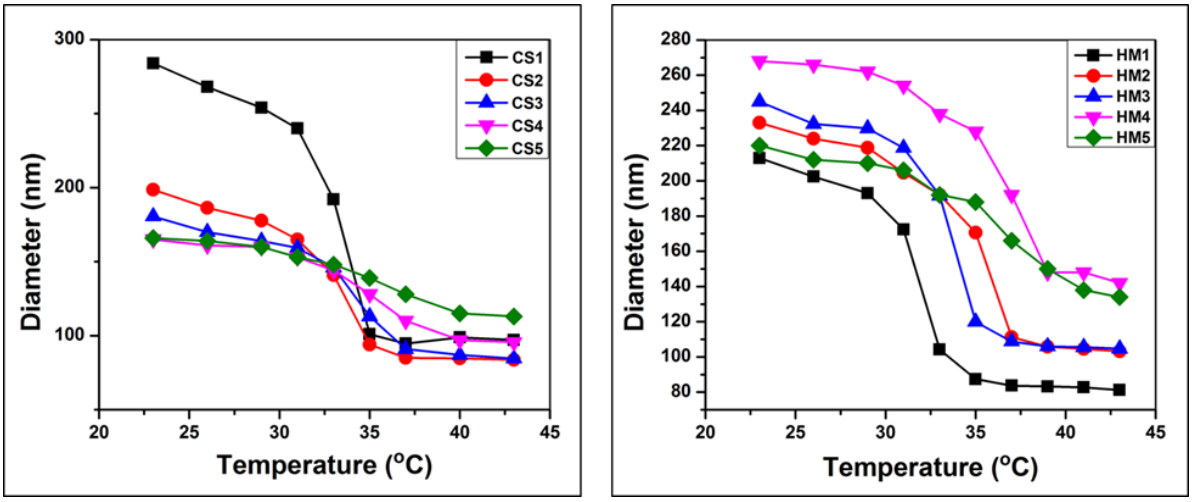

Figure 3.4: Hydrodynamic diameter (D_h) as a function of sample temperature obtained from dynamic light scattering (DLS) under dilute conditions for the core-shell samples (CS) and homogeneous samples (HM), with 5 different crosslink density, respectively.

Sample	BIS % (% of NIPAm)	Diameter at 23°C (nm)	Diameter at 43°C (nm)	VPTT (°C)	Swelling Ratio ($R_{h(43)}/R_{h(23)}$)
CS1	0.5	284	97.1	33	0.342
CS2	2.5	198.7	83.78	33	0.422
CS3	5	180.6	84.6	34	0.468
CS4	10	165	95.6	35	0.581
CS5	20	166	113	35	0.679
HM1	0.5	212	82	32	0.39
HM2	2.5	233	103.2	35	0.443
HM3	5	245	105	35	0.429
HM4	10	268	150	37	0.52
HM5	20	220	140	37	0.63

Table 3.2: Hydrodynamic diameter, VPTT and Swelling ratio of microgel particles.

The VPTT of the core-shell (CS) particles is seen to increase with the crosslinker content and is in the range 32°C to 35°C while for the homogeneous particles, it ranges from 32°C to 37°C. The VPTT of the core-shell particles (CS3) with 5% crosslinker content and its homogeneous analogue (HM3) are around 34°C& 35°C respectively. There is no trend in the size of particles with crosslinker amount but definitely there is an increasing trend in swelling ratio and VPTT. Core-shell particles with 5% crosslink density (CS3) shows a size of 180 nm at 23°C

with a swelling ratio of 0.468 while homogeneous particles with 5% crosslink density (HM3) shows a size of 245 nm at 23°C with a swelling ratio of 0.429. Core-shell particles with 0.5% crosslink density (CS1) show a swelling ratio of 0.342 and particles with highest crosslink density (CS5) has a swelling ratio of 0.679. Similarly, homogeneous particles with 0.5% crosslink density (HM1) have a swelling ratio of 0.39 and particles with highest crosslink density (HM5) have a swelling ratio of 0.63. This means that with the increase in crosslinker amount in the system, the particles show lesser tendency to shrink. Static light scattering was used to measure the radius of gyration R_g of the particles as well as the shape factor R_g/R_h.

Sample	R_g (nm)	R_h (nm)	R_g/R_h
CS1	62	142	0.4366
CS2	60.44	95	0.6362
CS3	59.6	90.3	0.66
CS4	56.53	80	0.707
CS5	63.17	83	0.7602
HM1	76	106.5	0.713
HM2	82.02	112.5	0.729
HM3	90.1	122.5	0.74
HM4	101.6	134	0.758
HM5	89.6	110	0.79

Table 3.3: Shape factor values of both core-shell and homogeneous samples depicting all particles with homogeneous crosslink density having hard sphere values and core shell particles with crosslinker content above 5% also near hard sphere values.

Table 3.3 summarizes the results of static light scattering measurements. It can be seen that R_g/R_h value for the core-shell (CS3) particles is 0.66 and for homogeneous particles (HM3) it is 0.74. It has been reported that the R_g/R_h value for hard spheres is around 0.778 and for microgels and other soft particles; it is much less than the hard sphere value.[21] The R_g/R_h value (shape factor) for the core-shell particles slowly increases from a minimum of 0.43 for CS1 (0.5% BIS) to a maximum of 0.76 for CS5 (20% BIS) proving that the morphology slowly changes from a soft sphere with long brushes on the surface to a hard sphere nature with shape factor value near 0.778. In the case of all homogeneous samples except for the sample with

lowest crosslink density (HM1 and HM2), the R_g/R_h value is near or above the hard sphere value of 0.778.

3.5.2. Linear rheology of dense PNIPAM glasses from core-shell and homogeneous microgel particles

In linear rheology, the storage modulus (G') and loss modulus (G") of the samples are measured as a function of oscillation frequency, ω under the application of a constant strain amplitude, γ. The frequency dependence of G' and G" in the linear regime (at small strain amplitude, γ= 0.5%) for the core-shell sample with 5% crosslinker content CS3 and homogeneous sample HM3 at a temperature of T = 20°C is shown in figure 3.5 for a constant volume fraction of ϕ = 1.5.

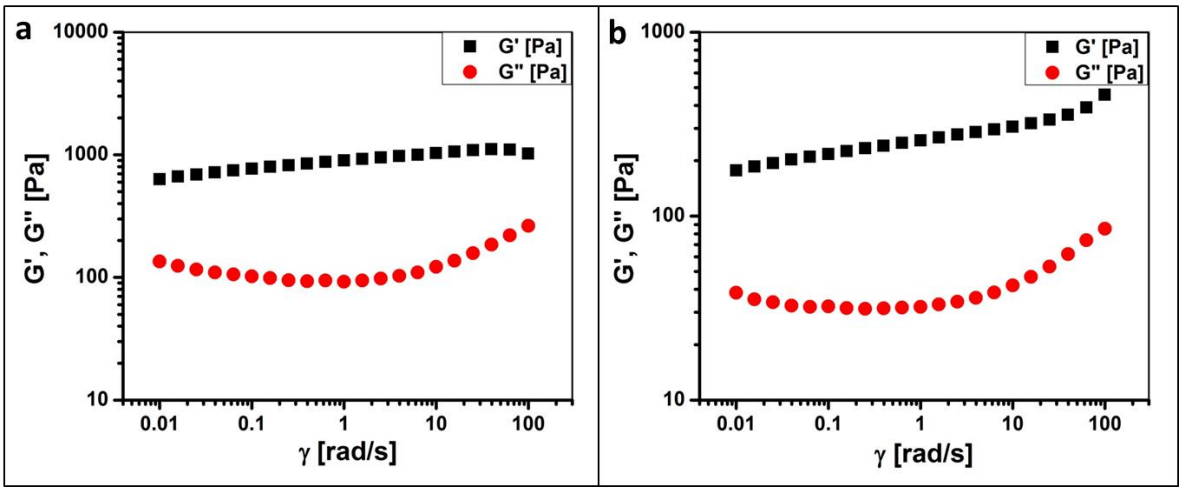

Figure 3.5: Storage modulus G' (solid symbols) and loss modulus G" (open symbols) as a function of oscillation frequency, ω at a small strain of γ= 0.5% for (a) core-shell microgel sample CS3 (5% BIS) and (b) homogeneous microgel sample HM3 (5% BIS) at a sample temperature of 20°C for a constant volume fraction of ϕ= 1.5

From figure 3.5 (a) it is evident that within the frequency range measured (10^{-2}–10^{2} rad/s), G' is always greater than G" and G' is almost independent of frequency for core-shell particles. Thus, the sample behaves like solid in this frequency range and for this small shear strain. The loss modulus G" shows a weak minimum at a frequency ω_β of around 1 rad/sec suggesting the linear rheological behavior of PNIPAM microgel glasses to be similar to that reported for other colloidal glasses.[22] According to a recent mechanical spectroscopic analysis of PNIPAM microgel suspension, plateau in G' and minimum in G" also implies that the microgel sample under

investigation (CS3) is repulsive glass.[23] The frequency ω_β scales with the fast or beta relaxation process of the colloidal glasses,[24] which arises due to the rattling of the particles within the near neighbor cage.[22] The frequency ω_β marks the crossover of dynamics from alpha relaxation to beta relaxation.[25] At frequencies lower than ω_β, a small upturn of G" was observed indicating a possible crossover with G', which corresponds to the slower structural relaxation (α-relaxation) arising from the escape of a particle from its cage. The crossover frequency ω_α corresponds to the α-relaxation time t_α. At frequencies above ω_β, viscous modulus increases again due to dissipation related to fast movement of particles inside the cage. The cage effect is maximum at β-relaxation frequency and so a dip in G". Since the alpha relaxation times in PNIPAM microgel glasses are very large, ω_α is very small and falls out of our measurement window.

Since the aim of our current work is to investigate the role of particle morphology on the yielding behaviour of PNIPAM microgel glasses, we also did rheological measurements on homogeneous PNIPAM particle suspensions synthesized using the continuous feed method described in the synthesis section 2.6.3 of chapter 2. Figure 3.5 (b) represents the frequency dependence of G' and G" for the homogeneous sample. The observation here is similar to that of core-shell particles. The sample behaves like solid in this frequency range and for this small shear strain. The beta relaxation frequency comes at around 1 rad/s. The α-relaxation frequency is out of the frequency range measured.

Figure 3.6 gives the dependence of G' and G" with frequency for samples for 4 different volume fractions ϕ=1.0, 1.25, 1.5 and 2.0 respectively. It can be seen from the figure that G' is always greater than G" and has only a weak frequency dependence whereas G" has a shallow minimum at the oscillation frequency of ω=1 rad/s. It was earlier proved that the change in the shape of G" plot from a curvy with a minimum at ω_β, to a flatter one represents the change in the phase of the particles from glassy to a jammed state.[26] In our case, for all the samples, the shape of G" curve remains the same and does not becoming plateau with increasing the particle volume fraction, implies that all the samples are below squeezed (or jammed state). This observation is similar for both core-shell and homogeneous particles.

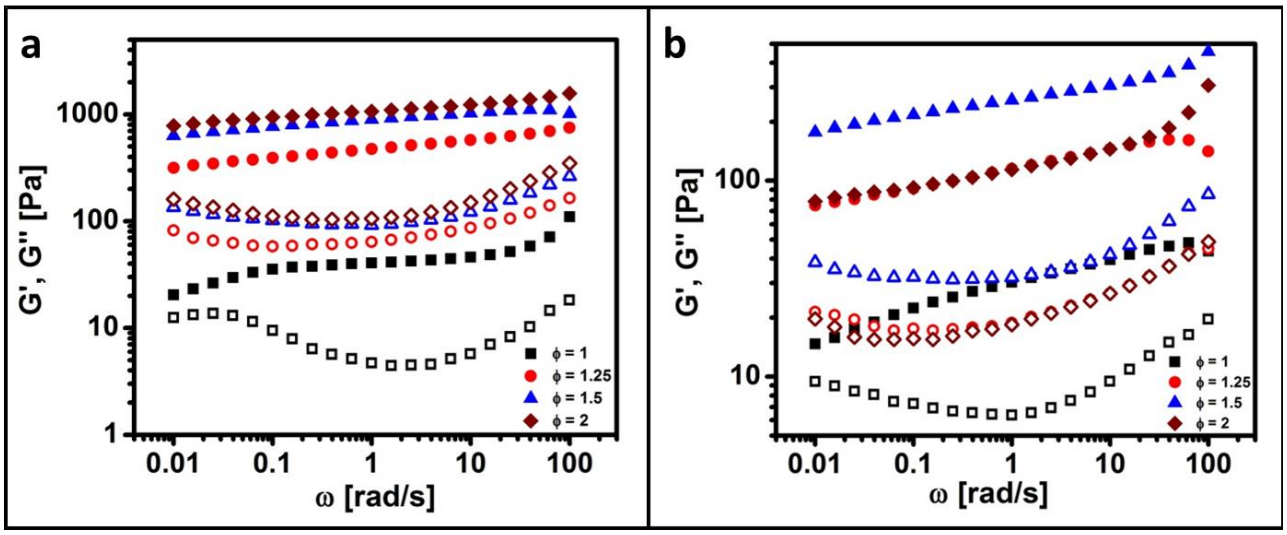

Figure 3.6: Storage modulus G' (solid symbols) and loss modulus G" (open symbols) as a function of oscillation frequency, ω at a small strain of γ= 0.5% for (a) core-shell microgel sample CS3 (5% BIS) and (b) homogeneous microgel sample HM3 (5% BIS) at a sample temperature of 20°C for 4 different volume fractions ϕ=1.0, ϕ=1.25, ϕ=1.5 and ϕ=2.0

3.5.3. Yielding behaviour of dense microgel glasses of core-shell and homogeneous microgel particles

Both the core-shell microgel samples (CS3) and homogeneous samples (HM3) are subjected to non-linear rheological measurements by performing dynamic strain sweep (DSS) measurements to understand the yielding process in these materials. In DSS, a sinusoidal strain is applied whose frequency ω is constant but whose amplitude γ is increased in steps, starting in the linear viscoelastic regime and progressing to non-linear regime. The stress response from the samples is recorded as a function of strain amplitude γ. The strain amplitude is varied over a wide range (0.1 – 1000%) at a fixed value of frequency. The intension of conducting DSS is to understand the role of particle morphology in the non-linear yielding behavior of microgel glasses. Since the beta relaxation frequency, ω_β is around 1.0 rad/sec we performed all our DSS experiments at frequencies above 1.0 rad/sec to see the role of the dangling polymer chains in the case of core-shell microgel particle suspensions. 4 oscillation frequencies (ω = 1.0, 10, 20 & 50 rad/sec) were chosen.

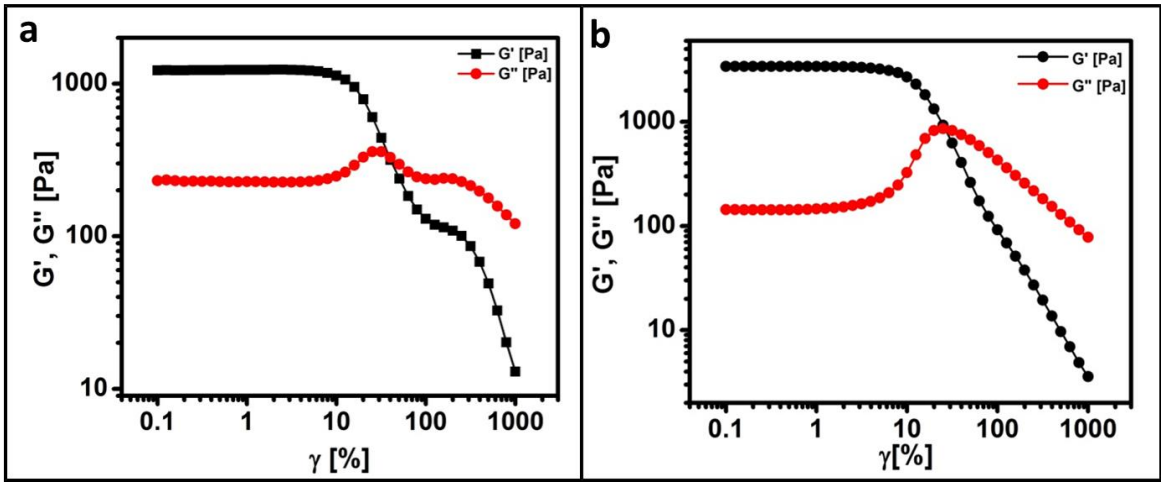

Figure 3.7: Dependence of the storage modulus G' (solid symbols) and loss modulus G" (open symbols) on the strain for oscillation frequency ω = 50 rad/sec for (a) core-shell microgel sample CS3 (5% BIS) and (b) homogeneous microgel sample HM3 (5% BIS) at a sample temperature of 20°C for a sample concentration of ϕ=1.5

Figure 3.7(a) shows the variation of storage modulus G' and loss modulus G" as a function of strain amplitude γ for the core-shell glass sample CS3 at a volume fraction of 1.5 at a frequency of 50 rad/s. Since our samples are in a highly dense glassy state, we chose the highest frequency of 50 rad/sec to see if the entanglement of dangling polymer chains has any role in the yielding of the microgel glasses made of core-shell particles. For lower values of γ, both G' and G" exhibit a plateau with G' > G" indicating the region over which the microgel glasses show linear response to the applied strain γ. For larger γ, G' starts decreasing indicating yielding of glasses under applied shear. With further increase in γ, G' further comes down and goes below G". The point at which the crossover of G' & G" takes place is called the crossover point and the corresponding values of strain γ_c and stress σ_c are called the crossover strain and crossover stress respectively. Beyond the crossover point, the sample CS3 behaves like a viscoelastic liquid (G' < G") due to the shear melting of glasses. In the non-linear regime, G' shows a monotonic decrease with increase in strain amplitude γ, a behaviour similar to that of hard sphere glasses reported in literature.[27] However, the viscous modulus, G" shows a completely different behaviour compared to the hard spheres. In contrast to the single peak in G" reported for hard spheres, G" for the microgel glass sample CS3 shows two peaks. G" exhibits 2 peaks at two different values of γ indicating that two microscopic mechanisms are operational during the yielding process of the PNIPAM microgel glasses. We interpret the yielding mechanism of dense

PNIPAm microgel glasses as i) breaking of entanglement of dangling polymer chains from the shells of neighboring microgel particles, giving rise to the first peak in G" at lower strain and ii) the breaking of the near neighbor cages giving rise to the second peak in G" at a larger strain. Although two step yielding has been observed in attractive colloidal glasses,[15] this is one of the first observation of two step yielding in pure PNIPAm microgel glasses. Very recently, Joshi and Tata observed the similar phenomenon in PNIPAm microgels.[28] In attractive colloidal glasses the two step yielding have been interpreted as due to i) breaking of near-neighbour bonds arising from attractive interactions leading to the first peak in the loss modulus (G") and ii) breaking of the cages of the neighbouring particles leading to the second peak in G". However, in our case, we are working at sample temperatures much below the volume phase transition temperature (VPTT), where the particle-particle interaction potential is purely repulsive. Hence, the first peak in G" in the PNIPAm microgel case is due to the disentanglement of dangling chains of the neighbouring microgel particles. The interpenetration of dangling chains gives rise to an attractive like potential in an otherwise purely repulsive system.

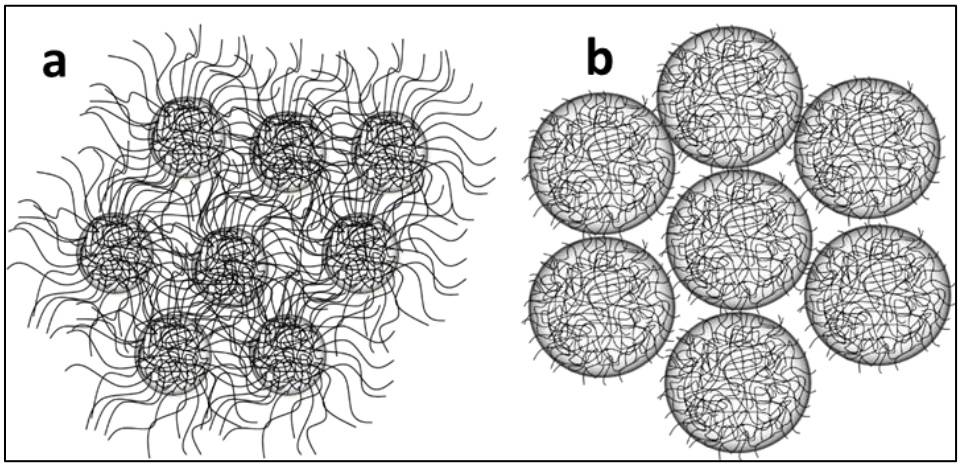

Figure 3.8: (a) Interaction between particles of core-shell morphology showing the interpenetration of surface brushes of particles and (b) Interaction between particles of homogeneous crosslink density where surface brushes are absent and hence the interpenetration also.

If the dangling chains play any role in the yielding mechanism, the absence of the same should show a difference in the yielding behaviour. To check this, we now subject the homogeneous microgel particle suspensions to non-linear rheology. Figure 3.7 (b) shows the variation of storage modulus G' and loss modulus G" as a function of strain amplitude γ for the homogeneous glassy sample HM3 at a volume fraction of $\phi = 1.5$ at an oscillation frequency of

ω =20 rad/sec. Experiment was also done at 50 rad/s where the moduli curves experienced disturbances. It can be seen that the homogeneous microgel glasses yield with a single yielding point similar to the hard sphere glasses. The nature of G' and G" for lower strains is similar to the core-shell microgel samples. For lower values of γ, both G' and G" exhibit a plateau with G' > G" indicating the region over which the microgel glasses show linear response to the applied strain γ. For larger γ, G' starts decreasing indicating yielding of glasses under applied shear. With further increase in γ, G' further comes down and goes below G".

Beyond the crossover point, all the samples behave like viscoelastic liquids (G' < G") due to the shear melting of glasses. In the non-linear regime, G' shows a monotonic decrease with increase in strain amplitude γ, a behaviour similar to that of hard sphere glasses reported in literature. However, unlike the core-shell glassy sample case, the loss modulus G" shows only one peak similar to the hard sphere glasses. The absence of the second peak in G" according to us is due to the homogeneous nature of the microgel particles synthesized by the continuous feed method. There are no dangling chains which can interpenetrate and give rise to the first peak as in the core-shell case. The only peak in G" is due to cage breaking as in the hard sphere glasses. From our static light scattering experiments explained in the experimental section 3.5.1, the R_g/R_h ratio for the homogeneous microgel particles is close to the value of 0.778 and hence the homogeneous microgel samples behave similar to hard spheres.

Figure 3.9 (a) shows the effect of concentration on the yielding of core-shell microgels samples CS3 for 4 different volume fractions ϕ = 1.0, 1.25, 1.5 and 2.0 at an oscillation frequency of ω= 50 rad/sec at 20°C. Some aspects of the behavior of the sample for all the volume fractions are qualitatively similar.

The inset in figure 3.9 (a) shows the double peak in G". It can be seen that with increase in volume fraction ϕ, the first peak in G" shifts to higher strains while the second peak shifts towards lower strain. With higher volume fraction, the interpenetration of the dangling chains of the neighbouring microgel particles is more. This will lead to the shift of the first peaks towards higher strain. However, with deeper interpenetration, the cores of the neighbouring microgel particles becomes more crowded, requiring a lower strain for the particles to move out of the cages, shifting the second peak in G" towards lower strain.

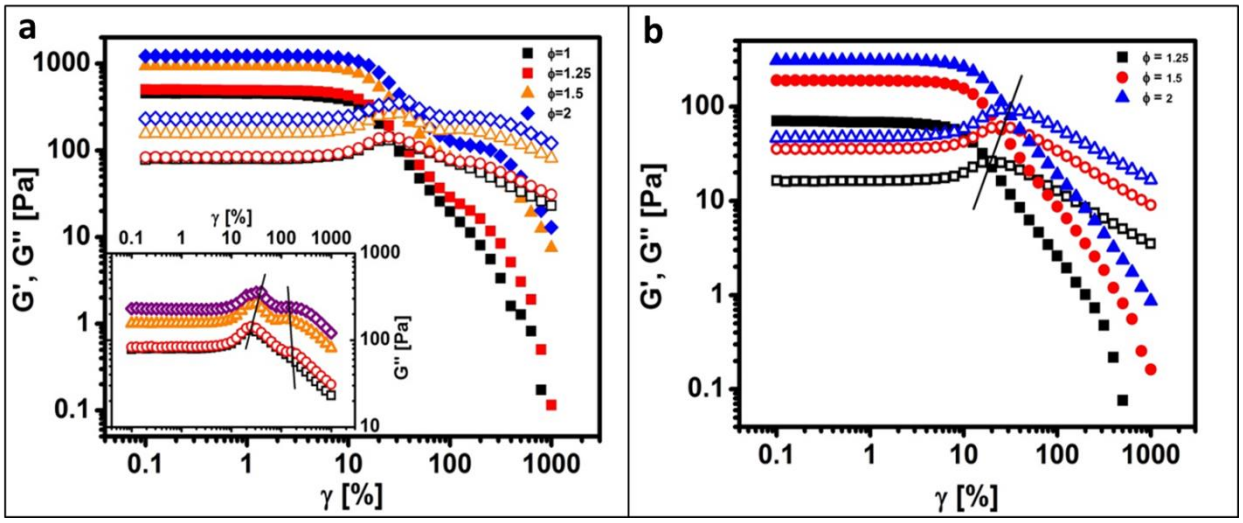

Figure 3.9: Dependence of the storage modulus G' (solid symbols) and loss modulus G" (open symbols) on the strain for oscillation frequency ω = 50 rad/sec for different concentrations of the glassy samples (a) CS3 and (b) HM3. Inset in (a) shows G" data plotted as a function of strain. Volume fractions of CS3 used are ϕ=1.0, ϕ=1.25, ϕ=1.5 and ϕ=2.0 and volume fractions of HM3 used are ϕ=1.25, ϕ=1.5 and ϕ=2.0. The temperature of the sample is T = 20°C.

Figure 3.9 (b) shows the variation of storage modulus G' and loss modulus G" as a function of strain amplitude γ for the homogeneous glassy sample HM3 for 3 different volume fractions ϕ = 1.25, 1.5 and 2.0 at an oscillation frequency of ω =20 rad/sec. The crossover point also shifts towards higher strain with increase in the volume fraction due to the higher compression of the homogeneous microgel particles at larger volume fraction requiring a larger strain to yield the material.

A recent paper on interpenetration of polymeric microgels at ultra-high densities also discusses about the interpenetration of the microgels and how entanglement of chains influences the flow properties of these microgel systems.[29] They measured the shape and size of PNIPAm particles at different volume fractions below and above close packing. Small angle neutron scattering with a zero-average contrast method was used for this. The studies were supported by SAXS and dynamic light scattering. They could also show that even at volume fractions much above the close packing, the particles does not considerably change their size and shape due to significant interpenetration. We expect a similar type of interpenetration in our particles also. This interpenetration eventually affects the yielding mechanism of the microgel at glassy regimes.

3.5.4. Frequency and temperature dependence of yielding of PNIPAm microgels

In order to explore more on the double yielding behaviour of the microgel glasses, we further carried out the non-linear rheology measurements as a function of polymer crosslinking density, oscillation frequency ω and temperature T of the sample. The results on the non-linear rheology measurements as a function of polymer crosslinking density are discussed in detail in later part of this chapter (section 3.5.5).

Figure 3.10(a) shows G' & G" for the core-shell microgel glassy sample CS3 (5% BIS) at a volume fraction of ϕ=1.5 and temperature of T=20°C for different oscillation frequencies (ω = 1.0, 10, 20 & 50 rad/sec). The inset in figure 3.10(a) shows the loss modulus G" values as a function of frequency.

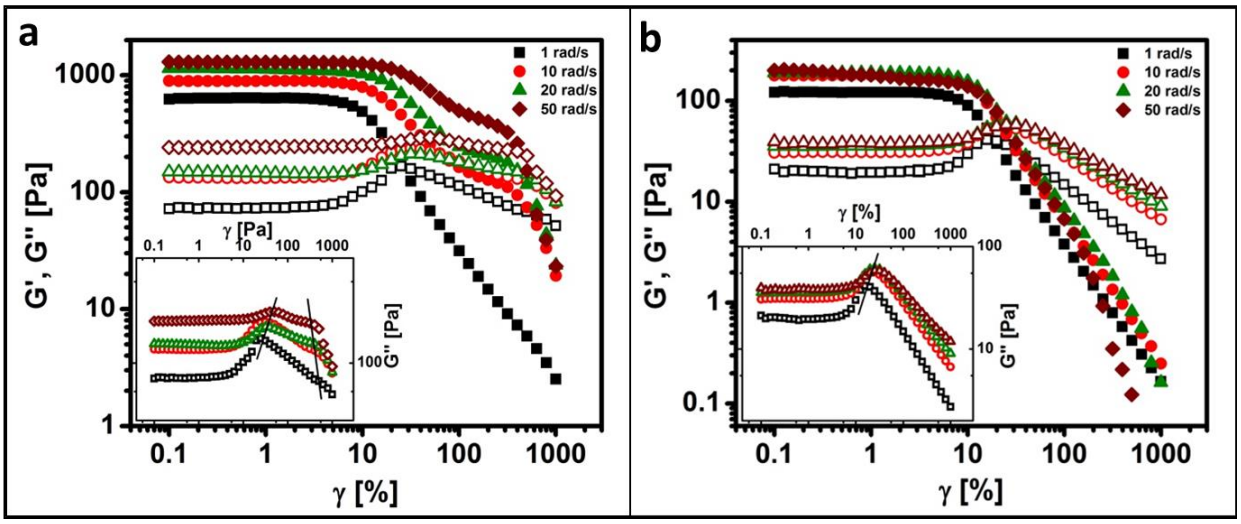

Figure 3.10: Dependence of the storage modulus G' (solid symbols) and loss modulus G" (open symbols) on the strain γ for different oscillation frequencies for glassy samples (a) CS3 and (b) HM3 at a volume fraction of ϕ=1.5 and at a sample temperature of T=20°C. Inset shows G" data plotted as a function of strain.

It can be seen that, for ω = 1.0 & 10 rad/sec, G" has only one peak. Whereas for ω = 20 & 50 rad/sec, there are 2 yielding peaks in G". This may be due to the fact that the beta relaxation frequency (ω_β) of our sample is only 1.0 rad/sec and hence to see the effect of entanglements of the dangling polymer chains on the yielding behaviour, one need to apply shear at oscillation frequency larger than ω_β. When shear is applied at ω close to or less than the beta relaxation frequency ω_β, the particles get enough time to rattle within the cage formed by the near neighbors causing the breaking of entanglements via beta relaxation before the effect of

shear comes in to play. Thus the effect of entanglements is seen only at oscillation frequencies much above the beta relaxation frequency.

Figure 3.10(b) shows G' & G" for the homogeneous microgel glass sample HM3 at a volume fraction of ϕ=1.5 and temperature of T=20°C for different oscillation frequencies (ω = 1.0, 10, 20 & 50 rad/sec). The inset in figure 3.10(b) shows the loss modulus G" values as a function of frequency. It can be seen that for all oscillation frequencies, there is only one peak in G" due to the cage breaking and the peak shift towards higher strain probably due to the effect of compression of the particles.

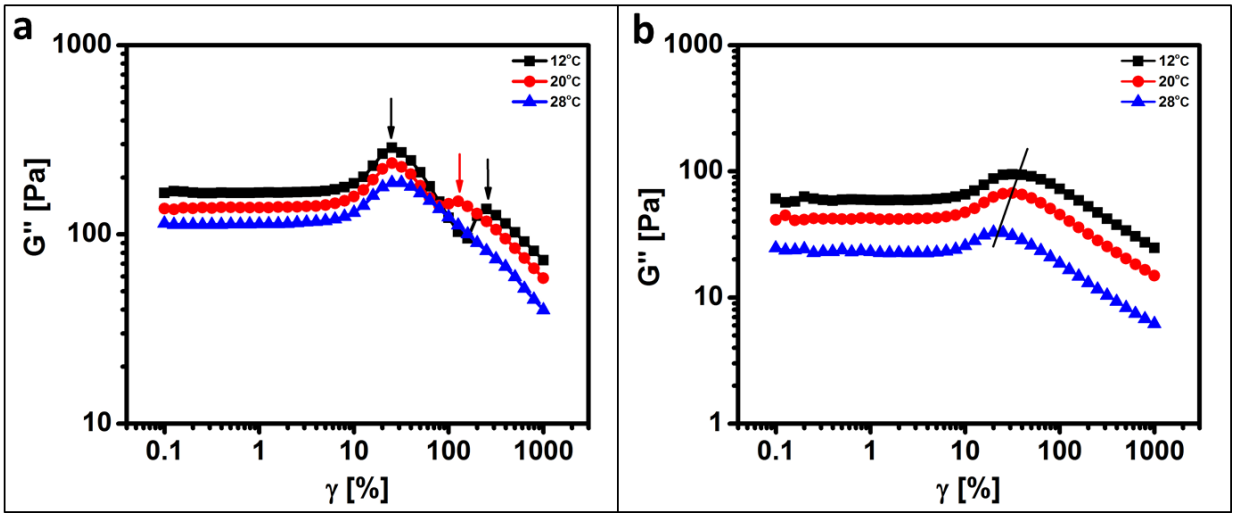

Figure 3.11: Dependence of the loss modulus G" on the strain for 3 different temperatures for the glassy samples (a) core-shell, CS3 and (b) homogeneous, HM3. The initial volume fraction of the sample at T=20°C was ϕ=1.5.

Figure 3.11(a) shows the loss modulus (G") as a function of strain for the sample CS3 for different sample temperatures T = 12°C, 20°C and 28°C respectively. The volume fraction of the sample at T=20°C was ϕ=1.5. For the lower temperature of T=12°C, the particle size is larger than that at 20°C and for T=28°C, it is smaller than that at 20°C. Thus the effective volume fraction ϕ_{eff} of the sample is much higher than 1.5 at T=12°C and lower at T=28°C.

It can be seen that the double peak in G" disappears with increase in temperature from 12°C to 28°C. This is due to the melting of the microgel glasses with increase in temperature. These observations imply that upon shearing at higher temperatures, the entanglements between neighbor particles goes off leading to the appearance of a single peak in G", which is the characteristics of most of the soft colloidal glasses. Thus the two step yielding behaviour changes

to single step yielding at higher temperatures where the entanglements between dangling chains decreases due to the shrinkage of PNIPAM microgel particles. The two-step yielding also disappears at oscillation frequencies comparable or lower than the beta relaxation frequency as the entanglements break due to the intrinsic fast structural relaxation (β relaxation).

Figure 3.11(b) shows the loss modulus (G") as a function of strain for the sample HM3 for different sample temperatures T = 12^{o}C, 20^{o}C and 28^{o}C respectively. The volume fraction of the sample at T=20^{o}C was ϕ=1.5. For the lower temperature of T=12^{o}C, the particle size is larger than that at 20^{o}C and for T=28^{o}C, it is smaller than that at 20^{o}C. Thus the effective volume fraction ϕ_{eff} of the sample is much higher than 1.5 at T=12^{o}C and lower at T=28^{o}C. At all experimental temperatures, the yielding behaviour is similar to that of hard spheres where only single peak is observed in viscous modulus curve. It can be seen that at lower temperature, the particles are larger in size and hence compress with other particles thereby shifting the yielding point to higher strain. With increase in temperature the peak in G" shifts towards lower strain as the compression of particles is less thereby breaking the cages at lower strains.

3.5.5. Effect of crosslinker density on the morphology of PNIPAm microgel particles

3.5.5.1. Linear Rheology: Frequency sweep

Linear rheology was done at a small strain amplitude of γ= 0.5%, as a function of oscillation frequency, ω and the elastic (G') and viscous moduli (G") were measured. The frequency dependence of G' and G" in the linear regime for all core-shell samples with different crosslinker content CS1- CS5 and homogeneous samples HM1- HM5 at a temperature of T = 20^{o}C is shown in Figure 3.12 for a constant volume fraction of ϕ = 1.5.

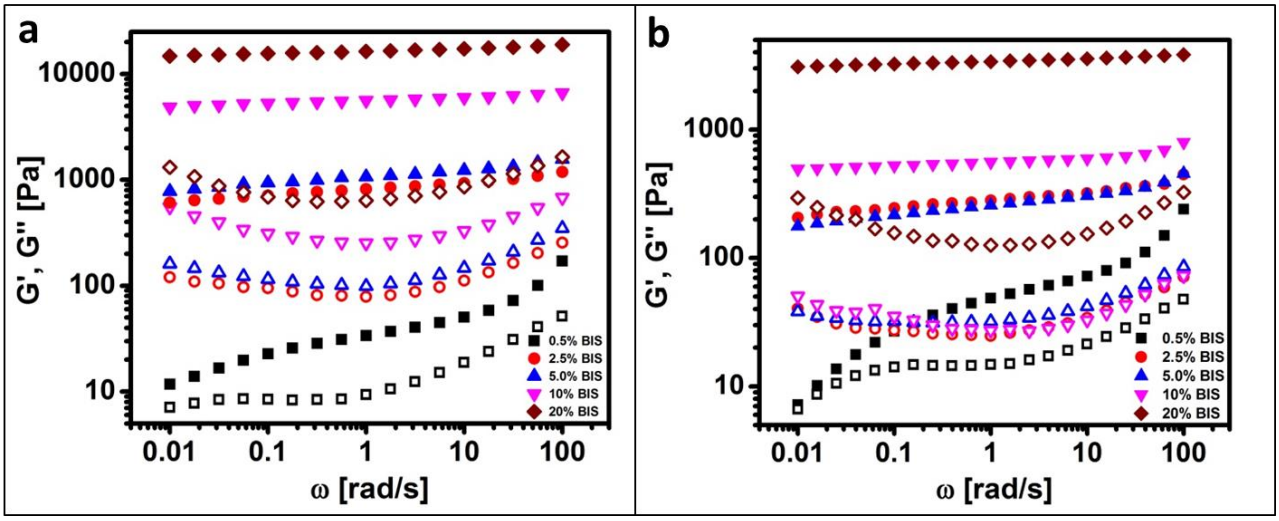

Figure 3.12: Storage modulus G' (solid symbols) and loss modulus G" (open symbols) as a function of oscillation frequency, ω at a small strain of γ= 0.5% for (a) core-shell microgel sample CS and (b) homogeneous microgel sample HM at a sample temperature of 20°C for 5 different crosslinker densities (0.5%, 2.5%, 5%, 10% & 20% BIS respectively) for a volume fraction of ϕ=1.5.

It is observed that within the frequency range measured (10^{-2}–10^{2} rad/s), G' is independent of frequency for all core-shell particles irrespective of the crosslinker content and G' is always greater than G" in all cases. Thus, all samples behave like solid in this frequency range and for this small shear strain. A minimum in the loss modulus G" at a frequency ω_β of around 1 rad/sec suggests that the linear rheological behavior of PNIPAM microgel glasses to be similar to that reported for other colloidal glasses. As observed and explained earlier in section 3.5.2 a small upturn of G" at frequencies below β- relaxation frequency hints a possible crossover with G', corresponding to α-relaxation arising from the escape of a particle from its cage. Since the alpha relaxation times in PNIPAM microgel glasses are very large, ω_α is very small and falls out of our measurement window except for the homogeneous particles with lowest BIS content (0.5%) which is observed near 0.01 rad/s.

3.5.5.2. Non-linear rheology: Strain sweep

Figure 3.13 shows the plot of the loss modulus (G") for 5 different core-shell particles suspensions (CS1-CS5) as a function of strain for a volume fraction of ϕ=1.5 at a temperature of T=20°C. It can be seen that lower crosslinking density particles show double yielding with two peaks in G".

However for higher crosslinking density (CS4 & CS5), there is only one peak in the loss modulus G". This may be due to the fact that the particles CS4 & CS5 behave similar to hard spheres. As per our static light scattering data (Table 3.3), CS4 and CS5 has an R_g/R_h ratio of 0.707 & 0.7602 respectively, which is closer to the hard sphere value of 0.778.

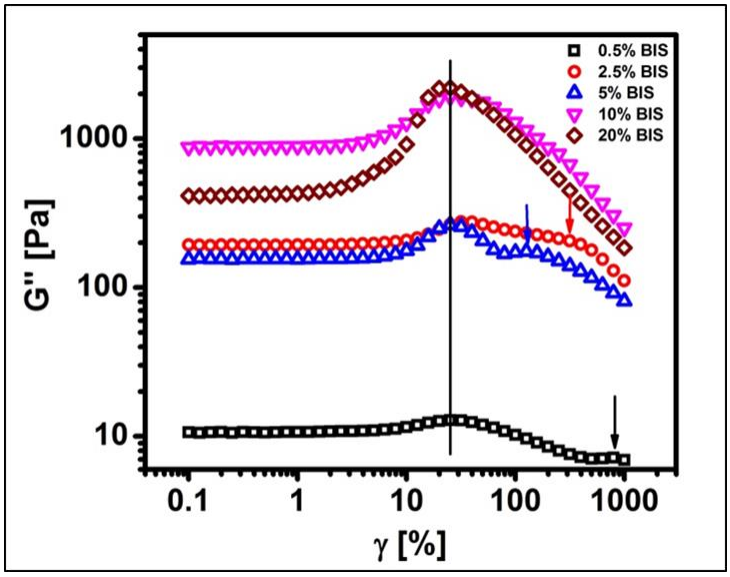

Figure 3.13: Dependence of the loss modulus G" on the strain for 5 different core-shell samples (CS1-CS5) with different crosslinking densities (0.5%, 2.5%, 5% 10% & 20% BIS respectively) for a volume fraction of ϕ=1.5 and the temperature of the sample T = 20°C.

Figure 3.14 shows the variation of storage modulus G' and loss modulus G" as a function of strain amplitude γ for all the homogeneous microgel glassy samples (HM1-HM5) at a volume fraction of ϕ = 1.5 and an oscillation frequency of ω = 20 rad/sec, which is much higher than the beta relaxation frequency of ω_β=1.0 rad/sec. The nature G' and G" for lower strains is similar to the core-shell microgel samples. At higher strains, G' starts decreasing indicating yielding of glasses under applied shear. With further increase in γ, G' further comes down and goes below G".

After the crossover of G' and G", all the samples behave like a viscoelastic liquids (G' < G") due to the shear melting of glasses. In the non-linear regime, G' shows a monotonic decrease with increase in strain amplitude γ, a behaviour similar to that of hard sphere glasses reported in literature.

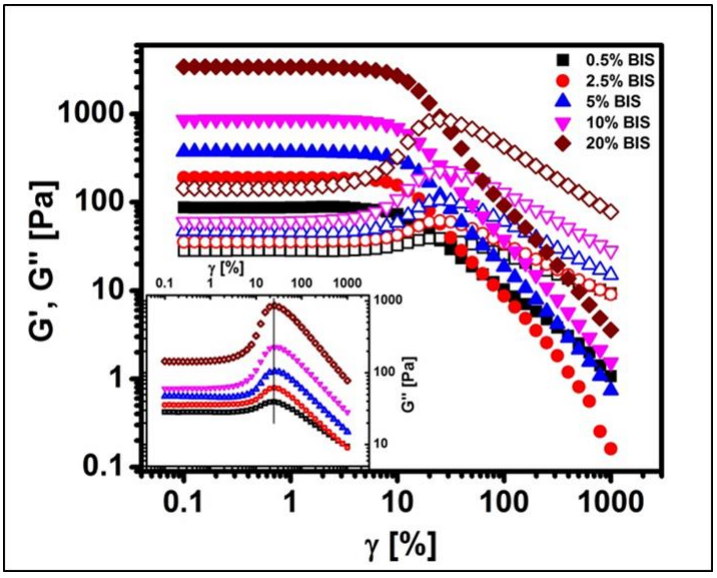

Figure 3.14: Dependence of the storage modulus G' and loss modulus G" on the strain for 5 different homogeneous samples (HM1-HM5) with different crosslinking densities (0.5%, 2.5%, 5%, 10% & 20% BIS respectively) for a volume fraction of ϕ=1.5 and the temperature of the sample T = 20°C. Inset shows the G" peaks separately.

However, unlike the core-shell glassy sample case, the loss modulus G" shows only one peak similar to the hard sphere glasses. There are no dangling chains to interpenetrate as in the core-shell case. So the single peak in G" is due to cage breaking. From our static light scattering experiments explained in the experimental section 3.5.1, the R_g/R_h ratio for the homogeneous microgel particles is close to the value of 0.778 and hence the homogeneous microgel samples behave similar to hard spheres. The inset of Figure 3.14 shows the plot of the loss modulus (G") as a function of the strain for homogeneous samples. It can be seen that there is only one peak in the loss modulus G" without a shift in the location of the peak.

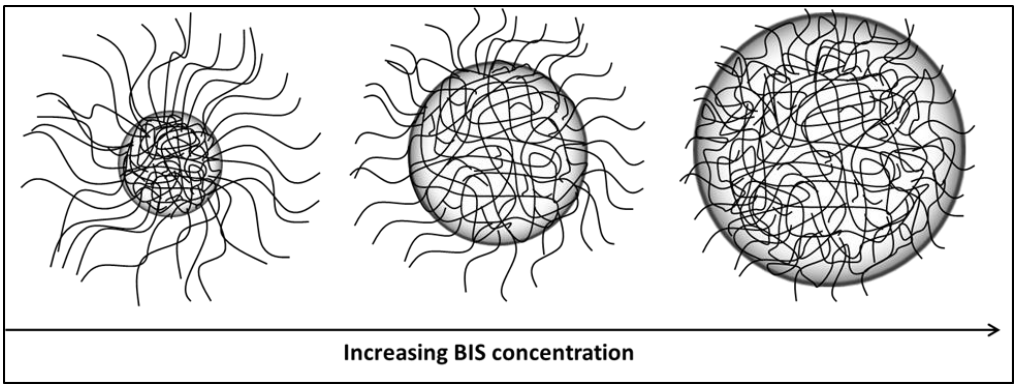

Figure 3.15: Effect of crosslinker content on PNIPAm microgel particle morphology.

3.6. Summary

Our experimental results suggest that the morphology of the microgel particles strongly influence the dynamics and flow behaviour under dense conditions. To summarise, we could show that particles having a heterogeneous morphology synthesized by conventional method yield with a double peak in viscous modulus while particles with homogeneous crosslink density made using continuous feed method yield with a single peak in G". It is interpreted that for the core-shell particles, the first peak in G" as due to the disentanglement of the dangling chains of the neighbor particles and the second peak due to the cage breaking process. In this chapter, we also conducted LAOS on particles at different frequencies and at different temperatures. Double yielding behaviour is shown to be greatly dependent on both oscillation frequency and the temperature of experiment. Particles with different crosslink density were also the subject of the study. The second peak in G" is seen to disappear for highly crosslinked microgel particles as they behave similar to hard sphere particles.

3.7. References

1 J. M. Brader, M. Siebenbürger, M. Ballauff, K. Reinheimer, M. Wilhelm, S. J. Frey, F. Weysser and M. Fuchs, *Phys. Rev. E - Stat. Nonlinear, Soft Matter Phys.*, 2010, **82**, 1–20.

2 T. G. Mason, J. Bibette and D. A. Weitz, *Phys. Rev. Lett.*, 1995, **75**, 2051–2054.

3 C. Bower, C. Gallegos, M. R. Mackley and J. M. Madiedo, *Rheol. Acta*, 1999, **38**, 145–159.

4 N. Altmann, J. J. Cooper-White, D. E. Dunstan and J. R. Stokes, *J. Nonnewton. Fluid Mech.*, 2004, **124**, 129–136.

5 H. G. Sim, K. H. Ahn and S. J. Lee, *J. Nonnewton. Fluid Mech.*, 2003, **112**, 237–250.

6 K. Hyun, S. H. Kim, K. H. Ahn and S. J. Lee, *J. Nonnewton. Fluid Mech.*, 2002, **107**, 51–65.

7 J. Mewis and N. J. Wagner, *Colloidal suspension rheology*, Cambridge University Press, Cambridge, 2011, vol. 9780521515.

8 R. H. Ewoldt, G. H. McKinley and A. E. Hosoi, *J. Rheol. (N. Y. N. Y).*, 2007, **52**, 1427–1458.

9 M. Stieger, J. S. Pedersen, P. Lindner and W. Richtering, *Langmuir*, 2004, **20**, 7283–7292.

10 J. Wu, B. Zhou and Z. Hu, *Phys. Rev. Lett.*, 2003, **90**, 4.

11 G. Huang and Z. Hu, *Macromolecules*, 2007, **40**, 3749–3756.

12 M. Stieger, W. Richtering, J. S. Pedersen and P. Lindner, *J. Chem. Phys.*, 2004, **120**, 6197–6206.

13 M. Kapnistos, A. N. Semenov, D. Vlassopoulos and J. Roovers, *J. Chem. Phys.*, 1999, **111**, 1753–1759.

14 R. Adhikari, M. Buschnakowski, S. Henning, S. Goerlitz, T. A. Huy, W. Lebek, R. Godehardt, G. H. Michler, R. Lach, K. Geiger and K. Knoll, *Macromol. Rapid Commun.*, 2004, **25**, 653–658.

15 N. Koumakis and G. Petekidis, *Soft Matter*, 2011, **7**, 2456.

16 R. H. Pelton and P. Chibante, *Colloids and Surfaces*, 1986, **20**, 247–256.

17 R. Acciaro, T. Gilányi and I. Varga, *Langmuir*, 2011, **27**, 7917–7925.

18 C. Urban and P. Schurtenberger, *J. Colloid Interface Sci.*, 1998, **207**, 150–158.

19 M. Schmidt, D. Nerger and W. Burchard, *Polymer (Guildf).*, 1979, **20**, 582–588.

20 J. Wu, G. Huang and Z. Hu, *Macromolecules*, 2003, **36**, 440–448.

21 H. Senff and W. Richtering, *J. Chem. Phys.*, 1999, **111**, 1705–1711.

22 M. E. Helgeson, N. J. Wagner and D. Vlassopoulos, *J. Rheol. (N. Y. N. Y).*, 2007, **51**, 297–316.

23 H. Wang, X. Wu, Z. Zhu, C. S. Liu and Z. Zhang, *J. Chem. Phys.*, 2014, **140**, 0–6.

24 T. G. Mason and D. A. Weitz, *Phys. Rev. Lett.*, 1995, **75**, 2770–2773.

25 A. Shukla, S. Arnipally, M. Dagaonkar and Y. M. Joshi, *Rheol. Acta*, 2015, **54**, 353–364.

26 D. A. Sessoms, I. Bischofberger, L. Cipelletti and V. Trappe, *Philos. Trans. R. Soc. A Math. Phys. Eng. Sci.*, 2009, **367**, 5013–5032.

27 K. N. Pham, G. Petekidis, D. Vlassopoulos, S. U. Egelhaaf, P. N. Pusey and W. C. K. Poon, *Europhys. Lett.*, 2006, **75**, 624–630.

28 R. G. Joshi and B. V. R. Tata, *Colloid Polym. Sci.*, 2017, **295**, 1671–1683.

29 P. S. Mohanty, S. Nöjd, K. Van Gruijthuijsen, J. J. Crassous, M. Obiols-Rabasa, R. Schweins, A. Stradner and P. Schurtenberger, *Sci. Rep.*, 2017, **7**, 1–12.

CHAPTER 4

ELECTRIC FIELD DRIVEN ASSEMBLY OF BINARY COLLOIDAL MIXTURE OF IONIC MICROGELS OF PNIPAM

Electric field driven self-assembly of deionized suspensions of binary ionic microgels of poly(N-Isopropyl acrylamide)-co-acrylic acid (P(NIPAm-co-AAc)) is studied in the current chapter. Microgel particles of similar cross-linking density (5 mol%) with a size ratio of 0.5 and labelled with two different dyes are used as the experimental model colloids. The AC field induced self-assembly behavior are studied under confocal microscope in the fluid regime for different number density ratio of big and small microgels.

4.1. Introduction

Colloids have been used as model systems to study phase behaviour and different interactions in atomic and molecular level because of the analogy in property.[1–6] Both hard and soft colloids were employed as model systems. Soft colloids like star polymers and microgels gained much attention in last decade.[7–11] Easy and advanced synthesis routes to prepare highly monodisperse microgel particles favoured the use of such system as model systems for phase transition studies.[12] Soft microgels of Poly(N-isopropyl acrylamide) (PNIPAm) is the most widely explored and extensively used as model colloid.[13–16] Introducing charge on NIPAm allows one to play with external stimuli like pH, ionic strength, electric and magnetic field etc. Moreover, ionic charge in the system makes the soft colloid softer, enriching the phase behaviour with many crystalline states.[17,18] Phase behaviour of ionic microgels can be tuned by use of external electric field. External electric fields are straightforward, efficient and powerful way to maneuver and assemble colloidal particles. Many reports have come where people use AC electric field to assemble highly monodisperse particles into well-defined arrays which can be tuned by the field strength and position.[9,19–23] The electric field studies on charged colloids are fairly a new idea which gained attention recently. Theoretical studies have also been carried out and come up with exciting results making use of Monte Carlo simulations.[24–27] Controlling the colloidal assembly by external electric field enable their application in many emerging fields such as crystal assemblies for biomedical applications,[28] microfluidic devices,[29,30] shock absorbers and clutches[31] etc. Field studies on binary mixture of colloids have become hot area of research.[32–37] Confocal laser scanning microscopy has been employed in tracking particles and the electric field studies are combined with this for accurate investigation of the behavior of microgels in both dilute and concentrated regimes.[38] Particle tracking softwares like IDL simplifies the studies.

Using confocal laser scanning microscopy, the directed self-assembly of a binary mixture of cross-linked ionic microgels differed by the hydrodynamic size under the influence of an applied alternating electric field at different effective volume fractions φ_{eff} in real space were studied. Concentrations ranging from dilute fluid regime to crystalline regime were investigated. The controls over the arrangement of the particles were achieved by three parameters: voltage and frequency of the electric field and the position of electrodes. The induced assembly was found to be fully reversible.

The objective of the current work is to apply an alternating electric field and study the self-assembly and structure formations in a binary mixture of microgels with a size ratio of around 2. The particles used for the study are micron sized polymeric gel particles of N-isopropylacrylamide with Acrylic Acid as the ionic component (P(NIPAM-co-AAc)). Electric field driven assembly of single microgel particles is well established system and it was found that that the particles align into chains at lower concentration on application of alternating current at fairly high frequency.[22,39] It was also proved that at concentration well above fluid regime, the crystal structural changes occur on applying electric field.

4.2. Synthesis and characterizations of microgel particles

The synthesis of larger sized PNIPAm microgels was done in the absence of the surfactant. The cross-linker amount taken was by weight of the total monomer. This produces increased crosslinking density and the refractive index of the microgels which intensifies the contrast when observed under the microscope. The synthesis protocol for both smaller and larger particles was similar except that the amounts of reagents taken are different.[12] A detailed synthesis protocol is provided in section 2.6.4 of chapter 2 and table 2.3 describes all the parameters for the synthesis. We prepared two different fluorescently labeled ionic microgels, one using methacryloxyethyl thiocarbamoyl rhodamine B (MRB) (excitation max 548 nm) as a covalently linked fluorescent label and the other using fluorescein isothiocyanate (FITC) (excitation max 490 nm). For preparing specific concentration of samples, freeze dried powder was redispersed in filtered DI water.

4.2.1. Light scattering studies

Dynamic and static light scattering (LS Instruments, Switzerland) studies were carried out to investigate the temperature dependent swelling behavior (See Figure 4.1 a) & b)) and

internal structure of both size microgel particles. The hydrodynamic radius (R_h) was extracted using a first order cumulant analysis from the measured intensity cross-correlation function. The particle form factor measured in the swollen state (T = 20°C) from static light scattering (SLS) (see Figure 4.2) and then fitted with fuzzy sphere model in order to estimate the core radius (R_{core}), shell thickness and R_{SLS}. Small and big size particles are denoted in the name as RNA670 and FNA1300 respectively.

Sample	**RNA670**	**FNA1300**
R_h at 20°C (nm)	336.5	658
R_h at 45°C (nm)	154.5	214
Swelling Ratio ($R_{h(45)}/R_{h(20)}$)	0.460	0.325
R_{core} at 20°C (nm)	221.5	458.2
Shell thickness (σ_s) (nm)	15.5	16.8
R_{SLS} at 20°C (nm)= R_{core}+2 σ_s	252.5	491.8

Table 4.1: Hydrodynamic radius (R_h) obtained from DLS, fuzzy sphere radius obtained from SLS (R_{SLS}) and swelling ratio of small and big microgel particles.

From dynamic light scattering, the temperature dependent swelling behavior of both size microgel particles are studied using cumulant analysis.[40] The average hydrodynamic radius of the bigger and smaller size particles in the swollen state (at T= 20°C) are 1300 nm and 670 nm respectively. The core-shell nature of the microgel particles are estimated by measuring the form factor (P_q) using static light scattering and then fitted with fuzzy sphere model (figure 4.2).[41] Both dynamic light scattering and static light scattering are clearly explained in the section 2.8.2 of chapter 2. The fuzzy sphere model is given by the equation:

$$\boldsymbol{P_q = \left[3\frac{\sin(qR) - \cos(qR)}{(qR)^3} e^{\left(-\frac{(\sigma_s q)^2}{2}\right)}\right]^2} \qquad \mathbf{4.1}$$

where, R is core radius and σ_s is fuzzy shell thickness.

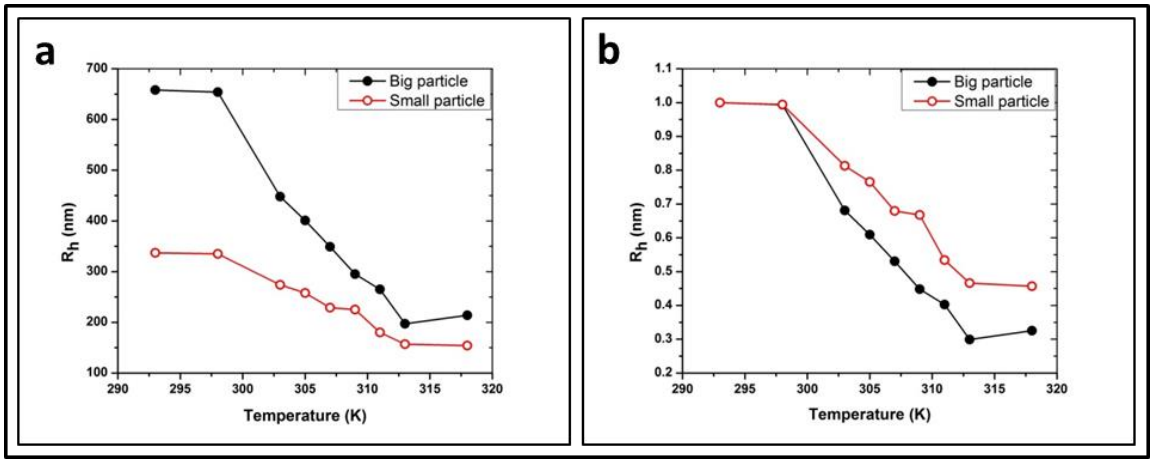

Figure 4.1: (a) Hydrodynamic radius vs Temperature graph for large and small P(NIPAm-co-AAc) microgel particles, (b) Normalized Hydrodynamic radius vs Temperature graph for large and small P(NIPAm-co-AAc) microgel particles.

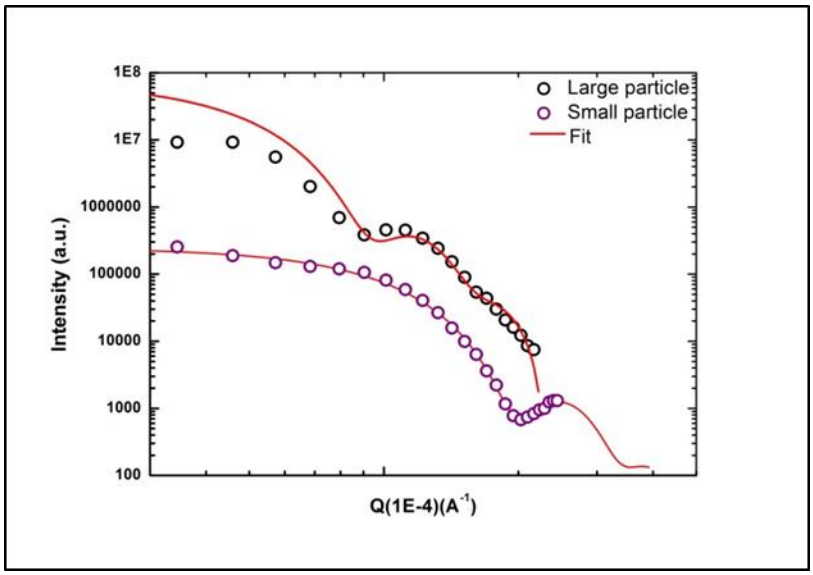

Figure 4.2: Form factor of big and small P(NIPAm-co-AAc) at T=20°C and fitted with fuzzy sphere model.

4.2.2. Electric field geometries

Electric field studies were conducted using confocal laser scanning microscope (CLSM) (Carl Zeiss LSM 710, Germany) with an upright objective (Axio imager Z2 M stand) with laser lines of Argon-ion (458, 488, 514) and Helium Neon (543, 633). Objective used was 63x oil immersion with a numerical aperture of 1.4. The fast resonant scanner accurately tracks particles at very low concentrations in the fluid regime. All experiments were done at a temperature 20

°C. The number density in the sample was varied from fluid regime to glass with a range of effective volume fractions (φ_{eff}) from 0.3 to nearly 1. Indium- Titanium oxide (ITO) coated cover slips of 18x18x0.15 mm size were used as a conducting medium. In parallel geometry, where applied electric field is parallel to XY-image plane, an insulated area of approximately 1 mm width is made across the length of the coverslip by etching the ITO coating off using concentrated acid. The sample is taken on a glass slide using spacer of 120 μm thick and is covered by the etched ITO coverslip in such a way that sample is in the insulated region. The coated region on both the sides is connected to a voltage source using thin wires and conducting tapes were used to fix the wires on the cover slide. In perpendicular geometry, electric field was applied along the Z-axis (perpendicular to the image plane), the sample was taken between two ITO-coated cover glasses separated by a spacer of 120 μm thick, and measurements were done around 10 particle diameters from the cover slide to minimize wall effects. Here, all the observations were made in the XY-image plane. We used two different field setups for our experiments carried out using confocal microscope. Since the resolution of microscope along z (perpendicular) direction is poor compared to xy plane (imaging plane), we used parallel setup (figure 4.3) to perform field experiments with the field along the x direction. Perpendicular setup (figure 4.4) was also done to reconstruct a three dimensional (3D) structure along the field direction.

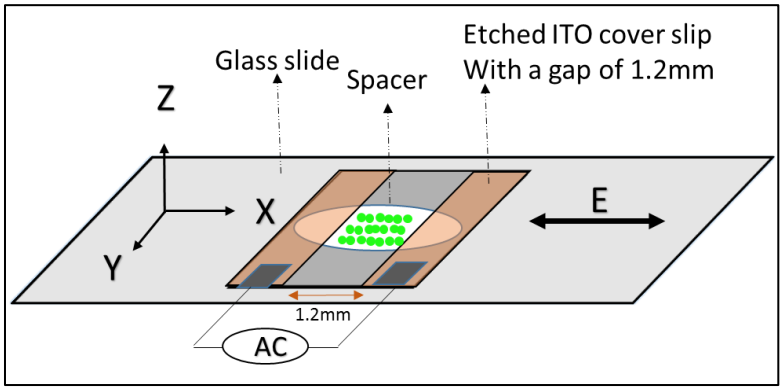

Figure 4.3: Parallel field setup. Microgel sample is taken between a glass slide and a conductive indium tin oxide (ITO) coated cover slip separated by a spacer of thickness 120 μ. The cover slip is etched with a gap of 1.2 mm. Under alternating field, charged microgels align along the field direction to form chains, parallel to the image plane itself. The z-axis is perpendicular to the image (xy) plane.

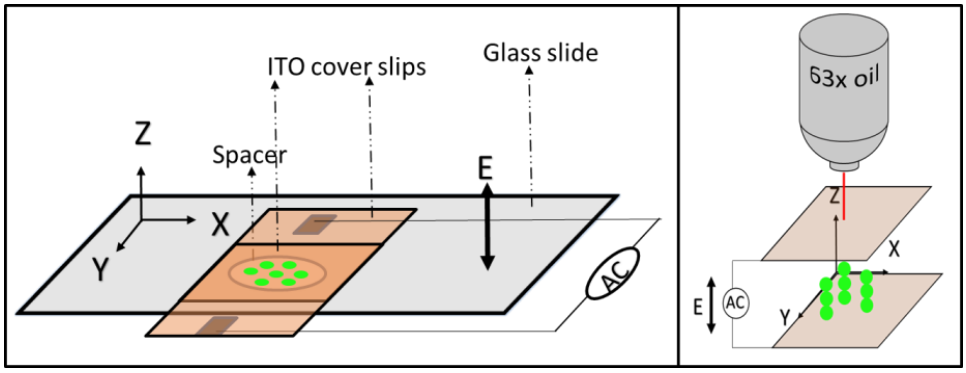

Figure 4.4: Perpendicular field setup. Microgel sample is taken between two cover slips coated with conductive indium tin oxide (ITO) separated by a spacer of thickness 120 μ. The structure is viewed along the applied electric field direction (along z), perpendicular to the image (xy) plane.

4.3. Results and Discussion

We used particles of P(NIPAm-co-AAc) having two distinct sizes (1300nm and 670nm) for the study. For identification under confocal microscope we incorporated dyes with the particle, fluorescein isothiocyanate (FITC) and methacryloxyethyl thiocarbamoyl rhodamine B (MRB) for larger and smaller particles respectively.

4.3.1. Zero-field density dependent equilibrium structure of big and small microgels

At high density, the particles arrange in a crystalline structure, which is in agreement with earlier studies.[39] The equilibrium zero field structure for both big (FNA1300) and small (RNA670) particles is of face centred cubic (FCC) type.

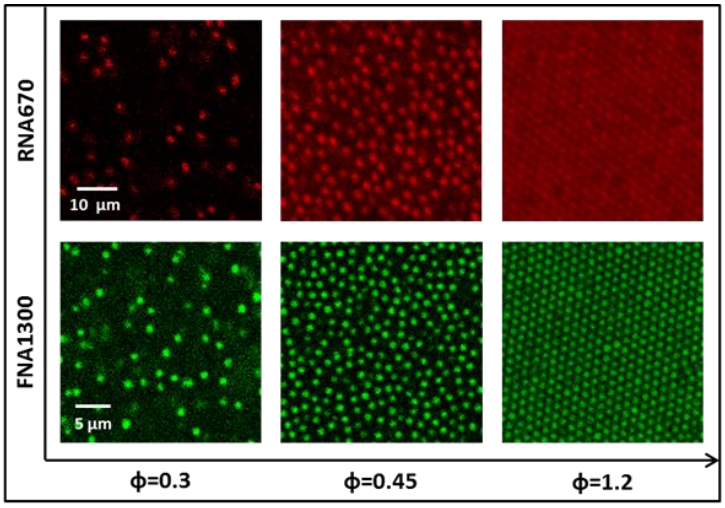

Figure 4.5: 2D CLSM images for individual particles as a function of concentration spanning from fluid to crystal state at the highest volume fraction.

The low density structural ordering is investigated by measuring the pair-correlation functions of individual microgel suspension. Figure 4.6 shows the experimental pair correlation function g(r) for a microgel suspension at low concentration obtained from the particle tracking of the CLSM time series images containing 5000 image frames at zero-field. Images were taken at a distance of 6μm away from the cover slip to minimize wall effects. The g(r)'s has a first peak and a weak second order peak which clearly demonstrate the signature of short-range order. Hence a liquid-like behaviour is confirmed for the individual microgel particles in the low density equilibrium phase at zero field. In the fluid phase, the microgels are well below overlapping regime and hence an electrostatic Yukawa type interaction is dominant.[21]

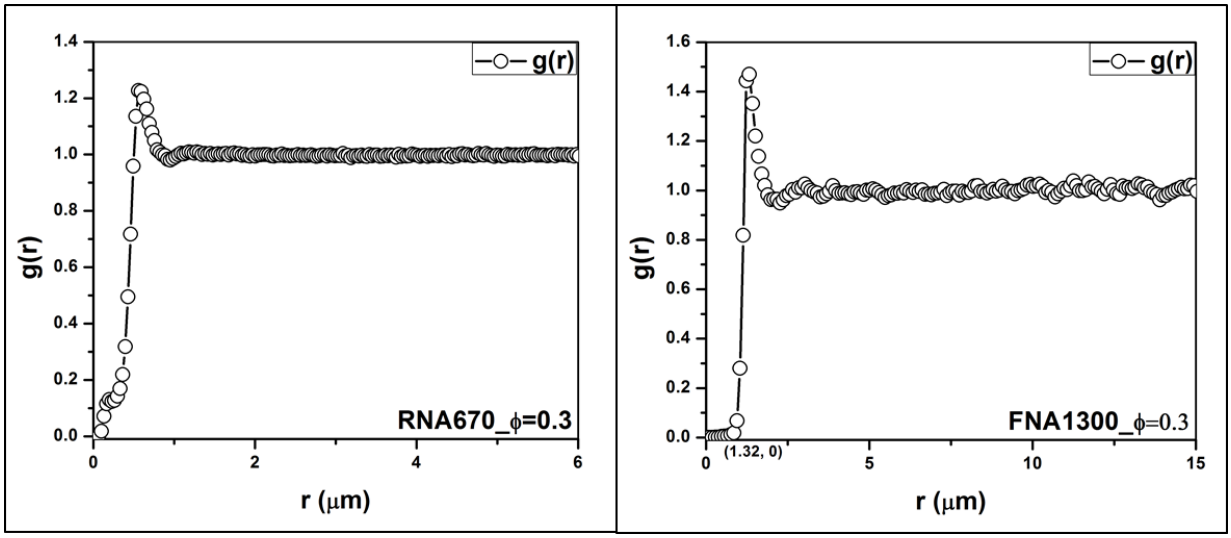

Figure 4.6: Experimental 2D- pair correlation functions of small and big size microgel particles.

4.3.2. Low density phase behavior of individual particles

Experiments were carried out in such a fashion that there are three variable parameters viz field strength, volume fraction and binary particle ratio. In the parallel geometry, the frequency was kept constant at 100 KHz. The phase behavior of individual microgel particles (both big and small) are shown in figure 4.7. The behaviour of the microgel particles towards electric field comes from many polarization contributions depending upon the frequency of the field.[22] The most important theory about the origin of response to electric field by colloidal particles is the dipolar interaction induced by the external electric field. This suggests that the particles in colloidal suspension are polarized by the external electric field and the interaction between the resulting dipoles causes the particles to form string-like structures along the

direction of electric field.[42] Bigger particles start forming chains at a voltage of 35V while the smaller particles need higher voltage to start forming the strings (85V). Being smaller in size, they require higher dipole moment to form chains and arrange.

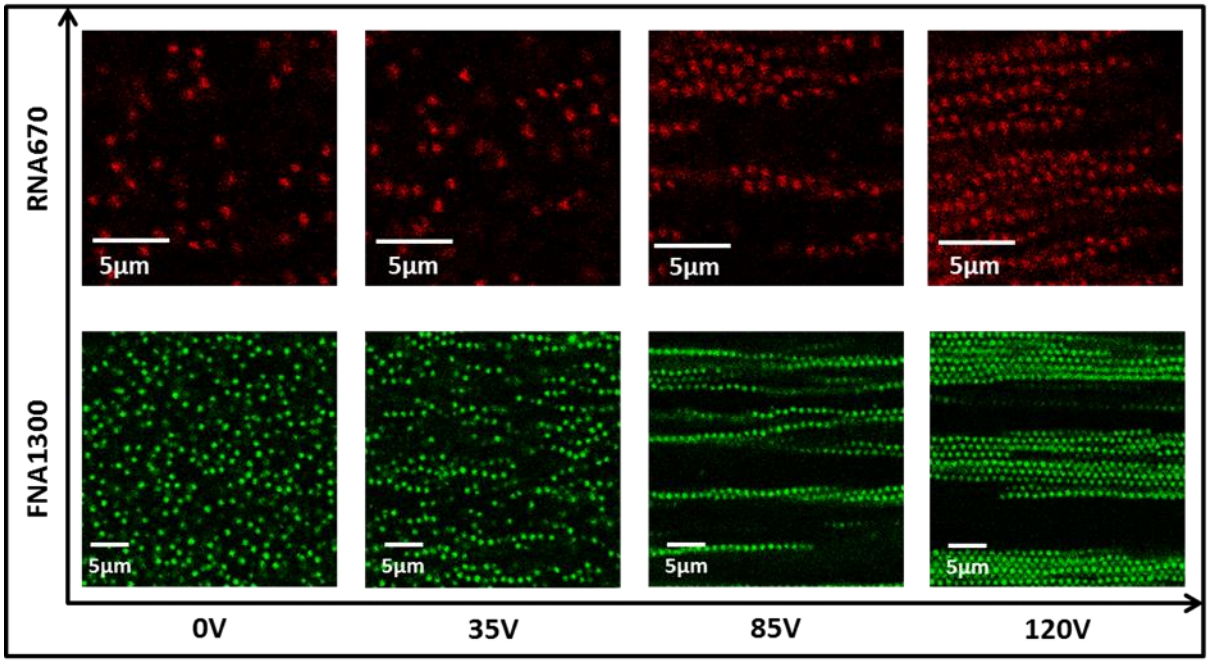

Figure 4.7: Response of individual microgel particles towards electric field.

As the field strength is increased further, the length of the chains increases and they slowly start aggregating to form bundles of chains. The driving force for this attraction between chains is the pair-wise dipole-dipole interactions between the particles of different strings. The interaction between chains is repulsive at longer distances but when the chains come near, there is an induced attractive interaction resulting in complex structure formation. At very high voltages, the density of bundles increases and eventually forms an ordered BCT crystal structure which is visible in perpendicular direction only. When the BCT crystalline structure is formed, there is a lot of space available in the bulk which is devoid of any particles. Thus it is observed that the particles in external field converts from a fluid phase to a string phase and finally to a gas- BCT phase. These findings are in agreement with previous studies.[39]

4.3.3. High density field-induced phase behaviour of individual particles

We investigated the field response of individual particles at volume fraction much above the freezing concentration. The samples at high concentration crystallize in FCC. The particles form bands/ chains in perpendicular direction, since we are interested in crystalline arrangement,

we conduct the experiment at crystalline volume fraction in perpendicular field set up only. Figure 4.8 shows the arrangement of the individual samples at different voltages. At zero voltage, particles are arranged in FCC lattice. As the voltage is increased, the FCC structure is disturbed due to the shear melting of particles. This shear molten state is a disordered glass at this very high concentration where the particles are kinetically arrested. For big particles, we get a BCT structure on further increase in voltage. Thus there is a crystal to crystal (FCC to BCT) transition through a glassy state. The applied voltage is insufficient for the smaller particles to fully convert in to a BCT structure, even though some parts are arranging into BCT.

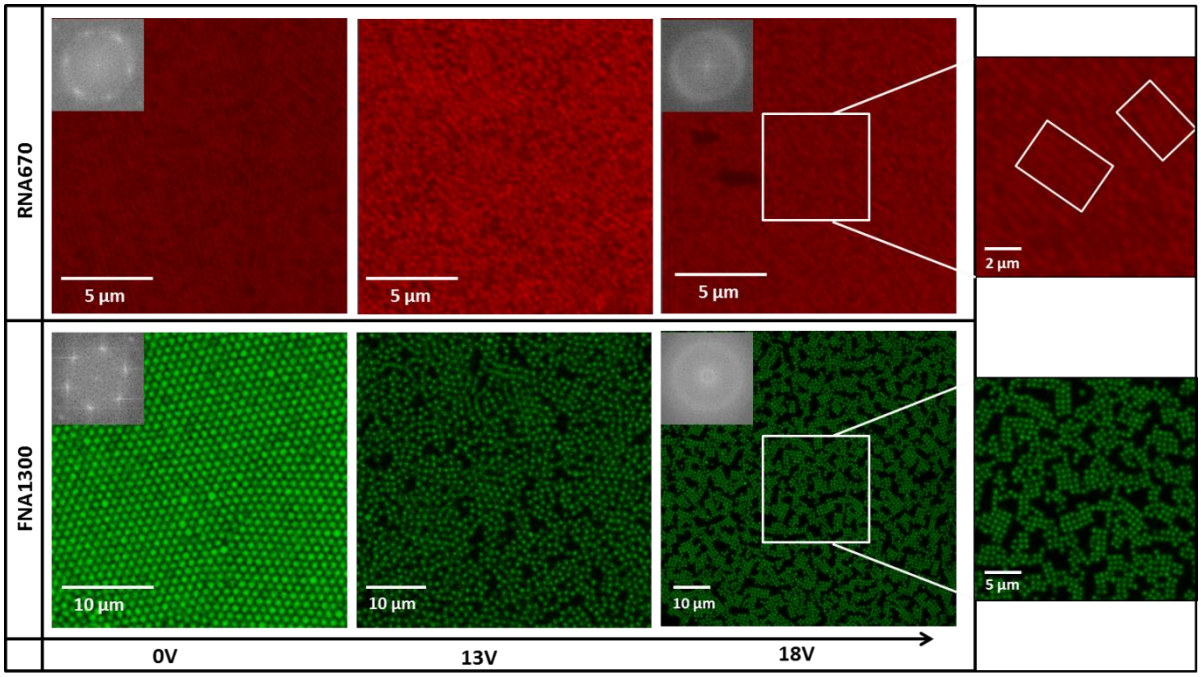

Figure 4.8: Response of microgel crystals to electric field. Inset shows the diffraction pattern obtained from Fourier transform of the images at crystal concentration.

4.3.4. Low density field induced phase behavior of binary mixtures

Electric field experiments were carried out in the mixture of binary microgel suspensions at different number density ratio (25:75, 50:50, 75:25) in the fluid regime at different field strength and at constant frequency of 100 KHz. 2D CLSM snaps of the field-induced phase behaviour of particles in the parallel field setup is shown in figure 4.9. Images show that particles are homogeneous distributed and have an isotropic order in the zero field (0V).

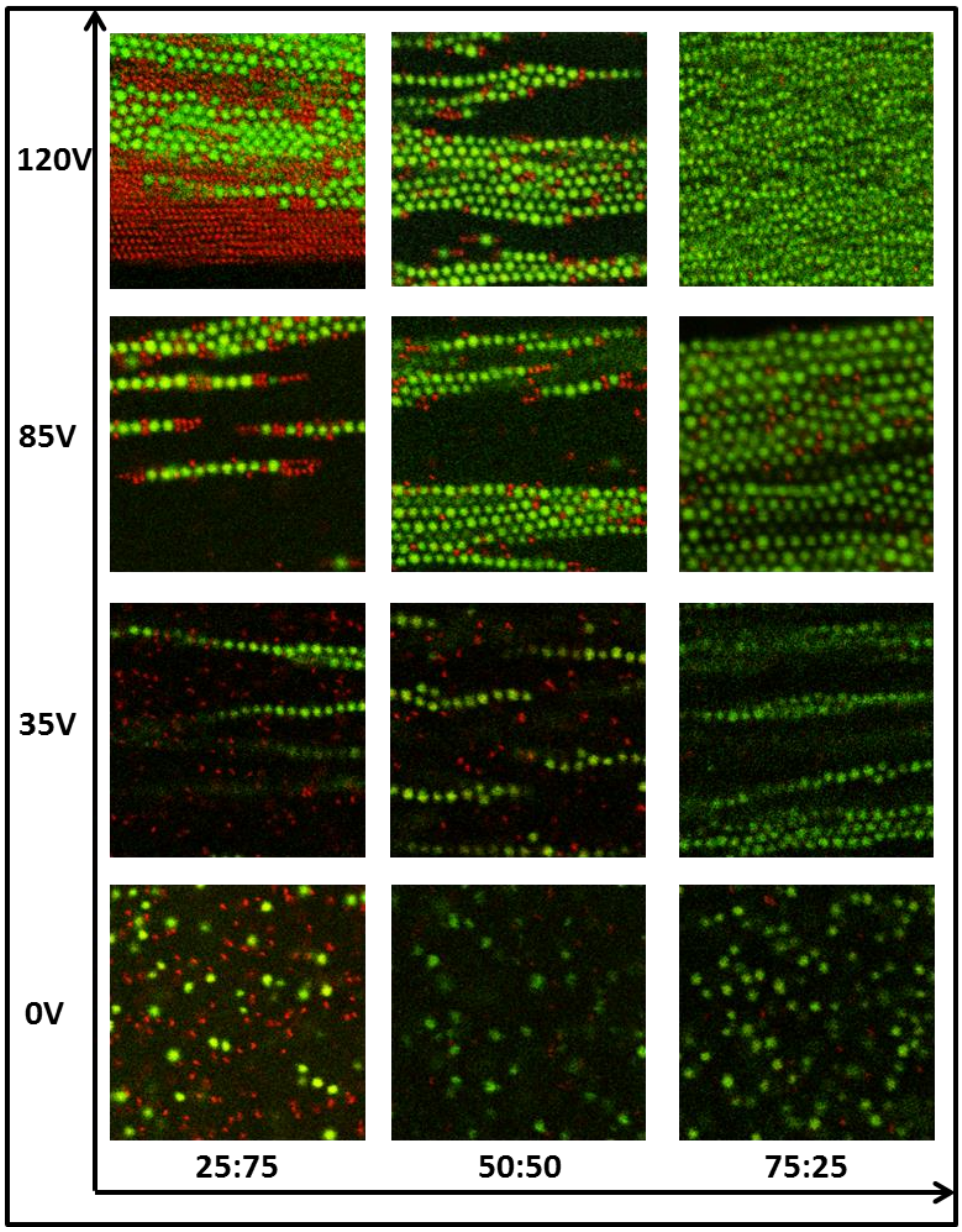

Figure 4.9: Behaviour of binary particles in low concentration under the application of electric field in the parallel geometry.

At ratio 25:75 (big: small), the volume fraction corresponds to φ_{eff} = 0.3. Time series images were continuously recorded with increasing steps of 5V. Big particles (green fluorescent) start forming chains along the field direction at lower voltage than the smaller ones. Around 35V, small particle starts to form chains due to increase of dipole interaction. Both particles start interacting together in special manner when the voltage reached sufficiently high (~80V). Small particles start to align themselves in between the chains of larger particles. About 4 small

particles surround one large particle in the image plane. At the same time small particles also form flame-like structure at the end of long chain of big particles at high this voltage. At slightly higher voltages, the chains of big particles are coming together to form bundles. At 120V, almost all the particles are seen to be arranged in chains and chains are in turn arranged to large bundles. Long flame-like chains of small particles at the end of the big particle chains are seen to be intact at this voltage. Recent simulations on assembly of binary mixture of particles under external electric field have predicted different types of assembly.[24,25] Flame-like endings were predicted for the binary mixture system with size ratio (size of small particle: size of big particle) around 0.25 by one group and 0.83 by another group.

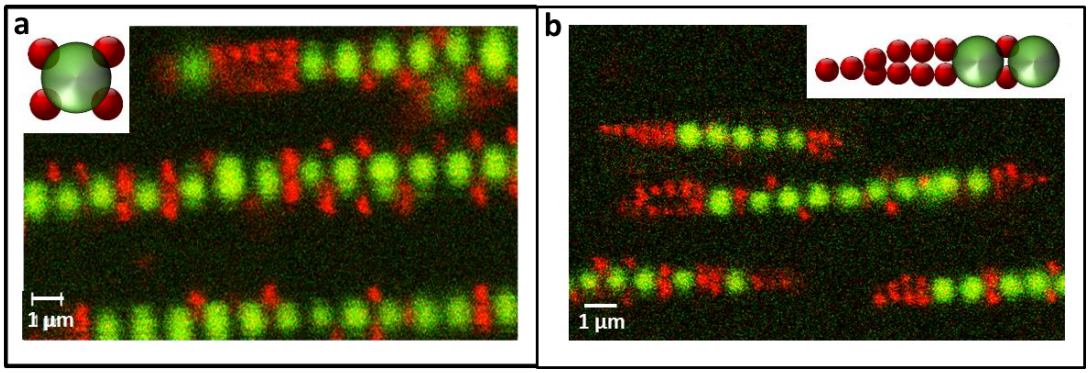

Figure 4.10: Assembly of microgel particles showing (a) small particles between big particles and (b) flame-like endings. Inset of (a) shows a schematic of the arrangement of small particles around one big particle. Inset of (b) shows the schematic of flame-like ending.

At ratio of 50:50, the threshold voltage at which big particles start forming chains is lower compared to the previous one. Moreover, probability of formation of ring-like alignment of smaller particles between big particles at higher voltage is reduced at this ratio. On increasing the voltage to 120V the chain arrange to large bundles. Here the tail formed by smaller particles on big particle chain ends is much smaller than that in the earlier case (25:75).

At a particle ratio of 75:25 (big: small), chains formed predominantly of large particles. Bundle formation at very high voltage has very little amount of small particles. Length of the tail formed of small particles also seemed to be reduced drastically.

4.3.5. High density field induced phase behavior of binary mixtures

Electric field experiments were carried out in the mixture of binary microgel suspensions at a number density ratio of 25:75 (FNA1300: RNA670) in the crystalline regime at different

field strength and at constant frequency of 100 KHz. Confocal images of the field-induced phase behaviour of binary mixture of particles in the perpendicular field setup is shown in figure 4.11.

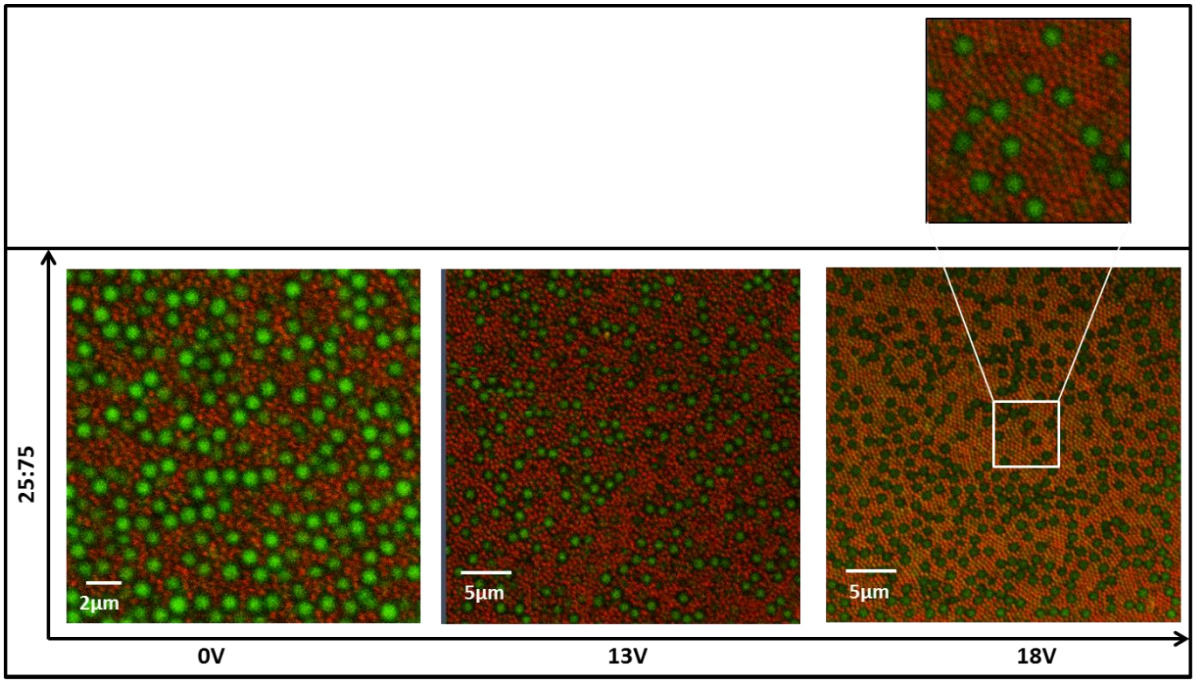

Figure 4.11: Response of binary mixture of microgels to electric field, at higher concentrations in the ratio 25:75.

The behaviour of the binary mixture of particles at higher concentration is different from that at fluid regime. In contrast to the individual particles system, we introduce polydispersity to the system by mixing two different sized particles. This suppresses the crystal formation and hence the zero field structure itself is kind of a glassy phase. In this case, the small sized particles (RNA670) have enough volume fraction to form crystals at higher voltages. Here, a glass to crystal transition is observed for RNA670. Bigger particles, FNA1300 are less in number and are kinetically trapped within the smaller particles restricting their mobility to form any kind of structures. At very high voltages, when RNA670 particles form a gas-BCT structure, there is possibility for big particles to move around and form strings. But in our measurement window, this does not happen.

4.4. Polarization mechanism at 100 KHz

Recent works on the dielectric spectroscopy on ionic microgel dispersions provides an idea on the origin of polarization induced on the ionic microgels with respect to the frequency of

electric field.[43] Contributions from the counter ions surrounding the particles, double layer around the particles, and from the polymer backbone itself along with the electrode polarization were observed depending on different electric field frequencies. Dipolar interactions dominate the field induced interactions at high frequencies. In our case, we used a frequency in range of 100 KHz. At this frequency range, internal counter ions polarization or the double layer polarization of the particles contribute to the self- assembly.

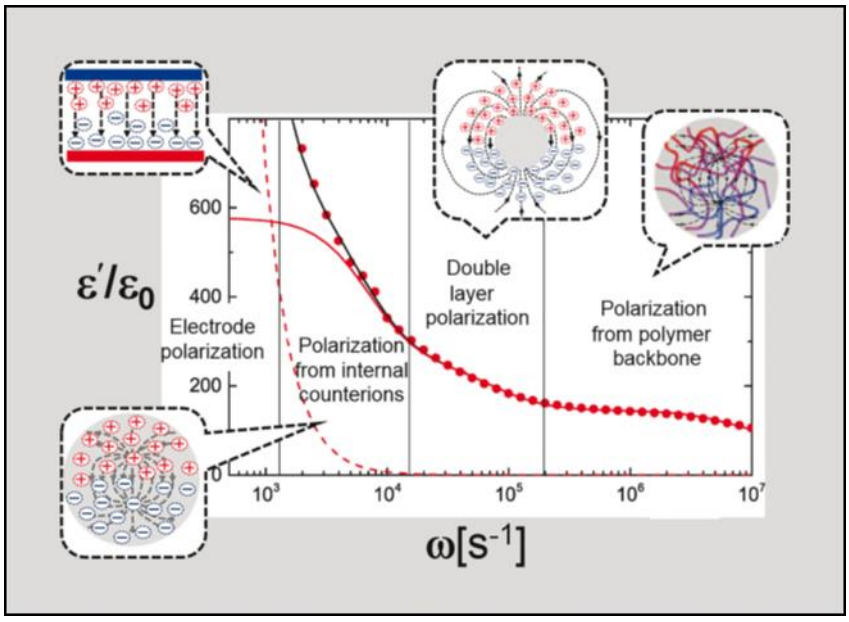

Figure 4.12: Contribution of different charges on polarization of ionic microgels with different electric field frequency [**DOI:** 10.1039/C6SM01683A].

4.5. Summary

Our study deals with the behaviour of P(NIPAm-AAc) particles of two different sizes mixed together in different proportions towards external field. Both individual microgels and binary mixture of microgels in different ratios are observed under confocal laser scanning microscope. A definite arrangement of the two different sized particle species into bands parallel to applied field at a definite frequency range is observed. The system returns to the equilibrium mixture when the field is turned off. Chain formation by the bigger particles is seen at lower voltages compared to smaller particles due to the higher dipole moment of bigger particles. Individual particles form chain bundles and arrange in crystalline structure at very high voltages. At crystalline concentration, individual particles crystals get convert from an FCC lattice to a BCT lattice through molten glassy state. In the binary mixture of particles, bigger particles

preferably form chains while the smaller particles falls into the potential well formed between bigger particles in the chain. At higher concentration, the binary mixture shows a different behavior. The smaller particles slowly transforms in to crystalline arrangement from a glassy state while the bigger particles, due to the kinetic arrest between smaller particles are unable to show any phase change in the given electric field window. Due to some technical issues, we could conduct the experiments on binary mixture at higher concentration at only one ratio (25:75). The current work is intended to be extended for other ratios (50:50 and 75:25) also.

4.6. References

1 P. N. Pusey and W. Van Megen, *Nature*, 1986, **320**, 340–342.

2 A. Van Blaaderen and P. Wiltzius, *Science (80-.).*, 1995, **270**, 1177–1179.

3 A. Yethiraj and A. Van Blaaderen, *Nature*, 2003, **421**, 513–517.

4 K. N. Pham, A. M. Puertas, J. Bergenholtz, S. U. Egelhaaf, A. Moussaid, P. N. Pusey, A. B. Schofield, M. E. Cates, M. Fuchs and W. C. K. Poon, *Science (80-.).*, 2002, **296**, 104–106.

5 E. R. Weeks, J. C. Crocker, A. C. Levitt, A. Schofield, D. A. Weitz, P. N. Pusey, A. B. Schofield, M. E. Cates, M. Fuchs and W. C. K. Poon, *Science (80-.).*, 2000, **287**, 627–631.

6 U. Gasser, E. R. Weeks, A. Schofield, P. N. Pusey and D. A. Weitz, *Science (80-.).*, 2001, **292**, 258–262.

7 D. M. Heyes and A. C. Brańka, *Soft Matter*, 2009, **5**, 2681–2685.

8 P. E. Ramírez-Gonzlez and M. Medina-Noyola, *J. Phys. Condens. Matter*, 2009, **21**, 075101.

9 D. Gottwald, C. N. Likos, G. Kahl and H. Löwen, *Phys. Rev. Lett.*, 2004, **92**, 068301.

10 Z. Zhang, N. Xu, D. T. N. Chen, P. Yunker, A. M. Alsayed, K. B. Aptowicz, P. Habdas, A. J. Liu, S. R. Nagel and A. G. Yodh, *Nature*, 2009, **459**, 230–233.

11 L. Berthier, A. J. Moreno and G. Szamel, *Phys. Rev. E*, 2010, **82**, 060501.

12 R. H. Pelton and P. Chibante, *Colloids and Surfaces*, 1986, **20**, 247–256.

13 J. J. Crassous, M. Siebenbürger, M. Ballauff, M. Drechsler, O. Henrich and M. Fuchs, *J. Chem. Phys.*, 2006, **125**, 204906.

14 H. Senff and W. Richtering, *J. Chem. Phys.*, 1999, **111**, 1705–1711.

15 F. Scheffold, P. Díaz-Leyva, M. Reufer, N. Ben Braham, I. Lynch and J. L. Harden, *Phys. Rev. Lett.*, 2010, **104**, 1–4.

16 M. Das, H. Zhang and E. Kumacheva, *Annu. Rev. Mater. Res.*, 2006, **36**, 117–142.

17 D. Gottwald, C. N. Likos, G. Kahl and H. Löwen, *J. Chem. Phys.*, 2005, **122**, 1–11.

18 P. S. Mohanty and W. Richtering, *J. Phys. Chem. B*, 2008, **112**, 14692–14697.

19 J. Dobnikar, A. Snezhko and A. Yethiraj, *Soft Matter*, 2013, **9**, 3693.

20 H. Löwen, *Eur. Phys. J. Spec. Top.*, 2013, **222**, 2727–2737.

21 J. Riest, P. Mohanty, P. Schurtenberger and C. N. Likos, *Zeitschrift für Phys. Chemie*,

2012, **226**, 711–735.

22 P. S. Mohanty, A. Yethiraj and P. Schurtenberger, *Soft Matter*, 2012, **8**, 10819.

23 A. van Blaaderen, M. Dijkstra, R. van Roij, A. Imhof, M. Kamp, B. W. Kwaadgras, T. Vissers and B. Liu, *Eur. Phys. J. Spec. Top.*, 2013, **222**, 2895–2909.

24 F. Smallenburg, H. R. Vutukuri, A. Imhof, A. Van Blaaderen and M. Dijkstra, *J. Phys. Condens. Matter*, 2012, **24**, 464113.

25 B. Bharti and O. D. Velev, *Zeitschrift für Phys. Chemie*, 2015, **229**, 1075–1088.

26 B. Bharti, F. Kogler, C. K. Hall, S. H. L. Klapp and O. D. Velev, *Soft Matter*, 2016, **12**, 7747–7758.

27 J. Zhou and F. Schmid, *Eur. Phys. J. Spec. Top.*, 2013, **222**, 2911–2922.

28 O. D. Velev and S. Gupta, *Adv. Mater.*, 2009, **21**, 1897–1905.

29 A. Terray, J. Oakey and D. W. M. Marr, *Science (80-.).*, 2002, **296**, 1841–1844.

30 E. S. Kyung, S. A. Vanapalli, D. Mukhija, H. A. McKay, J. M. Millunchick, M. A. Burns and M. J. Solomon, *J. Am. Chem. Soc.*, 2008, **130**, 1335–1340.

31 M. Parthasarathy and D. J. Klingenberg, *Mater. Sci. Eng. R Reports*, 1996, **17**, 57–103.

32 D. R. E. Snoswell, T. J. Rogers, A. M. Howe and B. Vincent, *Langmuir*, 2005, **21**, 11439–11445.

33 A. S. J. Iyer and L. A. Lyon, *Angew. Chemie - Int. Ed.*, 2009, **48**, 4562–4566.

34 Y. Hou, J. Ye, X. Wei and G. Zhang, *J. Phys. Chem. B*, 2009, **113**, 7457–7461.

35 R. J. Hall, V. T. Pinkrah, B. Z. Chowdhry and M. J. Snowden, *Colloids Surfaces A Physicochem. Eng. Asp.*, 2004, **233**, 25–38.

36 A. Ferna and A. Loxley, *Trends Colloid Interface Sci. XIV*, 2000, 84–87.

37 P. D. Hoffman, P. S. Sarangapani and Y. Zhu, *Langmuir*, 2008, **24**, 12164–12171.

38 T. Vissers, A. Imhof, F. Carrique, Á. V. Delgado and A. van Blaaderen, *J. Colloid Interface Sci.*, 2011, **361**, 443–455.

39 S. Nöjd, P. S. Mohanty, P. Bagheri, A. Yethiraj and P. Schurtenberger, *Soft Matter*, 2013, **9**, 9199.

40 D. E. Koppel, *J. Chem. Phys.*, 1972, **57**, 4814–4820.

41 M. Stieger, W. Richtering, J. S. Pedersen and P. Lindner, *J. Chem. Phys.*, 2004, **120**, 6197–6206.

42 A. P. Gast and C. F. Zukoski, *Adv. Colloid Interface Sci.*, 1989, **30**, 153–202.

43 P. S. Mohanty, S. Nöjd, M. J. Bergman, G. Nägele, S. Arrese-Igor, A. Alegria, R. Roa, P. Schurtenberger and J. K. G. Dhont, *Soft Matter*, 2016, **12**, 9705–9727.

CHAPTER 5

EFFECT OF PARTICLE MORPHOLOGY ON DRUG RELEASE BY PNIPAM MICROGELS

This chapter covers the study of the effect of particle morphology on the drug release from PNIPAm microgel particles. A water-soluble drug and a water insoluble drug were taken for the case study. Percentage drug release was measured using UV-Visible spectroscopy. Other characterizations were done using DLS, rheology and differential scanning calorimetry.

5.1. Introduction

5.1.1. Drug delivery

The process of administration or introduction of a pharmaceutical compound or drug in the form of solid, liquid or gas in to the body of a patient as part of treatment of any ailment or disease is called drug delivery. The different routes of administration are based on the application location. The different ways of introduction of the drug into the body are oral, transdermal, parenteral, inhalation etc. In the conventional drug delivery route, oral drug delivery is the oldest route and the most preferred one. Ease of administration and comfort makes this route the preferred one. This is one of the modes in enteral route, while the other is rectal. Parenteral route of drug delivery is another means of administering the drug in to the body through any route other than enteral and is the widest route. This includes intra-arterial, intramascular, intravenous, subcutaneous routes and many more. When the drug is introduced by inhalation method, it will directly reach the lungs. This method will avoid systemic effect i.e., increase the bioavailability of the drug in the system and is preferred one for treating respiratory diseases. Delivery is called topical when the application location and drug effect is local in the body. Transdermal drug delivery is done through body surfaces like skin. This type of delivery is fast because the drug is transferred directly to the blood stream rather than gastrointestinal metabolism.

5.1.2. Targeted drug delivery

Control of amount of dosage in to specific part of the body is always a challenge in drug delivery. Conventional delivery systems have these limitations as high dose in one go, delivery in unwanted areas of the body etc. Many of the therapeutics have very poor pharmacokinetic effects due to this. It is therefore necessary to develop a suitable drug delivery system which can distribute the therapeutically active drugs only to specific active site and importantly without affecting healthy tissues. A targeted drug delivery system is preferred when the drug is unstable or is having low solubility. Intelligent targeted drug delivery systems and controlled release

using smart microgel particles achieve the above requirements to some extent. Polymer micelles, liposomes, nanoparticles etc. are used as carriers in targeted drug delivery. Recently polymeric microgels also found attention as carriers due to the many advantages of microgels like size tunability (from nanometers to microns), easy incorporation of drugs inside, swelling and deswelling in response to several stimuli etc.[1]

5.1.3 Polymeric Microgels in targeted drug delivery

With the advent of new and improved biomaterials the drug delivery technology has improved a lot in recent years. The developments in drug delivery technology have improved the quality of life of patients which greatly depends on the amount and efficiency of drug administered by reducing the frequency of administration and increasing the efficiency of the drug. One class of new materials which showed the possibility of efficient drug delivery is smart polymeric materials. They offer extreme possibilities to control the delivery and dosage of drugs to specific area of the body. Smart materials are materials that respond to external stimuli like temperature, pH, ionic strength, electric and magnetic fields, and metabolites like glucose. Polymeric microgels whose structure can be tuned to respond to some environmental conditions, such as temperature, pH or ionic strength come under these "smart" materials.[2–6] Poly(N-Isopropyl acrylamide) microgels are one important group of microgels which are widely used in drug delivery applications.[7–11] There are potential limitations to this application such as accumulation in the body, problem with prolongation of delivery etc. Still, as a proof-of-concept, many researchers are using polymeric microgels of N-Isopropyl acrylamide as a drug delivery vehicle.[12–14] The ability to absorb solvents (water, usually) and to swell multifold allow PNIPAm microgels to absorb and store small molecules and ions with the solvent. This property along with their nanometer size range makes these microgels ideal for drug delivery applications. Absorbed water molecules along with the other molecules will be released when the particles shrink at a particular temperature (~32°C) which is called volume phase transition temperature (VPTT). Since the VPTT can be tuned to human physiological temperature, PNIPAm microgel can conveniently be used as drug delivery vehicle. VPTT can be tuned by addition of comonomers to the system which is explained in section in second chapter. Addition of carboxylic acid comonomers provides additional stimuli responses to pH, ionic strength etc. Interaction between the microgel particles and the drug molecules can also be tuned by appropriate selection of monomers. Since 90% of the microgel is water, it produces very low

inflammatory response when used in human body. The hydrophilic nature of the microgel can pose some problems in delivering hydrophobic drugs in to the system. So PNIPAm microgels can be used to deliver hydrophilic drugs allowing free release of drugs along with the release of water at VPTT. PNIPAm microgels can especially be used to deliver anticancer drugs to cancer tissues where the temperature is slightly higher than the body temperature. By fine tuning the VPTT of PNIPAm to the cancer cell temperature, the drugs can easily be released specifically on the cancer cells without releasing it during transportation.

Due to the heterogeneous morphology of PNIPAm with a highly crosslinked core and loosely bound brush-like surface of long polymeric chains, there are limitations for the drugs to get loaded into the particle. With a homogeneously crosslinked structure, more drug is expected to be incorporated into the microgel which can be subsequently delivered to the target site. A comparison of drug release from these two types of microgel morphologies i.e. core-brush type made by conventional synthesis method and homogeneous type made by two-step synthesis method is intended in this chapter.

Since a hydrophobic drug is also used in the study, the solvent system used is a mixture of water and ethanol in the ratio 90:10. Subsequently, there are slight changes in the particle size and the volume phase transition temperature (VPTT) due to the co-nonsolvency effect of alcohol with water.[15,16] Co-nonsolvency is a phenomenon in which a mixture to two solvents, in a particular range of ratios, becomes a nonsolvent for a polymer but individually is good solvent for the same. Light scattering data in section 5.5.1 provides an insight in to the comparison of particle sizes in water and water-ethanol mixture.

5.2. Drug loading and release

5.2.1. Loading

Loading of drug is the successful incorporation of a drug into the carrier in order to release it at a specific area of the body. The loading doses would usually be higher than the delivery dose to achieve more efficiency. Loading efficiency is represented in milligram of drug per milligram of polymer. The loading efficiency is shown by the following equation 5.1:

$$\text{Loading efficiency} = \frac{\text{Amount of drug loaded}}{\text{Amount of total drug added}} \text{X } 100 \qquad 5.1$$

There are different methods of loading viz. incorporation method where the drug is incorporated during polymerization of the microgel, breathing in method where the drug is made in suitable solution and polymer in dry powder state is added to the solution, and adsorption method where drug is incubated in solution and then introduced in to the microgel in solid form. The efficiency of the last method depends on the affinity between microgel and the drug. Breathing-in mechanism is easy and is followed in the current study. The drugs will be absorbed in to the microgel particles as soon as the microgel is swelled in the solvent.[17,18]

5.2.2. Release mechanisms

Drug release from PNIPAm microgels occur due to the deswelling of the particles that effectively expel out the drug along with the water molecules inside the particle. This happens at the VPTT of the polymer. Here the release rate greatly depends on the cross-linking density distribution throughout the particle.

Release can be a controlled release if there is a controllable interaction between the drug and the microgel particles. For instance, electrostatic interaction between an ionic microgel and a charged drug can be made use of the controlling parameter for desired release of drug. As explained earlier, other than temperature, external stimuli like pH, ionic strength, electric field etc. can also be used as trigger for releasing the drug in case of ionic microgels. Charge density distribution plays an important role in release kinetics here.[19]

The loading/release of drug and the loading mechanism onto PNIPAm particles is dependent on the amount of cross-linker, polymer network structure and hydrophilicity of polymer and drug.[19] For example, the swelling kinetics decreased when increasing the hydrophobicity with hydrophobic modification of PNIPAm microgel. By increasing the voids of crosslink network, loading and release can be increased by increasing the swelling-deswelling kinetics.

Moreover, some recent studies on gel particles with a core/shell structure showed more drug bound at the periphery or shell of the particles than in the to the interior part due to the less reachable core. The core is restricted by smaller polymer network.[20] Synthesis of PNIPAm microgel particles with a homogeneous crosslink structure is then expected to absorb and release more amount of drug.

The loading and release of a drug from a polymeric microgel network greatly depend on the interaction between them.[19] Loading of hydrophilic drugs will be easier if the microgel is hydrophilic or having some hydrophilic groups. Consequently, this will ease the release also.

In the present chapter of my thesis, drug release studies on two types of PNIPAm microgel particles (core-shell structure and homogeneous structure) are conducted and results were compared. Although there are many factors affect the loading and release of drugs from PNIPAm microgels, for my studies, two drugs were selected one of which is hydrophilic and other one is hydrophobic. To dissolve the hydrophobic drug 10% of the solvent (water) is replaced by **ethanol**. The drugs used are;

- Naproxen

  Naproxen is a non-steroidal anti-inflammatory drug. It is hydrophobic in nature.

- Naproxen Sodium

  Naproxen sodium is the salt form of naproxen. It is hydrophilic in nature and dissolves easily in water.

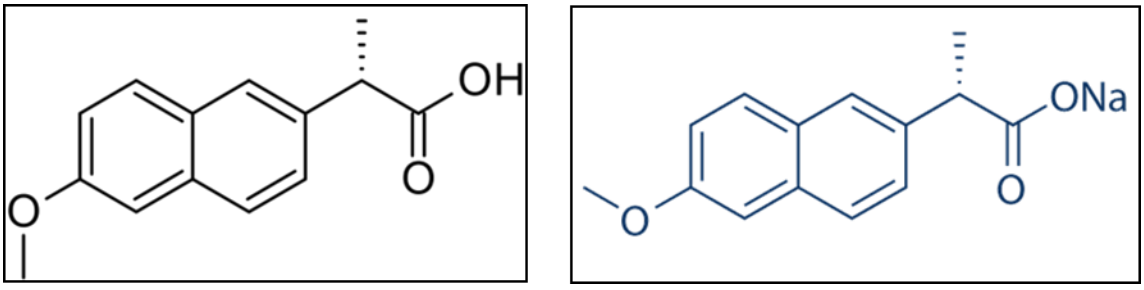

Figure 5.1: Structure of Naproxen and Naproxen sodium drugs.

5.3. Synthesis of microgels

Particles with a core-shell morphology synthesized using the conventional method and particles with a homogeneous crosslink density made by continuous feed method were used for the study. The detailed synthesis procedure is detailed in section 2.6.2 of second chapter. Both core-shell and homogeneous samples with 5% crosslinker content were synthesized and labeled as CS and HM respectively. Amount of crosslinker is represented in % per % of monomer content. Required concentration for characterizations were made by redispersing calculated amount of freeze dried sample in DI water after determining the volume fraction.

5.4. Characterizations

5.4.1 Dynamic light scattering

The hydrodynamic particle size (R_h) was measured as a function of temperature using 90 Plus particle size analyzer (Brookhaven Instruments Corporation, USA) with a laser wavelength of 632.8 nm at a fixed angle between incident laser and the detector at 90°. The temperature of the sample was maintained using a temperature probe inside the desktop instrument. Swelling ratios of the particles $R_h(43)/R_h(23)$ were found for each sample. Here, $R_h(43)$ is the hydrodynamic radius of the microgel particle at 43°C and $R_h(23)$ is the hydrodynamic radius at 23°C. Table 5.1 provides the DLS data of pure microgels and drug loaded microgels.

5.4.1.1. Sample preparation

For the drug release study, a hydrophobic drug Naproxen (Nap) and its water soluble salt Naproxen sodium (Nap-Na) were selected. Since Naproxen is not fully soluble in water, the solvent used was a 90:10 mixture of water and ethanol.

Drug is first dissolved in ethanol to make a 1mg/ml solution and is then diluted to 0.1 mg/ml with deionised (DI) water. Freeze dried microgels were weighed and added to the drug solution. Pure core-shell microgels were labelled as CS, Naproxen Sodium loaded core-shell microgels as Nap-Na-CS and Naproxen loaded core-shell microgels as Nap-CS. Similarly the homogeneous counterparts were labelled as HM, Nap-Na-HM and Nap-HM respectively.

5.4.2. Rheology

Rheology experiments were done on stress controlled rheometer (Physica MCR301, Anton Paar). The geometry used was cone and plate (cone angle 1°, diameter 25mm). To minimize water evaporation, a solvent trap was placed around the sample during the rheological experiments. The experiment protocol followed was exactly same as that explained in chapter 3 section 3.4.2.

5.4.2.1. Sample preparation

Highly dense samples of pure microgels for rheology were prepared by adding calculated amount of each microgel to 1 ml DI water to make the volume fraction near 1.5. Drug loaded microgels were prepared by dissolving calculated amount of each microgel to 1 ml 0.1% drug solution. All samples were kept undisturbed for 2 days for proper mixing.

5.4.3. UV-Visible spectroscopy

UV-Visible spectroscopy was done on the samples with Perkin Elmer Lambda 950 UV-Vis Spectrometer. To find the absorption spectra, the drugs were subjected to UV-Visible spectroscopy between 400 nm and 200 nm. Absorption maximum (λ_{max}) for Naproxen drug was found to be 271 nm and that for Naproxen Sodium was 284 nm. All experiments were done at these two wavelengths for the respective drugs. Samples were taken in 10 mm glass cuvettes from Optiglass limited, UK.

UV-Visible spectroscopy was conducted on drug samples with different concentrations viz. 0.01, 0.02, 0.03, 0.04 and 0.05 mg/ml and absorbance was used to draw the calibration curve.

Drug release studies were done by dialysis and subsequent UV-Visible spectroscopy. 10 ml drug loaded samples (equivalent to 10 mg of drug) were taken in a dialysis bag (cut-off of 14000 M_w) and dialysed in pure distilled water taken in a beaker. The distilled water was continuously stirred with a rotating magnetic needle inside. Temperature of the solution was slowly increased from room temperature to 37°C and kept constant at 37°C. 2ml of distilled water were taken from the beaker at predetermined times from 10 minutes to 4 hours (10, 20, 30, 45, 60, 120, 180, and 240 minutes. Each time, when 2ml sample was taken out same amount was replaced with fresh distilled water. UV visible spectroscopy of these samples was done and % release data was generated.

5.4.3.1. Sample preparation

Stock solution of 0.1 mg/ml was made from 1mg/ml of the samples in Ethanol which is diluted with deionised (DI) water so that the solvent ratio in the stock solution is 90% water and 10% Ethanol. Five different concentrations of both the drugs were made from the stock by adding required amount of solvent mixture. The concentrations were 0.01, 0.02, 0.03, 0.04 and 0.05 mg/ml. UV-Vis absorbance of all the prepared dilutions was recorded and used to plot a calibration curve.

5.4.3.2. Sample preparation for Drug release study

10 mg of drug (Naproxen or Naproxen sodium) powder was dissolved in 100ml 90:10 water-ethanol solvent mixture. After complete dissolution of drug in the solution, freeze-dried PNIPAm microgel powder was added to the solution. The solution is then heated just above the

VPTT of the microgel and then cooled so that when cooled, PNIPAm will absorb the solvent and consequently the drugs in to the microgel network.

5.4.4. Differential Scanning Calorimetry (DSC)

Thermal analysis of the freeze dried microgel was performed on a Thermal Advantage Q-100 instrument from TA Instruments under standard condition with a constant nitrogen gas purge of 50 ml/min. DSC was done to resolve first order transition peaks corresponding to the bound, interfacial and free water in the hydrophilic domain of the microgel particle. The samples were loaded in standard pans made of aluminium and covered with standard lids of known mass and thermal conductivity. An empty aluminium pan (with lid) was used for reference. The pans were cooled to -25°C at a cooling rate of 10°C/ min. Samples were then equilibrated at -25°C for 10 minutes. After keeping isothermal for 10 minutes, the samples were scanned for a temperature range from -25°C to 5°C with a heating rate of 3°C/ min in a single heating cycle.

5.4.4.1. Sample Preparation

1 mg/ml of each drug was prepared in 90:10 water-ethanol mixture. To dissolve the drug properly, the solution was heated below the boiling point of ethanol for 1 hour. PNIPAm microgels of core-shell morphology and homogeneous morphology were added to 1 ml of each drug separately and allowed to mix properly. Samples were appropriately weighed and taken in aluminium pans and closed with the lid and were freezed in deep freezer in a refrigerator. Freezed samples were taken out and weighed before the experiment. The sample weights were around 4-7 mg.

5.5. Results and discussion

5.5.1. Dynamic Light Scattering (DLS)

The particle size, volume fraction and swelling ratio of the core-shell are tabulated in table 5.1 while that of homogeneous samples are provided in table 5.2. Swelling ratio is the ratio of particle size at 43°C to that at 23°C. Dependence of particle size with temperature is depicted in figures 5.2 and 5.3 for core-shell and homogeneous particles respectively.

Sample	Particle size (nm)		VPTT (°C)	Swelling ratio ($D_{h(43)}/D_{h(23)}$)
	23°C	43°C		
CS in H_2O	198.0	82.0	34	0.414
CS in H_2O-EtOH	205.0	86.0	31	0.419
Nap-CS	187.7	78.5	31	0.418
Nap-Na-CS	177.1	72.4	30	0.409

Table 5.1: Particle size, VPTT and swelling ratio of CS in H_2O, CS in H_2O-Ethanol mix, Nap-Na-CS, Nap-CS

Sample	Particle size (nm)		VPTT (°C)	Swelling ratio ($D_{h(43)}/D_{h(23)}$)
	23°C	43°C		
HM in H_2O	233	103	35	0.442
HM in H_2O-EtOH	246.31	99.64	32	0.405
Nap-HM	215.02	85.8	30	0.399
Nap-Na-HM	216.96	87.45	31	0.403

Table 5.2: Particle size, VPTT and swelling ratio of HM in water, HM in H_2O-Ethanol mix, Nap-Na HM, Nap-HM.

As stated earlier in this chapter, the samples were made in a solvent mixture of water and ethanol (90:10). Due to the non-cosolvency of ethanol with water, the particle diameter and volume phase transition temperature is slightly different when compared to PNIPAm in water alone. According to Bischofberger et al,[16] the co-nonsolvency produces a coil-to-gobule-to-coil transition with increase in alcohol content. This in turn decreases the VPTT of PNIPAm. Below 5% volume fraction of ethanol in the solvent mixture, there is negligible effect of non-cosolvency. We have used 10% volume fraction of ethanol in the solvent. At this ratio, water and ethanol will have more affinity towards each other leading to less polymer-solvent interaction.[21] This will ease the release of solvent with increase in temperature leading to a lower value of VPTT. In other words, addition of alcohol into the system will decrease the enthalpy difference between the water molecules inside and outside the microgel particles. This eventually eases the formation of hydrophobic interaction between isopropyl groups of polymer molecules thus

decreasing the VPTT. From the figure 5.2 and table 5.1, it is observed that the VPTT of core-shell (CS) type particles is around 34°C while that of CS in water-ethanol mixture is 31°C. In the case of homogeneous (HM) type (figure 5.3 and table 5.2) the corresponding values are 35°C and 32°C. Addition of drugs into the system decreases the particle size but does not affect the swelling ratio. The decrease in size may be due to the close interaction of drug with the solvent molecules. These observations are same for particles of both morphologies i.e. CS and HM.

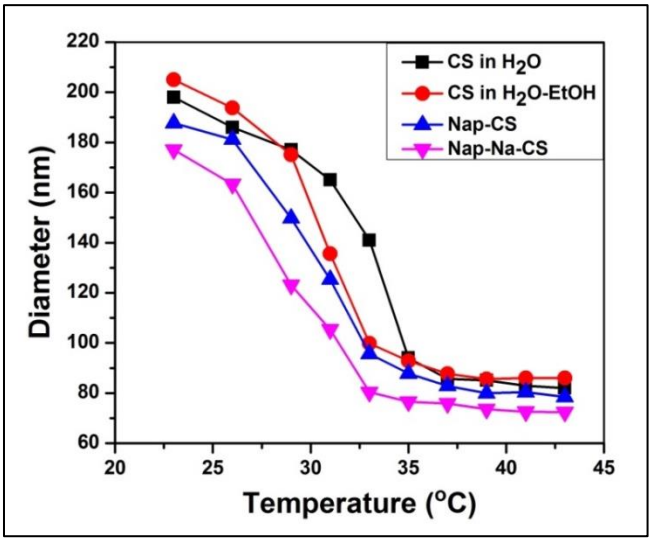

Figure 5.2: Variation of particle size of PNIPAm core-shell particles with different drugs as a function of temperature (°C).

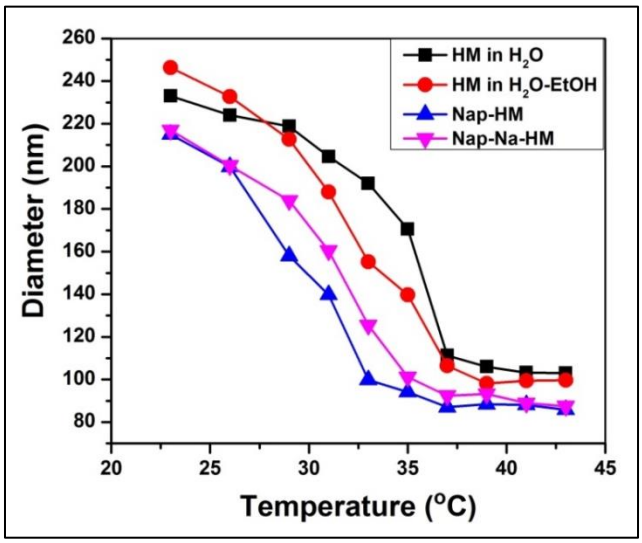

Figure 5.3: Variation of particle size of PNIPAm homogeneous particles with different drugs as a function of temperature (°C).

5.5.2. Non-linear rheology

Non-linear rheology was done on all samples to check any morphology changes or interaction changes in the system on addition of ethanol and drugs in to the microgel system. The yielding behaviour was compared with pure PNIPAm system in DI water.

The figure 5.4 shows storage (elastic) modulus and loss (viscous) modulus curves of amplitude (γ) sweep for core-shell (CS) and homogeneous (HM) particles at a constant frequency of 50 rad/s. Storage modulus is the stored energy which shows the elastic property of polymer, denoted as G'. The loss modulus measures the energy dissipated, showing viscous property of the polymer. Figure 5.4 a, b and c shows the strain sweep data of pure PNIPAm CS, Naproxen-Na drug in CS and Naproxen drug in CS respectively and d, e and f represents corresponding homogeneous samples.

The loss modulus (G") curve exhibits a peak at higher strains which corresponds to the yielding of the microgel. Core-shell particles yield with a double peak in G" curve due to the bond breaking and cage breaking phenomena while homogeneous samples yield in single peak in G". The phenomenon of double yielding is clearly explained in chapter 3 section 3.5.3.

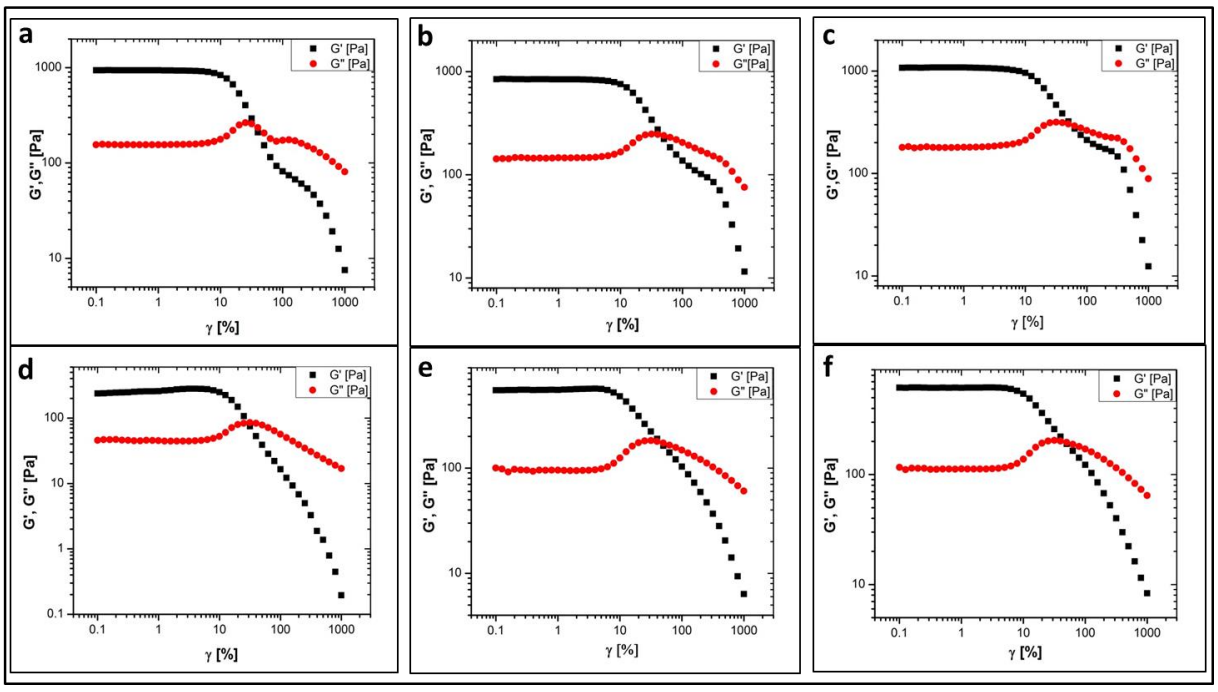

Figure 5.4: Strain sweep experiment data of (a) Pure PNIPAm CS, (b) Naproxen-Na in CS, (c) Naproxen in CS, (d) Pure PNIPAm HM, (e) Naproxen-Na in HM and (f) Naproxen in HM.

From the figure 5.4, it is seen that all the samples having core-shell morphology has a double yielding behaviour irrespective of drug loading while the particles with homogeneous crosslink distribution shows single yielding. Comparison of non-linear rheology data of concentrated gels of pure PNIPAm and drug loaded PNIPAm reveal that the double yielding property of core shell type particles are retained even after drug loading and homogeneous type particles retain their single yielding behaviour.

5.5.3. UV-Visible Spectroscopy

5.5.3.1. Calibration Curve

UV-Visible spectroscopy was conducted on drug samples with different concentrations viz. 0.01, 0.02, 0.03, 0.04 and 0.05 mg/ml and absorbance was used to draw the calibration curve. Calibration curves for both the drugs Naproxen and Naproxen Sodium are shown in figure 5.5. The slope values are 2.53 and 1.94 respectively for Naproxen and Naproxen Sodium. Regression coefficient values (R^2) indicates linearity between drug concentration and absorbance. When R^2 approaches 1, it confirms the linearity. Here, calibration curves of Naproxen has a regression coefficient very close to one (R^2 = 0.983) and that for Naproxen Sodium is 0.982. This indicates the linearity between concentration and absorbance. It also suggests suitability of analytical method which can be used in the current work for further studies.

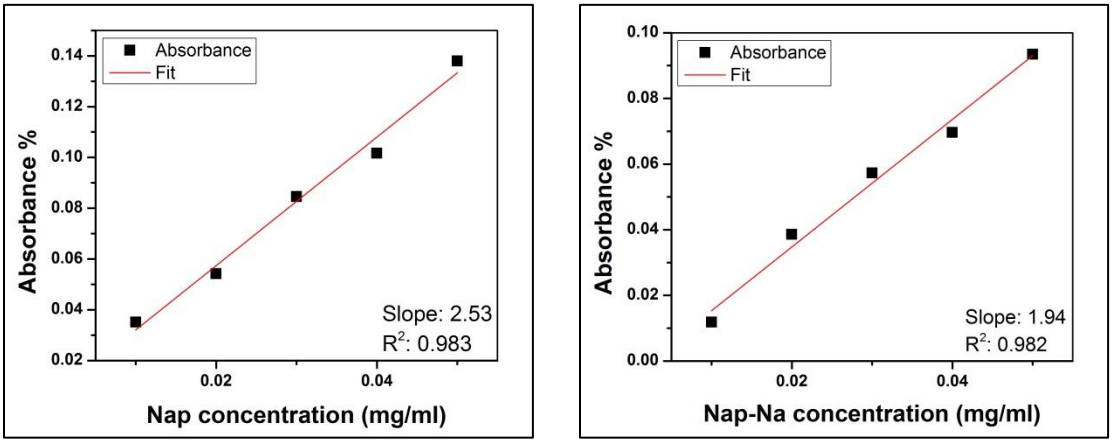

Figure 5.5: Calibration curves for the drug samples (a) Naproxen (b) Naproxen-Na.

5.5.3.2. In vitro drug release studies

Drug release studies were done by dialysis and subsequent UV-Visible spectroscopy as explained in section 5.4.3. UV visible spectroscopy of the samples was done and percentage release data was generated.

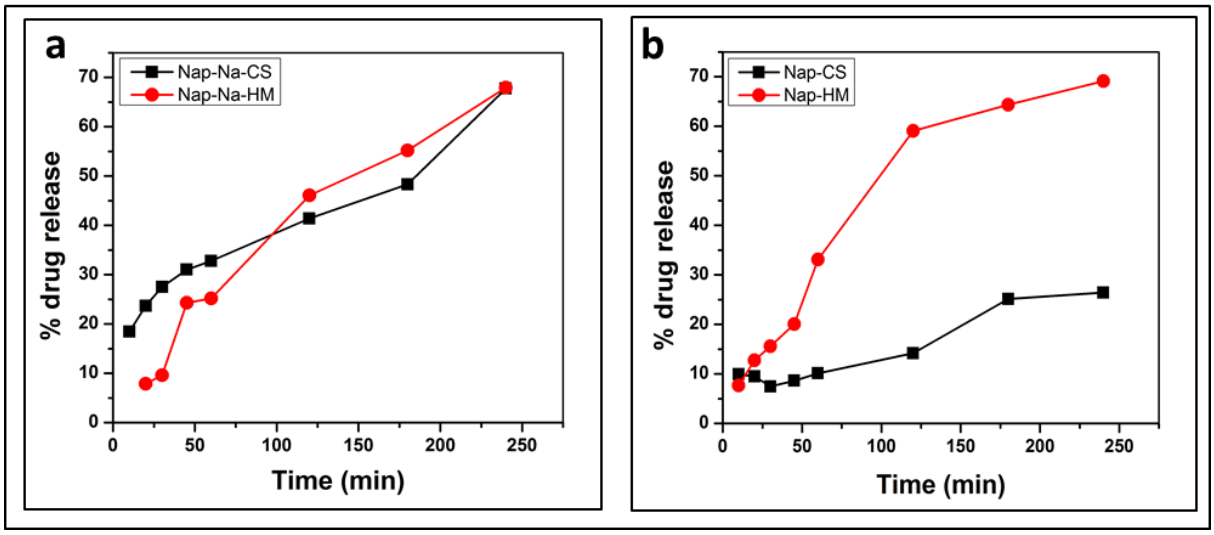

Figure 5.6: Percentage of drug release with time of (a) Naproxen-Na in Core-Shell (CS) and Homogeneous (HM), (b) Naproxen in Core-Shell (CS) and Homogeneous (HM).

The graphs in the figure 5.6 show the percentage release of drugs by PNIPAm particles of core-shell and homogeneous morphology. Figure 5.6 a represents Naproxen sodium and 5.6 b represents Naproxen drug. For Naproxen sodium, the release pattern is almost similar and the final release amount is same for both morphologies. Irrespective of the morphology, about 70% of Naproxen sodium drug is released in 4 hours. Since Naproxen sodium is a water soluble drug, it can interact well with the water- ethanol solvent mixture. Hence when the solvent molecules are expelled out at the VPTT of the microgel, the drug may also be released boosting the release efficiency of the microgel.

Drug release is very different in core-shell particles and homogeneous particles loaded with naproxen drug. Particles with homogeneous density distribution release 70% of drug while particles with core-shell morphology could release only around 20% of loaded drug. The higher % of drug release for homogeneous samples can be attributed to the more volume to absorb the drugs, higher deswelling ratio and bigger network to release them. The density of isopropyl group per area inside the microgel network will be more for core-shell particles. This may

increase the chance of hydrophobic bond between naproxen drug and hydrophobic isopropyl group in the microgel network hindering the release resulting in less percentage release in core-shell particles.

5.5.4. Differential Scanning Calorimetry

Subzero temperature differential scanning calorimetry was conducted on frozen samples taken directly from the deep freezer. The pans were cooled to -25°C at a cooling rate of 10°C/ min. Samples were then equilibrated at -25°C for 10 minutes. After keeping isothermal for 10 minutes, the samples were scanned for a temperature range from -25°C to 5°C with a heating rate of 3°C/ min in a single heating cycle. Nature of water associated with the gelling of microgel can be determined by the position of endotherm peak in DSC thermogram. There are three possibilities of presence of water in the system. Water can be bound associated with the hydrophilic groups in the system, or can be interfacial water which is found in the interface of the dispersed system or can be free water. All the three have distinct melting temperatures. Bound water melts below -10°C, interfacial water melts at -10°C and free water melts at around 0°C.[22,23]

Figure 5.7 shows the DSC thermogram of the freeze dried samples. All samples have an endotherm peak between 0°C and -5°C indicating the presence of interfacial water. Amount of sample taken in the pan plays an important role in deciding the heat flow and thus the endotherm peak size.

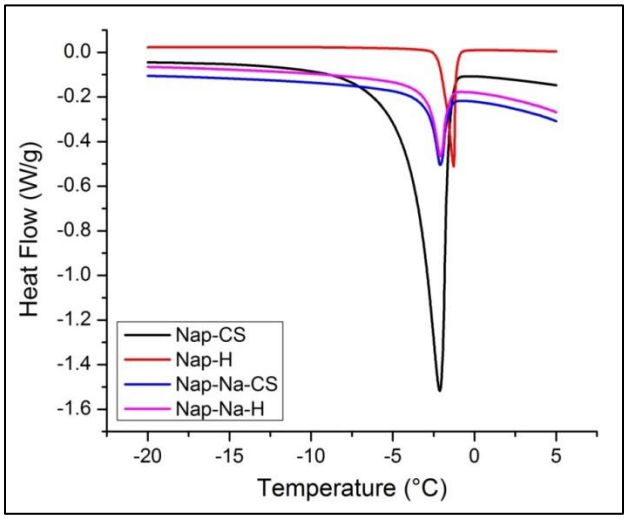

Figure 5.7: DSC endotherm of PNIPAm (core-shell and homogeneous particle distribution) with different drugs.

There was a significant rise in enthalpy for Naproxen dissolved in core-shell PNIPAm particles (Nap-CS) compared to others. This indicates that the addition of a hydrophobic drug into the system induces a dehydration effect causing significant change in the thermodynamic properties of water associated with the microgel system. But this observation is absent in Naproxen-homogeneous system.

5.6. Summary

The drug release capacity of PNIPAm microgels with different morphology were studied in this chapter. One hydrophobic drug and its hydrophilic salt were selected and to dissolve the hydrophobic drug, 10% of the solvent (water) was replaced by ethanol. Consequently, considerable decrease in volume phase transition occurred due to the non-cosolvency effect. Non-linear rheology on dense microgels loaded with drugs suggested the retention of the morphologies even after loading of drugs. UV-Visible spectroscopy was made use of for finding % drug release. In the case of hydrophobic drug Naproxen, particles with core-shell morphology (CS) released 20% of the loaded drug after 4 hours while particles with homogeneous crosslink density (HM) could release 70% of the loaded drug. Most of the drug molecules having biological action are water insoluble and thus many approaches such as cyclodextrin complexation, cocrystallization, solid dispersion and use of nanoparticles as carriers are used to improve their solubility (dissolution rate).[24] In the current work HM showed significant improvement in percent release of hydrophobic naproxen when compared to CS microgels. These results suggest utility of HM in effective loading and release of hydrophobic drugs and thus can be a promising carrier system for poorly water soluble drugs. The higher release capacity of homogeneous particles may be attributed to the more volume to absorb the drugs and bigger network to release them. In the case of hydrophilic drug Naproxen Sodium, both CS and HM could release 70% of the absorbed drug. Since the drug is hydrophilic, it will have strong affinity towards the solvent molecules and when the solvent is expelled out at the VPTT of the microgel, the drug is also expected to be released.

5.7. References

1 C. Ramkissoon-Ganorkar, F. Liu, M. Baudyš and S. W. Kim, *J. Control. Release*, 1999, **59**, 287–298.

2 D. Chakraborty, *Front. Biosci.*, 2013, **18**, 1030.

3 S. K. Sahoo, T. K. De, P. K. Ghosh and A. Maitra, *J. Colloid Interface Sci.*, 1998, **206**, 361–368.

4 K. S. Soppimath, A. R. Kulkarni and T. M. Aminabhavi, *J. Control. Release*, 2001, **75**, 331–45.

5 D. J. Bharali, S. K. Sahoo, S. Mozumdar and A. Maitra, *J. Colloid Interface Sci.*, 2003, **258**, 415–423.

6 V. C. Lopez, J. Hadgraft and M. J. Snowden, *Int. J. Pharm.*, 2005, **292**, 137–147.

7 L. E. Bromberg and E. S. Ron, *Adv. Drug Deliv. Rev.*, 1998, **31**, 197–221.

8 J. Gu, F. Xia, Y. Wu, X. Qu, Z. Yang and L. Jiang, *J. Control. Release*, 2007, **117**, 396–402.

9 T. R. Hoare and D. S. Kohane, *Polymer (Guildf).*, 2008, **49**, 1993–2007.

10 N. M. B. Smeets and T. Hoare, *J. Polym. Sci. Part A Polym. Chem.*, 2013, **51**, 3027–3043.

11 S. Nayak, H. Lee, J. Chmielewski and L. A. Lyon, *J. Am. Chem. Soc.*, 2004, **126**, 10258–10259.

12 N. Murthy, M. Xu, S. Schuck, J. Kunisawa, N. Shastri and J. M. J. Fréchet, *Proc. Natl. Acad. Sci. U. S. A.*, 2003, **100**, 4995–5000.

13 W. Xiong, W. Wang, Y. Wang, Y. Zhao, H. Chen, H. Xu and X. Yang, *Colloids Surfaces B Biointerfaces*, 2011, **84**, 447–453.

14 K. Madhusudana Rao, B. Mallikarjuna, K. S. V Krishna Rao, S. Siraj, K. Chowdoji Rao and M. C. S. Subha, *Colloids Surf. B. Biointerfaces*, 2013, **102**, 891–7.

15 F. M. Winnik, H. Ringsdorf and J. Venzmer, *Macromolecules*, 1990, **23**, 2415–2416.

16 I. Bischofberger, D. C. E. Calzolari and V. Trappe, *Soft Matter*, 2014, **10**, 8288–8295.

17 M. H. Smith and L. A. Lyon, *Acc. Chem. Res.*, 2012, **45**, 985–993.

18 C. M. Nolan, L. T. Gelbaum and L. A. Lyon, *Biomacromolecules*, 2006, **7**, 2918–2922.

19 H. Bysell, R. Månsson, P. Hansson and M. Malmsten, *Adv. Drug Deliv. Rev.*, 2011, **63**, 1172–1185.

20 G. R. Hendrickson, M. H. Smith, A. B. South and L. A. Lyon, *Adv. Funct. Mater.*, 2010,

20, 1697–1712.

21 T. Takahashi, H. Fukazawa and H. Kawaguchi, in *Aqueous Polymer Dispersions*, Springer Berlin Heidelberg, Berlin, Heidelberg, 2004, pp. 164–167.

22 D. Senatra, L. Lendinara and M. G. Giri, in *Trends in Colloid and Interface Science V*, Steinkopff, Darmstadt, 1991, pp. 122–128.

23 P. C. Schulz, J. E. Puig, G. Barreiro and L. A. Torres, *Thermochim. Acta*, 1994, **231**, 239–256.

24 P. Khadka, J. Ro, H. Kim, I. Kim, J. T. Kim, H. Kim, J. M. Cho, G. Yun and J. Lee, *Asian J. Pharm. Sci.*, 2014, 9, 304–316.

CHAPTER 6

CONCLUSIONS AND FUTURE WORK

6.1. Conclusions

The work reported in this thesis provides an insight in to the microstructural changes and its effect on the properties of dense aqueous suspension of Poly(N-isopropyl acrylamide) microgels. Light Scattering, rheology and confocal microscopy were used to investigate the properties of microgels. Small microgels, preferably size less than 500 nm were used to study yielding of colloidal glasses and the effect of particle morphology on the yielding. Large particles of ionic microgels of NIPAm and acrylic acid having size above 500 nm were used to study the effect of applied external electric field on the structural arrangement of microgels. Monodisperse PNIPAm microgels were synthesized by precipitation polymerization in the presence of a cross-linker. The size of the microgel was controlled by adding an anionic surfactant sodium dodecyl sulphate (SDS) during the polymerization while large particles were synthesized in the absence of surfactant. Particles with two different morphologies were synthesized. Due to the faster reaction rate of crosslinker, conventional synthesis method yielded particles with a core-shell like morphology with a highly cross-linked inner core and a loosely cross-linked brush-like surface. New synthesis strategies like continuous feed method yielded particles with uniform crosslinker density. Static light scattering and dynamic light scattering methods were made use of to measure the radius of gyration and the hydrodynamic radius respectively. The main objectives and results of this thesis work have been explained in three chapters.

The notable conclusions of the non-linear rheological studies, confocal microscopy studies and drug delivery investigations are described below.

6.1.1. Rheology studies

Two types of thermosensitive microgel particles of PNIPAm were synthesized, one using a conventional synthesis procedure and the other one using a continuous monomer feed method. The conventional synthesis method produced core-shell (CS) particles and the continuous feed method yielded homogeneous microgel (HM) particles. Dense suspensions of these microgel particles with volume fractions much above the glass transition were analyzed using linear and non-linear rheology to understand the yielding mechanism in these dense microgel suspensions. In the non-linear regime, we found that the core-shell (CS) glassy microgel samples undergo a two-step yielding with two distinct peaks in the loss modulus (G”). The first peak in G” is expected to be due to the disentanglement of the dangling chains of

the neighboring particles and the second peak due to the cage breaking process. With increase in the volume fraction (φ) of the samples, the first peak in G" is seen to move to higher strains due to the deeper interpenetration of the dangling chains of the neighbouring microgel particles. However, the second peak in G" is seen to shift towards lower strains with increasing volume fraction. This is due to the fact that with deeper interpenetration, the cores of the neighbouring microgel particles become more crowded, requiring a lower strain for the particles to move out of the cages. The second peak in G" is seen to disappear for highly crosslinked microgel particles as they behave similar to hard sphere particles. The second peak in G" is observable only at oscillation frequencies (ω) much above the beta relaxation frequency ω_β. When shear is applied at frequency close to or less than the beta relaxation frequency ω_β, the particles get enough time to rattle within the cage of the near neighbours causing the breaking of entanglements via beta relaxation before the shear does it. The double yielding mechanism is also found to depend on the sample temperature. At lower temperature, the particle size is larger and the sample is in a highly compressed state. The second peak in G" is seen to disappear with increase in temperature. This is due to the melting of the microgel glasses with increase in temperature. At higher temperatures, the entanglements between neighbour particles goes off leading to only a single peak in G", which is the characteristics of most of the soft colloidal glasses. Thus the two step yielding behaviour changes to single step yielding at higher temperatures where the entanglements between dangling chains decreases due to the shrinkage of PNIPAM microgel particles. The results of this work suggest that the morphology of the microgel particles strongly influence the dynamics and flow behaviour under dense conditions and provide an insight into the tuning of the interaction between the particles by changing the crosslinker content and the particle morphology.

6.1.2. Confocal Microscopy studies

Our study deals with the behaviour of P(NIPAm-AAc) particles of two different sizes mixed together in different proportions towards external field. Both individual microgels and binary mixture of microgels in different ratios are observed under confocal laser scanning microscope. A definite arrangement of the two different sized particle species into bands parallel to applied field at a definite frequency range is observed. The system returns to the equilibrium mixture when the field is turned off. Chain formation by the bigger particles is seen at lower voltages compared to smaller particles due to the higher dipole moment of bigger particles.

Individual particles form chain bundles and arrange in crystalline structure at very high voltages. At crystalline concentration, individual particles crystals get convert from an FCC lattice to a BCT lattice through molten glassy state. In the binary mixture of particles, bigger particles preferably form chains while the smaller particles falls into the potential well formed between bigger particles in the chain. At higher concentration, the binary mixture shows a different behavior. The smaller particles slowly transforms in to crystalline arrangement from a glassy state while the bigger particles, due to the kinetic arrest between smaller particles are unable to show any phase change in the given electric field window.

6.1.3. Drug delivery studies

Smart microgels have become promising materials in the field of targeted drug delivery in the recent past. In the final part of my work, an investigation in to the effect of particle morphology on the drug release capacity of PNIPAm microgels was done. Particles with core-shell morphology and homogeneous crosslinker morphology were prepared. Non-linear rheology on dense microgels loaded with drugs suggested the retention of the morphologies even after loading of drugs. UV-Visible spectroscopy was made use of for finding % release. In the case of hydrophobic drug Naproxen, particles with core-shell morphology (CS) released 20% of the loaded drug after 4 hours while particles with homogeneous crosslink density (HM) could release 70% of the loaded drug. The higher release capacity of homogeneous particles may be attributed to the more volume to absorb the drugs and bigger network to release them. In the case of hydrophilic drug Naproxen Sodium, both CS and HM could release 70% of the absorbed drug. Since the drug is hydrophilic, it will have strong affinity towards the solvent molecules and when the solvent is expelled out at the VPTT of the microgel, the drug is also expected to be released.

6.2. Recommendation for future work:

6.2.1. Non-linear rheology of mixture of colloids

The effect of addition of small polymer chains in to a colloidal system and the dynamics of the system were studied in detail in the past and well-established. The effect of particle morphology on the yielding of a soft sphere was the intention of my thesis work. The results of this work opens up several interesting opportunities for future investigations. A binary mixture of colloids of different size ratio and/ or of different charges is expected to exhibit more complex but interesting dynamics. Some recent works proved wide range of behaviours for hard sphere

mixtures like fluid to crystal transitions, glass to glass, double yielding etc.[1–3] A detailed investigation on the structure and dynamics of a binary mixture of hard sphere and soft sphere is highly desirable as a fundamental point of view.

6.2.2. Electric field driven assembly of mixture of oppositely charged colloids

In my thesis work, a binary mixture of soft colloids of different sizes but same charge were investigated under external electric field and shown to provide interesting phase behaviour. Due to some technical issues, we could conduct the experiments on binary mixture at higher concentration at only one ratio (25:75). The current work is intended to be extended for other ratios (50:50 and 75:25) also. The behaviour towards electric field will be more complicated if a binary mixture of colloids of different charges is used. An investigation in this regard will contribute towards different perspectives like mixture of microgels and active colloids.[4] We have made initial attempts to prepare a mixture of PNIPAm microgels and active materials and study the effect of external field on the movement and arrangement of particles and bacteria. The preliminary results of our study suggest possible use in future in biomedical field as biosensors.

6.3. References

1 T. H. Voigtmann, *EPL*, 2011, **96**, 36006.

2 T. Sentjabrskaja, E. Babaliari, J. Hendricks, M. Laurati, G. Petekidis and S. U. Egelhaaf, *Soft Matter*, 2013, **9**, 4524.

3 T. Sentjabrskaja, M. Hermes, W. C. K. Poon, C. D. Estrada, R. Castañeda-Priego, S. U. Egelhaaf and M. Laurati, *Soft Matter*, 2014, **10**, 6546–6555.

4 P. Teratanatorn, R. Hoskins, T. Swift, C. W. I. Douglas, J. Shepherd and S. Rimmer, *Biomacromolecules*, 2017, **18**, 2887–2899.

List of Publications

1. **"Two step yielding in dense thermosensitive microgel suspensions: Role of particle morphology"**
   Kiran Kaithakkal Jathavedan, Fayis Kanheerampockil and Suresh Bhat (Under revision, *Colloid and Polymer Science*).

2. **"Directed self-assembly of binary mixtures of soft repulsive ionic microgels under an external alternating electric field"**
   Kiran Jathavedan, Suresh Bhat and Priti Mohanty (Manuscript submitted to *Journal of Colloid and Interface Science*)

3. **"Template-Free Assembly in Living Bacterial Suspension under an External Electric Field"**
   Kunal Samantaray, Bhabani Sahoo, **Kiran Jathavedan**, Bikash Ranjan Sahu, Mrutyunjay Suar, Suresh K. Bhat and Priti Sundar Mohanty. *ACS Omega* 2017, 2, 1019−1024

4. **"Synthesis and characterization of novel polymer-hybrid silver nanoparticles and its biomedical study"**
   Suresh Kumar Verma, Ealisha Jha, **K J Kiran**, Suresh Bhat, Mrutyunjay Suar and P S Mohanty. *Materials Today: Proceedings* 2016, 3, 1949–1957